SOLUTIONS TO SOME ILL-POSED PROBLEMS IN SENSOR ARRAY IMAGING

A THESIS

Submitted for the Award of the Degree

. of

DOCTOR OF PHILOSOPHY

in

COMPUTER SCIENCE AND ENGINEERING

by

Joseph Chakravarti P. MARIADASSOU

DEPARTMENT OF COMPUTER SCIENCE AND ENGINEERING

INDIAN INSTITUTE OF TECHNOLOGY

MADRAS-600 036.

FEBRUARY 1990

CERTIFICATE

This is to certify that the thesis entitled **"SOLUTIONS TO SOME ILL-POSED PROBLEMS IN SENSOR ARRAY IMAGING"** is the bonafide work of Mr. Joseph Chakravarti P. Mariadassou, carried out under my guidance and supervision, at the Department of Computer Science and Engineering, Indian Institute of Technology, Madras, for the award of the degree of Doctor of Philosophy in Computer Science and Engineering.

(B.Yegnanarayana)

ACKNOWLEDGEMENTS

It is with a deep sense of gratitude that I thank Prof.B.Yegnanarayana for his constant help and guidance throughout the course of this work. I thank Prof.R.Nagarajan, Head, Department of Computer Science and Engineering, for making available to me the various facilities in the department. Most of the work presented here was performed during my tenure as project associate for the Department of Electronics, Govt. of India, project, 'Signal Processing in Acoustic Imaging'. I thank the Department for the financial assistance provided. I thank Mr.Pramod Saini, my colleague in the project for the many fruitful discussions I had with him.

I thank Mr.V.P.Sandlas, Director, Defence Electronics and Applications Laboratory, Dehra Dun for granting me the leave and my senior colleagues Dr.V.V.Rampal and Mr.S.C.Jain of Defence Electronics and Applications Laboratory, for their encouragement to complete this thesis.

Mr.C.Chandrasekhar and Mr.A.Ravichandran helped me in no small measure in getting the thesis ready. I owe my special thanks to the two of them. Mrs.Hema Murthy, Mr.Ramana Rao, Mr.Sundar and Mr.Ramaseshan proof read parts of my thesis. Among my many friends who have helped me in one way or other I must mention Mr.Eswar, Mr.Madhu Murthy, Mr.Ravi Subba Rao, Mr.Rajesh Kumar, Mr.Rajendran, and Mr.Vaidyanathan.

My parents and my parents-in-law have been a constant source of moral support. Finally I thank my wife Stella, who has been in many ways responsible for the completion of this work.

Solutions to Some Ill-Posed Problems
in
Sensor Array Imaging.

Major Contributions of the Thesis

Topic: **Ill-Posed Problems in Sensor Array Imaging** (Chapters **1,2)**

***Discussion*:** (a) Ill-Posed Problems especially in the context of Sensor Array Imaging (SAI)

(b) Solutions based on the method of Projection Onto Convex **Sets(POCS)**

Results: Identification of ***tasks*** for study - Image reconstruction from digital holograms

***Issues to be addressed*·** Reconstruction from (a) Sparse data (b) Noisy sparse data

(c) Noisy phase data

***Problem*:** **Image Reconstruction from Sparse Data (Chapter 3)**

Techniques: (a) Solution by collecting data at multiple frequencies

(b) Mapping the problem of SAI as finding a common point of a collection of convex sets and applying the method of Projection Onto Convex Sets to find a solution

Result: The **first** major contribution is **that** using even a small array (8x8) an image (64x64 pixel) **can** be reconstructed

Problem: **Image Reconstruction from Noisy Sparse Data** (Chapters **4,5)**

Techniques: (a) Computation of a "feasible solution" by the method of POCS

(b) New method of reconstruction based on the method of Projection Onto Non Intersecting Convex Sets (PONICS)

Result: The second major contribution is to show that the method of PONICS converges to a solution in the case of noisy sparse data

Problem **Image Reconstruction from Noisy Phase Data** (Chapter **6)**

Discussion: **Image** Reconstruction from full and quantised phase of noisy data

Result: The third major contribution is the development of techniques for reconstruction from partial information such as sparse and quantised noisy phase data

CONTENTS

Chapter 5

IMAGE RECONSTRUCTION BY THE METHOD OF PROJECTION ONTO NONINTERSECTING CONVEX SETS

Chapter 6

IMAGE RECONSTRUCTION FROM NOISY PHASE

ABSTRACT

of the Thesis on

Solutions to Some Ill-Posed Problems in Sensor Array Imaging

Ill-posed problems are those for which there may not be a solution or there may be many widely varying solutions. Sensor Array Imaging (SAI) is a problem of reconstructing an image from data collected by an array of sensors. Since the data is sparse, image reconstruction in SAI is an ill-posed problem. This thesis addresses some issues in SAI and suggests some new methods of solving the problems in SAI. We discuss the theory and develop a method of reconstructing an image from sparse data measured at multiple frequencies. We study the effects of noise in the measured data on the reconstructed image, and develop a method to reconstruct an image from noisy sparse data collected at multiple frequencies. We extend the studies to the case when the measured data is partial. In particular, we consider phase only data. We study methods for image reconstruction from partial noisy sparse data collected at multiple frequencies. As the data available becomes lesser and more noisy, the image reconstruction problem becomes more ill-posed, and it becomes more difficult to formally characterise the situation. We will have to rely on visual observation to assess the performance of any method for image reconstruction.

In a typical SAI situation, such as acoustic holography, the number of sensors is small. Hence the amount of initial data available to reconstruct an image is sparse giving rise to a wide variety of possible solutions. To reduce the size of the solution set, we propose that the array data be collected for

different frequencies of the waves illuminating the object. The problem is now to find an image that generates the measured array data obtained at various frequencies. We show through simulation studies that the quality of the reconstructed image improves as the number of frequencies is increased. The iterative procedure used for reconstructing an image is based on the method of Projection Onto Convex Sets (POCS).

If the initial data is noisy, as it is likely to be in a practical situation, the method of POCS will not be directly applicable. We propose two solutions to this problem. Our first attempt is to compute a "feasible" solution that matches the original data to within a certain degree. The second approach is to apply the method of Projection Onto NonIntersecting Convex Sets (PONICS) which is proposed in this thesis. PONICS is essentially a modification of the method of POCS and uses a relaxation technique to converge to a solution. The relative merits of the two methods are brought out by means of simulation studies. We argue that the method of PONICS is better suited for image reconstruction from noisy sensor array data.

The problem of image reconstruction from the noisy phase of the sensor array data is also considered. An iterative method for image reconstruction is proposed. In this figure of merit for terminating the iterative procedure. Studies show that an image can be reconstructed from full as well as 2-bit quantised noisy phase data.

In a nutshell, the thesis suggests a method of reducing the number of sensors and the measurement complexity at sensor elements by increasing the computational complexity.

Chapter 1

INTRODUCTION

1.1 Major Objectives

This thesis addresses some issues in Sensor Array Imaging (SAI) and discusses solutions to some of these imaging problems. We view SAI as a general problem of recovering a signal or information from partial and noisy data available from a sensor array [21]-[24]. In general, as these problems are ill-posed and hence, we explore the use of some available techniques for solving ill-posed problems [44],[58]. Some of these techniques involve the use of both symbolic and numeric constraints of a given problem, together with some empirical and heuristic procedures to obtain an acceptable solution [5],[43]. In order to study the performance of these techniques in imaging context we consider a simplified imaging setup, where the conditions of ill-posedness can be simulated easily. Before we discuss ill-posed problems we describe the problem of information recovery from partial data.

1.2 Information Recovery from Partial Data

When two systems communicate with one another, the signal that is transmitted from one system to the other undergoes some transformation. In this process part of the signal may be distorted or even lost. In addition noise may also be added to the signal. Usually there is redundancy in the transmitted data. Therefore the transmitted information can still be recovered from the partial noisy signal. But if the adverse effects of noise and loss of signal dominate, it may be impossible to retrieve the signal unambiguously. In some cases only part of the signal needs to be recovered and pattern recognition/artificial intelligence techniques can be used to recover useful information from this partial signal [5],[43]. However no precise characterization of what constitutes useful information has been made for any practical domain, although there have been several attempts to model some restricted domains like the blocks world [62]. We restrict our attention to signal recovery problems that can be stated formally.

1.3 Inverse Problems

Signal recovery is an inverse problem and may be posed in all its generality as follows: Let g be the transmitted signal transformed by an operator T to produce a signal f. That is,

$$f = Tg. \tag{1.1}$$

It is required to compute $g = T^{-1}f$, given f and T, and hence the name inverse problem.

As mentioned earlier there is usually loss of signal information upon transmission. Signal recovery may be possible in spite of the loss because of the redundancy in the data. Of all possible signals that could be transmitted, only a small subset of them carries meaningful information in a given context. The set of transmitted signals can be characterized by certain known properties. From the data available at the receiver, it is required to conjecture a signal at the transmitter end that satisfies the known properties, and which could have given rise to the data at the receiver end. Obviously the derived signal must depend on the known data, otherwise there would be no need to transmit the signal. The problem may have no solution at all if, for example, the received signal is noisy and there exists no signal belonging to the class of solutions which could have given rise to the known data. If the data is sparse, there may exist more than one solution, each different from the other. This is because for a given partial data there may be many solutions that could have given rise to the known data and satisfying the constraints known a priori. The partial data situation may arise due to poor sampling or quantisation or collection of only a part of the signal. Problems such as these which have no solutions or very different solutions are referred to as ill-posed problems.

1.4 Ill-Posed Problems[57]

1.4.1 What are Ill-Posed Problems

Ill-posed problems occur in many areas like pattern recognition, computer vision and speech processing. A problem is ill-posed if it has no unique solution that is robust to small changes in the initial data. A formal definition is as follows[57]:

Definition : *A* problem is said to be well-posed if a solution exists, is unique and depends continuously on the initial data. A problem that is not well-posed is ill-posed.

Some of the methods of solving ill-posed problems are: (a) to reformulate them as well-posed problems by the use of some cost functions to be optimized and (b) to compute any arbitrary solution from among the set of possible solutions that satisfy some constraints/properties known a priori. The first approach is used for example in Wiener filtering and maximum entropy methods. The second approach which we try to adopt in this thesis is suitable if the size of the solution set is small. This approach may in fact be reduced to the problem of finding a common element of a collection of sets. In other words if multiple solutions to a given initial data are possible and it is required to find one that satisfies some constraints or properties known a priori, then the problem can be formulated as one of finding a solution that (a) belongs to the set of all functions satisfying the initial data and (b) belongs to the set of all functions satisfying the given constraints/properties.

1.4.2 Methods of Solving Ill-Posed Problems

Let $T:G \to F$ denote an operator T whose domain G and range F are metric spaces[1]. Our first attempt at solving ill-posed problems is to convert them to a well-posed problem if possible. Such a method, known as the selection method attempts to find a unique g for a given f such that $f = Tg$ and $g \in G_o$, where G_o is a known set. The following Theorem 1.1 states that the selection method can be applied if G_o is compact. A compact set is defined as follows [63]:

....

1. A brief introduction to metric and Hilbert spaces is given in Appendix,

Definition: A set G_o in a metric space G is said to be compact if every sequence in G_o contains a subsequence that converges to a limit in itself.

Theorem 1.1 *[57]:* Suppose that a compact (in itself) subset G_o of a metric space G is mapped onto a subset F_o of F. If the mapping $G_o \to F_o$ is continuous and one to one, then the inverse mapping $F_o \to G_o$ is continuous and one to one.

If, as it usually happens, the known signal is noisy, the selection method cannot be applied as there may exist no solution $g \in G_o$ such that f=Tg. Hence we restrict our attention to finding g such that $g \in G_o$ and

$$\rho_F(f,Tg) = \min_{g_o \in G_o} \rho_F(f,Tg_o), \tag{1.2}$$

where ρ_F is a metric on the space of received signals. Such a solution is called a quasisolution. Sufficient conditions for the existence and uniqueness of a quasisolution can be stated through Theorem 1.2 and Theorem 1.3.

Theorem 1.2 *[57]:* If the equation f = Tg can have more than one solution on the compact set G, and if the projection of each element of the set F onto the set T_G is unique, then the quasisolution of 'the equation f = Tg is unique and depends continuously on the initial data f. Here

$$T_G = \{f=Tg: g \in G\} \tag{1.3}$$

and F is the space of functions containing f.

The projection of an element x onto a set C is an element

Px of C such that

$$\rho(x,Px) = \min_{y\in C} \rho(x,y) \tag{1.4}$$

Informally, Px is a point in C that is closest to X. If $x \in C$ then $Px=x$. If T is a linear operator, a more general theorem may be stated as follows [57]:

Theorem 1.3 *[57]:* If T is a linear operator and the homogeneous equation $Tg = 0$ has only the zero solution on the convex set $G_o \subset G$, and if every sphere in the set G is strictly convex, then a quasisolution to the equation $f = Tg$ on the compact set G_o is unique and depends continuously on f.

Notice that when the conditions required by the above theorems are satisfied the problem is no longer ill-posed. If the solution set G_o is not compact then we need other techniques to tackle the problem of signal reconstruction. One of these is to make use of a stabilizing functional Dg optimizing which, will hopefully give a solution that is at least close to the desired solution. This method is known as regularization. In general there are three methods of using the stabilizing functional. These are [42]:

1. Min $\rho_F(f,Tg)$ such that $Dg \leq d$, for given d,
2. Min Dg such that $\rho_F(f,Tg) \leq d$, for given d.
3. Min $(\rho_F(f,Tg) + \alpha Dg)$.

The last functional is known as the smoothing functional and a is a relaxation parameter. In the next section we shall see examples of some well known regularization procedures.

1.4.3 Regularization

Some well known statistical methods of signal reconstruction like Wiener filtering and maximum entropy method can be cited as examples of regularization. In this section we shall see how some ill-posed problems are regularized. Note, however that the regularization merely suggests a solution to the problem, but the manner of computing a regularized solution is sometimes quite involved and hence approximations are made to the actual problem. Let us begin with Wiener Filtering. For convenience, we restrict our attention to the discrete one dimensional space.

Wiener Filtering

Let

$$f = Tg + n, \tag{1.5}$$

where f is the received signal, g is the transmitted signal and n is the noise signal. Let Qg be the stabilizing functional where Q is a linear operator. It is required to minimize

$$\|Qg\| \text{ subject to } \|f - Tg\|^2 = \|n\|^2. \tag{1.6}$$

Here $\|.\|$ refers to a norm in a normed vector space. By using the method of Lagrange multipliers [29],[53] we can show that the desired solution satisfies the following equation [1], [45]:

$$(T'T + \alpha Q'Q)g = T'f \tag{1.7}$$

where T' and Q' denote the adjoint of the operator T and Q respectively and $1/\alpha$ denotes the Lagrange multiplier to be chosen such that

$$\|f - Tg\|^2 = \|n\|^2. \tag{1.8}$$

In the case of one dimensional vectors the operators T and Q are matrices and the adjoint of these matrices are their Hermitian transposes. This method of signal recovery is referred to as constrained restoration [1],[43]. By substituting $Q'Q = R_{gg}^{-1}R_{nn}$ where R_{gg} and R_{nn} represent the autocorrelation matrices of g and n respectively, the above filter reduces to the parametric Wiener filter. Hence g may be estimated as,

$$g = (T'T + \alpha Q'Q)^{-1}T'f \tag{1.9}$$

In addition if $\alpha=1$, then we obtain the Wiener filter. If $\alpha>1$ in the parametric Wiener filter, then the effect of noise and signal statistics is emphasized and if $\alpha<1$, then it is de-emphasized. To compute an optimal solution a must be chosen to satisfy (1.8). Note that g and n are assumed to be wide sense stationary [1],[45].

In the two dimensional case, using the block circulant properties of certain square matrices (1.4) can be written as [1]:

$$G(u,v) = \frac{F(u,v)}{T(u,v)} \; \frac{1}{T(u,v)T^*(u,v) + \alpha S_n(u,v)/S_g(u,v)} \tag{1.10}$$

Here $G(u,v)$, $F(u,v)$, $T(u,v)$, $S_n(u,v)$ and $S_g(u,v)$ represent the Fourier transforms of $g(x,y)$, $f(x,y)$, $t(x,y)$, $R_{nn}(x,y)$ and $R_{gg}(x,y)$ respectively (The superscript * denotes complex conjugate). In practice $S_n(u,v)$ and $S_g(u,v)$ are not usually known and some empirically determined constant is used in place [1]. The stabilizing functional used so far reflected noise and signal statistics. It can also be used to reflect a measure of smoothness [45]. We shall not go into the details. Suffice here to say that the stabilizing functional can be used to reflect many an objective or subjective criterion.

Maximum Entropy Method [1],[9]

Let us consider the maximum entropy method which has been used extensively for image restoration [1], [7], [61], [74]. Here the stabilizing functional is the entropy function $g[\ln(g)]^t$. (The superscript 't' denotes transpose and g denotes a vector of values of g at discrete points in the 1-D case). The problem can be formulated as

$$\text{Min } g[\ln(g)]^t \text{ subject to } \|f - Tg\|^2 = \|n\|^2 \quad (1.11)$$

Again applying the Lagrange multiplier method we derive [1],[9]:

$$\hat{g} = \exp\{1 - 2\alpha T^{*t}(f - T\hat{g})\} \quad (1.12)$$

Here g denotes the estimated value of g. Notice in this method that $\hat{g}$ is positive and if $\hat{g}[i]$ is close to zero then the computation is numerically unstable. Also note that a must again be chosen such that

$$\|f - Tg\|^2 = \|n\|^2 \quad (1.13)$$

One inherent drawback of this method is that the method is numerically unstable when the signal to noise ratio (SNR) is low. Moreover it can be used only for reconstructing real positive signals.

Minimum Norm Solution

The minimum norm solution for a set of simultaneous equations [18] is also a method of regularization when the set of equations is underdetermined. In the overdetermined case it is akin to the computation of linear predictor coefficients in signal estimation and hence is really a quasisolution. In the underdetermined case the stabilizing functional is $\|g\|$, the norm being defined in the Euclidean sense. The method of computing the solution is by Singular Value Decomposition (SVD) [18]. In [44] a method similar to SVD has been described. Here the desired solution is assumed to belong to a compact set of the Hilbert space and can be computed by expanding it in terms of the eigenfunctions of the operator $T'T$.

A note regarding regularized solutions is well in place here. In Weiner filtering, for example, we could ignore noise effects altogether by setting a to zero. However the resulting inverse operator is numerically unstable since the denominator might tend to zero at a faster rate than the numerator. To avoid this instability we have to settle for an operator that cannot in general yield exact results even in the absence of noise. Hence a regularized procedure will necessarily produce estimates that loose some of the detail and fine structure of the reconstructed signal. The exact way in which the fine structure is lost ultimately depends upon the noise level. Notice in this context the use of the name smoothing functional to a method of regularization mentioned in Section 1.7. In short, regularization is a compromise between numerical instability arising due to noise and loss of detail.

The main drawback of these methods is that they do not make explicit use of constraints in various domains such as band-limitedness or finite support. In iterative procedures where the solution is refined at every iteration these constraints can be applied easily. Hence we advocate the use of iterative techniques.

1.5 Iterative Methods of Signal Recovery

1.5.1 Gerchberg-Papoulis Iterative Procedure

The iterative method is resorted to if there exists no closed form solution for the problem. But the main difference between an iterative method like the method of Projection Onto Convex Sets (POCS) - to be described later - and an algorithm is that the latter must terminate after a finite number of steps, while the former merely tends to a solution. There are some situations where even the POCS method can be shown to compute a solution in a finite number of steps but such cases are not often encountered in ill-posed problems. In practice, the result after a few iterations is sufficiently close to the desired solution. Thus iterative methods are also advantageous in terms of speed and numerical stability, as they are less prone to roundoff error.

Iterative methods of signal reconstruction have been in vogue for a long time [8],[10],[39],[44],[50],[54],[59]. There are many instances where a noniterative procedure, even if available, is not used due to numerical instability [59]. Moreover there are instances where noniterative algorithms are not available. Iterative methods for signal reconstruction were proposed by Gerchberg [10], Papoulis [39], Feinup [8] besides several others. In literature they are referred to as 'Papoulis', 'Gerchberg-Saxton' or 'Feinup' iterative method. The methods are essentially the same although they have been applied to different problems. As an example of an instance where iterative methods are applied we shall discuss the problem and its solution as given in [38]. The problem is interpolating a bandlimited discrete signal. In the Papoulis method the values to be interpolated are initialized to some bounded value say zero and the procedure consists of the following steps at every iteration:

1. Compute the Fourier transform of the signal and set the value outside the known band to zero
2. Take inverse Fourier transform of the resulting function and replace the computed signal values with the known ones where they are available.

The Papoulis method was shown to converge. Let us now briefly trace the history of such iterative methods 'or more specifically their proof of convergence. We start with Von Neumann's theorem on alternating projections in the Hilbert space [69].

1.5.2 Alternating Projection Theorem

Let H denote a Hilbert space [24], [63] with inner product denoted by $<x,y>$ and norm $\|x\| = <x,x>$. Let P_a and P_b denote the projections onto linear subspaces C_a and C_b. The orthogonal complement of a set C denoted as $\perp C$ is the set $\{y: <x,y> = 0$, for $x \in C\}$. Let Q_a and Q_b denote the projection operators onto $\perp C_a$ and $\perp C_b$ respectively. The alternating projection theorem [70] states that

$$\lim_{k\to\infty} (P_a P_b)^k f = f_c \qquad (1.14)$$

for any $f \in H$, where f_c is the projection of f onto the Closed Linear Manifold (CLM), $P_c = P_a \cap P_b$. If $f \in P_b$, then Youla's theorem

(Theorem 1 of [70]) states that f is uniquely determined by its projection onto P_a if and only if

$$C_a \cap \perp C_b = \{0\} \tag{1.15}$$

Furthermore, the following sequence converges to f in norm (strong convergence):

$$f_{k+1} = g + Q_a P_b f_k \tag{1.16}$$

The above iterative procedure of computing a solution is called the method of alternating projection. Youla's theorem can be used to show uniqueness of solution for various problems [54]. In fact it can also be used to show convergence of the Papoulis method. Now if noise changes g to $g+\Delta g$ and if we assume that $C_a \cap \perp C_b = (0)$ (implying that the solution is unique), then for $\lim_{k\to\infty} f_k = f_o$ (where $f_o = f+\Delta f$) in (1.16) it can be shown that [70]

$$\|\Delta f\| \leq \frac{\|\Delta g\|}{\sin(\psi(C_a, \perp C_b))} \tag{1.17}$$

where

$$\cos(\psi(C_a, \perp C_b)) = \inf_{\substack{x \in C_a \\ y \in \perp C_b}} \frac{<x,y>}{\|x\| \cdot \|y\|} \tag{1.18}$$

(Here 'inf' refers to the greatest lower bound, or loosely speaking, minimum). Thus, in the presence of noise the change in the reconstructed signal depends on the noise in the transformed signal and the divergence between the two closed linear manifolds.

1.6 Method of Projection Onto Convex Sets (POCS)

The method of Projection Onto Convex Sets (POCS) extends the method of alternating projections to include an arbitrary collection of closed convex sets with nonempty intersection. The earliest references to this method are in [2] and [13]. However we shall present our discussion based on a later work by Youla and Webb [71].

1.6.1 Theoretical Basis of the POCS Method

Let $C_1, C_2, \ldots, C_n$ be a collection of closed convex subsets of a Hilbert space H and let P_C denote the projection operator onto a closed convex set C. Define $T = 1+\lambda(P_C-1)$ with $0<\lambda<2$. Here 1 denotes the identity operator. Let T_i be the corresponding operator for the closed convex set C_i. The theorem to follow suggests an iterative method of computing an element of C_n', where $C_n' = \bigcap_{i=1}^{n} C_i$. But first we shall define the notion of strong and weak convergence [26],[71]. These ideas are required for a discussion of the POCS method.

Definition: A sequence $\{f_k\}$ is said to converge strongly to f if $\lim_{k\to\infty} f_k = f$ and is written as $f_k \to f$. It converges weakly if $\lim_{k\to\infty} (f_k, g) = (f, g)$ for every $g \in H$, and is written as $f_k \rightharpoonup f$.

Note that strong convergence implies weak convergence but not vice versa. The theorem' regarding the proof of convergence of the POCS method can now be stated as:

Theorem 1.4 [71]: Let C_n' be nonempty. Then for every $x \in H$ and every choice of relaxation constants $\lambda_1, \lambda_2, \ldots, \lambda_n$, in the interval $0<\lambda_i<2$, the sequence $\{T_o^N(x)\}$ converges weakly to a point in C'_n. The convergence is strong if and only if at least one of the subsequences of $\{T_o^N(x)\}$ converges strongly. Here $T_o = T_1 T_2 \ldots T_n$.

Note that if the result of every iteration belongs to a compact set [26],[69], then the sequence converges strongly. Methods based on POCS will be used in many of our later studies. For the sake of future reference, a result which may in fact be taken to be the definition of projection onto a convex set, is given below.

Lemma 1.5 [71]: Let Px denote the projection of $x \in H$ onto a closed convex set $C \subset H$ and let y be an arbitrary element of C. Then $\mathrm{Re}\langle x-Px, y-Px \rangle \leq 0$, where Re refers to the real part.

In the next subsection we shall present some examples of convex sets. Prior to that we would like state some of the applications of the method of POCS. One of the areas where POCS has found extensive use is in signal reconstruction. The method has been used for imaging even in the presence of noise [52],[60]. This is done by reducing the constraint that the reconstructed signal must satisfy the initial data exactly to the condition that it must be satisfied to within a certain degree. Of late the method has been applied in image enhancement [4] and acoustic imaging [46],[64]-[66]. In the next section we shall see some examples of convex sets which are found in many signal reconstruction problems.

1.6.2 Convex Sets Defined by .the Fredholm's Operator

In this section we shall see some examples of convex sets. In keeping with our earlier objective of considering a general signal recovery problem we consider the Fredholm's operator of the first kind. Without loss of generality we shall consider the one dimensional case.

The Fredholm's equation of the first kind [23] is given by:

$$f(y) = \int_a^b h(x,y)g(x)\ dx = Rg(x) \tag{1.19}$$

where $h(x,y)$ is a continuous function in both x and y, and $f(y)$ is defined in the interval $[c,d]$. Let R denote the Fredholm's operator. Some examples of convex sets for given $f(y)$ are given below.

(i) Define

$$B_p = \{g(x): Rg(x) = f(y) = 0, \text{ for } |y| > w\} \tag{1.20}$$

where w is a real constant

(ii) Define

$$C_a = \{g(x): Rg(x) = f_a(y), \text{ for } f_a(y) \text{ known at } y \in I_a\} \tag{1.21}$$

where I_a is a closed convex set.

(iii) Define

$$C_\phi = \{g(x): Rg(x) = A(y)\exp(j\phi(y)), \text{ for a given phase function } \phi(y)\}. \tag{1.22}$$

(iv) Define

$$C_{fsc} = \{g(x): g(x) = 0 \text{ for } x \notin C_p\}, \tag{1.23}$$

where C_p, known as the region of support, is a compact set. Although convex sets have been defined for various operators, an attempt has been made here to define it for a general operator such as the Fredholm's operator. The extension is quite straightforward though. The following theorem holds:

Theorem 1.6: B_p, C_a, C_ϕ, and C_{fsc} are closed convex sets.

Proof:

(i) B_p is a closed convex set devoid of interior points [71].

(ii) It has been shown that the set of $f(y)$ whose value in the set I_a is $f_a(y)$ is a closed convex set [71]. Since $g(x)$ is transformed by a bounded linear operator to $f(y)$ it follows that C_a is a closed convex set.

(iii) C_ϕ is a closed linear manifold [71].

(iv) C_{fsc} is a closed convex set devoid of interior points [71].

(End of proof)

We shall now see how the projection onto these sets are computed. We consider only those cases where the problem of

$$\min_{g_2 \in C} \|g_1-g_2\| \tag{1.24}$$

for given g_1 can be reduced to the problem of

$$\min_{Rg_2 \in R(C)} \|Rg_1-Rg_2\|. \tag{1.25}$$

Define the operation $R^{-1}Qg(x)$ as follows:

$$g_0(x) = R^{-1}Qg(x) \tag{1.26}$$

if

$$\|g_0(x)-g(x)\| = \text{Min } \|g'(x)-g(x)\| \tag{1.27}$$

such that

$$Rg'(x) = Q_R Qg(x) = Rg_0(x). \tag{1.28}$$

Here Q_R is the projection onto the range of R and Q is an operator to be defined. Notice that $g_0(x)$ is the projection of $g(x)$ onto the set C_g defined as

$$C_g = \{g'(x): Rg'(x) = Q_R Qg(x)\}. \tag{1.29}$$

The projection is unique if the range of R is closed and convex.

Let P_b, P_a, P_ϕ and P_{fsc} denote the projection operators onto the sets B_p, C_a, C_ϕ and C_{fsc} respectively.

(i) $P_b g(x) = R^{-1}(p_b(y)R(x))$ (1.30)

where

$$p_b(y) = 1, \quad \text{for } y \leq w, \qquad (1.31)$$
$$= 0, \quad \text{otherwise.}$$

(ii) $P_a g(x) = R^{-1}(p_a(y)f_a(y) + (1-p_a(y))Rg(x))$ (1.32)

where

$$p_a(y) = 1, \quad \text{for } y \in I_a, \qquad (1.33)$$
$$= 0, \quad \text{otherwise.}$$

(iii) Let $\phi(y)$ represent the phase function of $Rg(x)$ and $\phi_o(y)$, the known phase. Now,

$P_\phi g(x) = R^{-1}Qg(x)$ (1.34)

where

$$Qg(x) = |Rg(x)|\cos(\phi(y) - \phi_o(y)) \exp(j\phi_o(y)),$$
$$\text{for } \cos(\phi(y) - \phi_o(y)) \geq 0$$
$$= 0, \quad \text{otherwise.} \qquad (1.35)$$

(iv) $P_{fsc}g(x) = g(x), \quad \text{for } x \in CI_p,$
$$= 0, \quad \text{otherwise.} \qquad (1.36)$$

The derivation of these equations can be found in [71]. The POCS method has one serious restriction that the collection of sets must have at least one element in common. In some cases this is not possible as the problem may have been formulated in such a way that there is no common element. Such situations can occur if the initial data is noisy and the noise characteristics are not known. One way of dealing with such problems is to expand the sets by reducing the constraints and thus ensure a point of intersection among them. This can be done, for example, by allowing the solution to satisfy the initial data not exactly but to within a certain degree. For such an approach to work, the sets must be expanded as to be so large that there is always a common element. This will result in a situation where, for most cases, the solution set will be so large that an arbitrary element of the solution set will not be close to the desired solution. The approach that we suggest is to find a solution that satisfies the known constraints and fits the initial data to the best possible extent. The new method which we call the method of projection onto nonintersecting convex sets will be discussed in detail in Chapter 5.

1.7 Iterative Methods of Computing a Regularized Solution

In Section 1.4.3 we saw how a problem could be regularized. Some methods of computing a regularised solution were also given for certain case. In this subsection we shall see some iterative methods of regularizing a solution. Such methods of computing a solution have been reported in literature. In fact most of the regularized solutions discussed earlier can be computed iteratively. However iterative methods are resorted to when the inverse operator is not well defined. For example in Wiener filtering the operator $(T'T + \alpha Q'Q)^{-1}$ may not be well defined for some operators T and Q. Let us consider one such problem where a regularised solution is computed iteratively.

Consider the problem of solving the Fredholm's equation of the first kind. It is required to compute g(x) given f(y), where R is an ideal low pass filter and it is known that $g(x) \in C_{fsc}$. The method of POCS can be applied for computing a solution. In fact, as we shall show later, the method can be modified to compute a quasisolution even if f(y) is noisy (See Chapter 5). We shall now see an approach using some energy constraints for the noise and reconstructed signal [30].

The problem is to compute $g(x)$ such that $\|f-Rg\|^2<\|n\|^2$ and $\|g\|^2<E^2$ for given $\|n\|$ and E. Although even this problem could be solved by the method of POCS it was reformulated to

$$\mathrm{Min}\ (\|f-Rg\|^2 + (\|n\|^2/E^2)\|g\|^2) \tag{1.37}$$

Note that we have come across this problem earlier while discussing Wiener filtering. Here the relaxation parameter is n^2/E^2. After suitable manipulation we can show that the desired solution satisfies the following equation [30]:

$$g = P_{fsc}\{P_b g+(1-\|n\|^2/E^2)(1-P_b)P_{fsc}g\}, \tag{1.38}$$

where P_{fsc} and P_b are as defined in (1.36) and (1.30). Moreover the following iterative scheme was shown to converge:

$$g_k = P_{fsc}\{P_b g + (1-\|n\|^2/E^2)(1-P_b)P_{fsc}g_{k-1}\}, \tag{1.39}$$

where g_k is result of the k-th iteration and $g_o = 0$.

A similar approach was used in [31]. Here the non-negativity constraint was sought to be applied. This can be done in an iterative procedure by simply setting all the negative values in g_o to zero. These methods have not been extended to the case where more than two convex sets are involved. Such a situation occurs in image reconstruction from digital holograms which will be discussed later.

1.8 Sensor Array Imaging (SAI)

1.8.1 A Typical *SAI System*

Sensor array imaging (SAI) can be formulated as a problem of numerically solving the **Fredholm's** equation of the first kind. In this thesis we shall consider mainly one instance of SAI, namely digital holography. We shall now discuss some of the basic principles of SAI.

Fig.1.1 shows the block diagram of a typical sensor array imaging system. The received signal is the transmitted or reflected wavefield from the object of interest. This signal is first sensed by a sensor array, which converts the incoming acoustic or electro-magnetic wave into an equivalent electrical form, by a process known as transduction. Detection which follows next is the process of digitizing the electrical signal so as to be able to store it in a digital computer. From the data thus collected the wavefield at the object plane of interest is computed by means of suitable inverse transformation. This is known as spatial processing.

1.8.2 Issues in SAI

Since all sensor array imaging systems follow the same basic procedure there are a number of issues that are common to all of them. Consider the input to the system first. Due to noise and other medium disturbances this signal is not the actual reflected or transmitted signal from the object plane but a corrupted form of it. Moreover the transformation the signal undergoes in its path from the object plane to the receiver is known only approximately. Hence in practice it is almost impossible to recover the original object wavefield accurately. Noise also creeps in through the poor fidelity of the sensors. But the most important problem with sensor array imaging systems is that, due to the small number of sensors the received signal is known only at a few points. That is, we have problems of poor sampling and truncation. In fact the goal is to obtain an acceptable quality of image using as few sensors as possible. In the detection stage the issue is the level of quantization. Fine quantization requires high fidelity sensors and precise analog to digital converters, neither of which is economical. Coarse quantization, on the other hand, yields poor results since the data is not accurate.

1.8.3 Ill-Posed Nature of the SAI Problem

We consider sensor array imaging(SAI) as an illustration of finding solutions to ill-posed problems. The problem in SAI is to reconstruct an image from the data collected by an array of sensors in a certain fashion. SAI is an ill-posed problem, the ill-posed nature of the problem arising due to (a) the sparsity of data, (b) noise in the data and (c) inadequate knowledge of the process of imaging.

The sparsity of the data results in a large number of solutions that could have given rise to the known data. Thus the solution set is large and two possible candidate solutions could be very different from one another. Consider the set

$$C_a = \{g(x): f(y) = Tg(x), \text{ for } f(y) \text{ known for } y \in I_a\} \quad (1.40)$$

where $T: C_1 \to C_2$. For the problem to be well-posed, $C_1 \cap C_a$ must contain a unique element. However if the data were sparse, C_a is a large set in that the diameter of C_a is large. Hence $C_1 \cap C_a$ will admit very different feasible solutions. In other words the variance of the estimate of an arbitrary solution will be quite large. This, for obvious reasons is not desirable.

Noise in the data causes ill-posedness because there may be no solution (with the known constraints) that could have given rise to the known data. More formally, let $T:C_1 \to C_2$ be a mapping from C_1 to C_2. Let f be the known noisy data. There may be no $g \in C_1$ such that f = Tg. In other words $C_1 \cap C_a$ may be empty. Now if the data were sparse the size of C_a will be large. Hence even in the presence of noise, if the initial data is sparse the solution set may be nonempty. Notice that the effect of noise is to shift the set C_a so that there is no point of intersection. If the data were sparse, C_a is expanded and hence it is likely that $C_1 \cap C_a$ will have a common point of intersection. This suggests one way of noise reduction and was used in [42] for image reconstruction from digital holograms. Here the data is made deliberately sparse by discarding the less significant phase bits. The drawback of this method is that it does not make full use of the known initial data. A more appealing solution is to find $g \in C_1$ such that $\|f-Tg\|$ is minimized for an appropriate norm.

Inadequate knowledge of the transformation operator T will have the same effect on the solution set as noise. Iterative methods are sometimes not used when T is not known accurately, since the error might propagate over successive iterations [44]. In our work we shall not consider this issue, as we wish to focus our attention on the computational aspect of the problem.

1.8.4 Definition of a Solution in SAI

A solution in SAI is one that could have given rise to the known initial data and portrays the image of a real and possible object. Hence the set of possible objects must be characterized precisely. This is a complex task and no successful attempt has been reported for any (practical) domain. Some simple heuristics are possible. For example, the reconstructed image may be known to have large homogeneous regions, or to be enclosed within a known compact region of support. Ultimately the goodness of a solution depends on how much relevant information it gives to the human viewer.

1.8.5 Mapping SAI to Finding a Common Point of a Collection of Sets

SAI is a problem of finding an image function that (a) could be a possible solution to the initial data and (b) has some properties known a priori. Hence it is a problem of finding a common element of two or more sets. Moreover if the sets are convex then the POCS method can be used. If the initial data is noisy then there may exist no image function with the constraints known a priori satisfying the initial data. Here the method of projection onto nonintersecting convex sets can be applied. This method converges to a function whose exact nature is not understood fully. In the case of two nonintersecting sets it can be shown that it converges to a quasisolution. For more than two sets the method converges to a fixed point of the operator applied in the method. Experimental verification is required to show that the fixed point is indeed acceptable.

1.8.6 Imaging and Image Processing

Some image processing techniques like histogram equalization, edge enhancement and mean/median filtering for noise reduction can be used on an image to bring out some of its essential features. These methods, while good, are not sufficient to overcome the poor resolution due to the sparsity of the data and noise. Moreover image processing methods are not applicable on poorly sampled images. Thus noise cleaning and improvement of resolution must be done during imaging itself.

1.8.7 Image Characterization

For a human being who is familiar with the class of objects being imaged it is not very difficult to eliminate certain images as being unrealistic. But it is difficult to characterize formally the class of plausible images. Hence attempts have been made to take recourse to heuristics that are more often than not effective in eliminating implausible images, and retaining the plausible ones [5], [39]. The use of such heuristics might, in some cases, lead to divergence in the iterative reconstruction procedure. Hence they must be employed carefully.

1.9 Digital Holography

1.9.1 A Simplified Model

In order to study the issue of imaging from sparse data, we consider the implementation of a typical SAI problem namely digital holography. A simplified model of the system is used so as to focus our attention on some of the problem solving issues mentioned earlier.

1.9.2 Description of Imaging Setup

In this thesis we shall consider the problem of image reconstruction from digital holograms [15],[63]. Fig.1.2 shows a typical digital holographic system. A plane wave is incident on the object plane and the reflected wave is received at the receiver plane by an array of sensors which transduces the wave at the receiver point into a suitable electrical signal, which is then digitized and fed into a computer. The received signal is assumed to be a steady state periodic signal of one temporal frequency and hence the magnitude and relative phase at every point can be measured. The goal is to compute the field distribution on the object plane using the phase and magnitude data thus collected. The intensity of the field distribution in the object plane gives the image of the object.

Thus the problem of image reconstruction from digital holograms is one of signal recovery from partial and noisy data. Hence without restricting the class of reconstructed signals no worthwhile signal recovery is possible, since for any sensor array data it is possible to conjecture a large number of widely different signals that could have given rise to the known data.

1.9.3 Theory of Imaging

The theory of imaging can be derived from the Rayleigh-Sommerfield equation [11]. Let $f(x,y)$ be the wavefield at the receiver plane and $g(x,y)$ be the wavefield at the aperture also referred to as object plane. Neglecting constant factors the relation between $f(x,y)$ and $g(x,y)$ can be given by the following equation after suitable approximation [51]:

$$f(x,y) = \frac{1}{j\lambda r} \iint_{-\infty}^{\infty} g(x_o,y_o) \exp(j2\pi r/\lambda)\ dx_o dy_o, \qquad (1.41)$$

where

$$r = [(x-x_o)^2 + (y-y_o)^2 + z^2]^{1/2}, \qquad (1.42)$$

z is distance between the object and receiver planes,

and λ is the wavelength of the transmitted wave.

(For a derivation of the above equation from first principles [11] is a good reference). Note that the object and image planes are assumed parallel to one another.

1.10 Outline of Thesis

In this thesis we consider the problems of sparse data and noise for a particular implementataion of sensor array imaging namely digital holography. We have seen that sensor array imaging is an ill-posed problem and we have discussed some ways of solving ill-posed problems. Some of these methods are considered in the context of imaging through digital holography. Prior to discussing the solutions we have to investigate the nature of digital holography to decide what are the more fundamental issues. We decided to use a simplified model of an actual imaging setup in order to study the computational problems involved. Simulation studies show that accurate knowledge of parameters like wavelength, sampling rate and distance between object and receiver plane is necessary for a good reconstruction of the image of the object. We also show that as the number of samples is reduced the quality of the reconstructed image degrades rapidly.

We restrict our attention to the problem of poor sampling and noise. The samples are sparse because the receiver array is usually small and contains only a few sensors. However we need to have more information regarding the object field to obtain a 'good' quality for the reconstructed image. One way of doing this, which we have not considered, is to put some restrictions on the class of objects to be imaged. Such methods have been attempted with varying degrees of success for some narrow domains. In our work we have not considered any particular domain although we feel that a good image reconstruction procedure is 'good' because it yields meaningful information to the human viewer. Thus although we shall prove convergence of our iterative procedures with respect to the squared norm we must point out that squared error is not a good indicator of the quality of the reconstructed signal.

The other way of obtaining more information would be to collect more data on the same sensor array by altering the transformation operator. This is achieved by changing some parameters that are involved in the transformation. The parameter that we have in mind is the wavelength. For some practical reasons to be discussed later we do not consider changing other parameters. Thus on the same array many different set of data can be obtained for the same object. The data thus collected can be combined to produce a better quality image. Earlier methods using, what will henceforth be referred to as multispectral data, combined the reconstructed images for each set of data as a weighted sum. In this thesis we have made use of such data in an iterative algorithm so that the computed solution satisfies the known data. Moreover iterative methods are better because many nonlinear constraints can be imposed on the solution. Simulation studies showed that this method is indeed effective in reconstructing a good quality image.

We consider next the problem of noise. Some existing methods of image reconstruction in the presence of noise are investigated. In particular we study the performance of the POCS method for noise reduction. These methods are not found satisfactory as they require too much a priori knowledge regarding the signal. Hence we develop a new method of image reconstruction in the presence of noise. This method, which we call the method of projection onto nonintersecting convex sets, is found to perform much better than the methods considered earlier, and yet required little additional data about the signal. Signal reconstruction from phase has received considerable attention in recent years [16],[17],[27],[52],[67]. We address in this thesis the problem of signal reconstruction from the noisy phase of digital holograms. The relative merits of quantised phase over full phase are also discussed. We conclude this report by summarizing some of the new results in this thesis. Some issues that warrant further investigations are also pointed out.

1.11 Thesis Organization

The rest of this thesis is organized as follows. In Chapter 2 we shall discuss two methods of reconstructing an image from its hologram. These methods are known as backward propagation and Fresnel/Fourier transform respectively. We shall see the need for simulation studies. A description of the simulation setup and the results of some preliminary investigations are presented. Chapter 3 describes a way of using the data collected at multiple frequencies. This method is suggested as a means to overcome the sparsity of sampling points. Simulation studies bring out the effectiveness of our proposed method. In Chapter 4 we consider the problem of error in the measurement of data. Here we assume that the error is bounded. If the error were due to the addition of random noise then the boundedness assumption will not hold. To overcome this drawback we develop the method of PONICS which is essentially a modification of the method of POCS. This is discussed in Chapter 5. Some simulation studies are presented to bring out the efficaciousness of the method of PONICS. Chapter 6 discusses the problem of image reconstruction from phase of digital holograms. The last chapter (Chapter 7) gives a summary of the thesis. The broad conclusion is that measurement complexity can in some cases be traded for computational complexity without losing image quality.

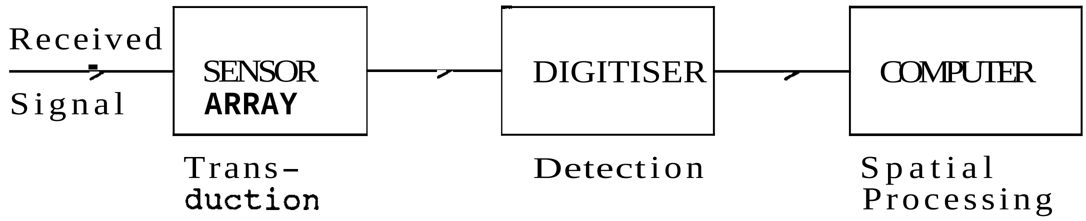

Fig.1.1 Block diagram of a typical sensor array imaging system.

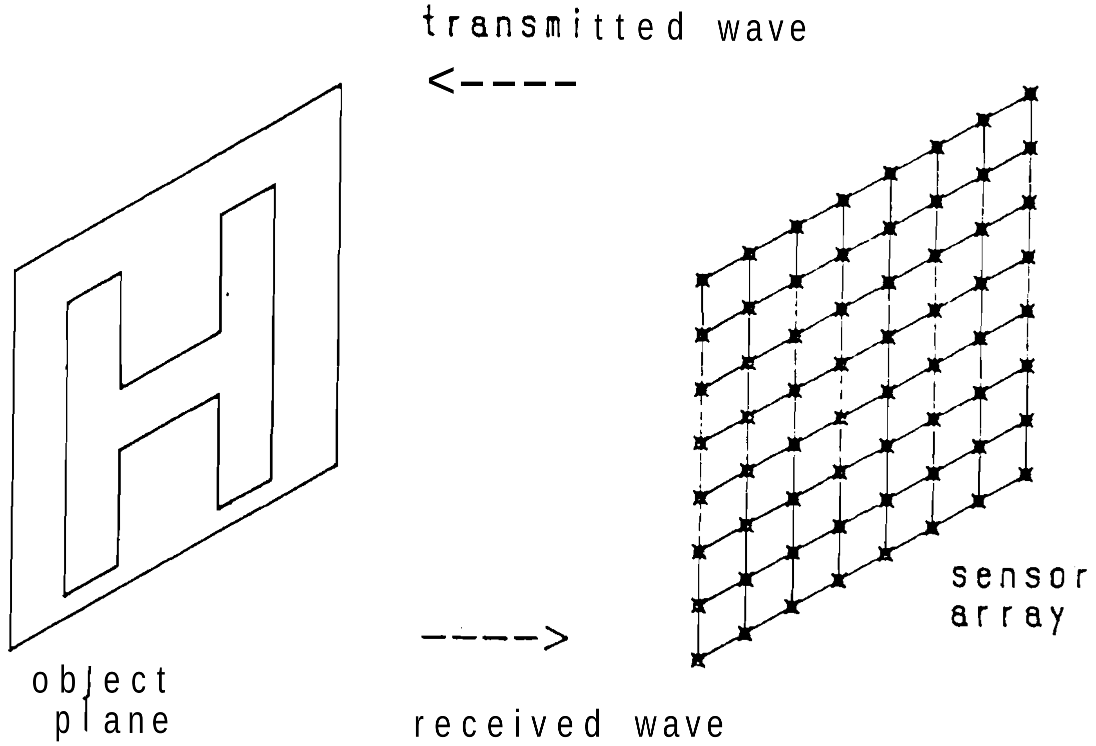

Fig.1.2 A typical sensor array imaging system.

Chapter 2

SIGNAL RECONSTRUCTION FROM DIGITAL HOLOGRAMS

2.1 Introduction

We view sensor array imaging (SAI) as an ill-posed problem and consider digital holography as an instance of SAI, where conditions of ill-posedness can be easily simulated and studied. In this chapter we describe the methods of image reconstruction from digital holograms and some practical problems that arise in implementing these reconstruction procedures.

As described earlier hologram formation is a function dependent on the wavelength and the distance between object and image planes. Thus these two parameters must be known a priori. In addition when the data is digitised, the choice of the sampling rate, the quantisation and the choice of the components of data such as phase and magnitude must be made. If the data available is noise free and precise, and if sufficient quantity of data is available, image reconstruction from digital holograms would be fairly simple. In practice such ideal conditions are seldom encountered. In fact in some applications even the wavelength and the distance between the object and image planes are not known precisely. Studies are made to investigate the quality of the image reconstructed under various adverse conditions. It is found that that wavelength and sampling rate must be known precisely. This result can be explained theoretically. Moreover as in other signal recovery problems we find that phase is more important than magnitude for a good reconstruction. Inadequate number of samples results in poor quality of the reconstructed image.

The sparsity of samples arises due to the inevitably small number of sensors. However with a few sensors it is still possible to collect a large number of data and Chapter 3 discusses a new method of collecting and using the data. The other important aspect of the problem of digital holography is noise. Standard methods of of filtering are inadequate for our problem and hence some new methods are proposed in Chapter 4 and Chapter 5.

There are two methods of reconstructing a signal in digital holography namely Fresnel/Fourier transform and backward propogation. A discussion of these methods of image reconstruction follows in the next section. The issues of performance of these methods with regard to resolution of the reconstructed image and computational complexity are also addressed. In Section 2.3 we point out the advantages and inadequacies of simulation studies. We make use of simulation studies in all our investigations. A description of our simulation setup and the results of our preliminary investigations with regard to noise, sparsity of data and error in measurement of parameters are presented in Section 2.4. We conclude with a summary of the problems encountered in digital holography and point out the issues which we shall address in the rest of our thesis.

2.2 Theory of Image Formation

The equation relating the field distribution on the object plane denoted as $g(x,y)$ and the field distribution on the receiver plane denoted as $f(x,y)$ is given as:

$$f(x,y) = \frac{1}{j\lambda r} \iint_{-\infty}^{\infty} g(x_o,y_o) \exp(j2\pi r/\lambda)\, dx_o dy_o \qquad (2.1)$$

where

$r = [(x-x_o)^2 + (y-y_o)^2 + z^2]^{1/2}$

x,y are the co-ordinates along the x and y axes in the receiver plane

x_o,y_o are the co-ordinates along the x and y axes in the object plane

z is the distance between the image and object plane

$k = 2\pi/\lambda$ is the wavenumber

and λ is the wavelength of the transmitted wave.

The above equation can be viewed as a convolution. Hence, we can write

$$f(x,y) = h(x,y) * g(x,y) \qquad (2.2)$$

where $*$ denotes convolution and

$$h(x,y) = \exp(jk(x^2+y^2+z^2)^{1/2}). \qquad (2.3)$$

2.2.1 Fresnel/Fourier Transform

When $r \approx z[1+(x-x_o)^2/(2z)+(y-y_o)^2/(2z)]$, some approximations can be made in (2.1) resulting in the following equation:

$$f(x,y) = \frac{1}{j\lambda z} h'(x,y) \exp(jkz) \iint_{-\infty}^{\infty} [h'(x_o,y_o)\, g(x_o,y_o)] \exp(j2\pi(xx_o+yy_o)/z\lambda) dx_o dy_o \qquad (2.4)$$

where

$h'(x,y) = \exp(j\pi(x^2+y^2)/(\lambda z))$.

Note that the above approximation holds only in the Fresnel zone where $D<z<D^2/\lambda$ and D is the size of the aperture along the x or y axis. In the above equation the integral is the Fourier transform of the term within square brackets. Thus

the computation of $f(x,y)$ involves one Fourier transform operation if we use (2.4) to compute $f(x,y)$ from $g(x,y)$. Now let Δx and Δx_o represent the sampling interval in the object and image planes respectively along the x-axis and Δy and Δy_o represent the sampling interval in the object and image planes respectively along the y-axis. Let N represent the number of samples along every row and column. For proper computation of the Fourier transform the following relations must hold:

$$N\Delta x_o = \lambda z/\Delta x \tag{2.5a}$$

$$N\Delta y_o = \lambda z/\Delta y \tag{2.5b}$$

Furthermore, if the phase is to be computed accurately, we have [58]:

$$\Delta x_o \leq \lambda z/l_{ox} \tag{2.6a}$$

$$\Delta y_o \leq \lambda z/l_{oy} \tag{2.6b}$$

where l_{ox} and l_{oy} are the size of the aperture and may be given by $l_{ox}=N\Delta x_o$ and $l_{oy}=N\Delta y_o$. Hence from (2.5a) and (2.6a) we derive $\Delta x_o \leq \Delta x$. Similar relations may be derived if it is required to compute $g(x,y)$ from $f(x,y)$. In this case the resolution in the reconstructed image is lower than the sampling interval on the receiver plane. The advantage is that a large object can be imaged using a small array. If the phase of $f(x,y)$ has to be computed from $g(x,y)$, or vice versa, then the sampling interval on both the planes must be equal and

$$\Delta x = \Delta x_o = (\lambda z/N)^{1/2} \tag{2.7a}$$

$$\Delta y = \Delta y_o = (\lambda z/N)^{1/2} \tag{2.7b}$$

2.2.2 Backward Propagation

Another method of computing $f(x,y)$ from $g(x,y)$ is by applying the convolution theorem [33] and is referred to as backward propagation [51]. Here the hologram or the received signal can be viewed as a linear shift invariant system. Hence using convolution theorem we can write

$$F(u,v) = G(u,v)H(u,v) \tag{2.8}$$

where $F(u,v)$, $G(u,v)$ and $H(u,v)$ are the Fourier Transforms of $f(x,y)$, $g(x,y)$ and $h(x,y)$ respectively. $H(u,v)$ is given as [51]:

$$H(u,v) = \exp(jkz(1 - (\lambda u)^2 - (\lambda v)^2)^{1/2}), \text{ for } (\lambda u)^2+(\lambda v)^2 \le 1$$
$$= 0, \qquad \text{otherwise} \tag{2.9}$$

Computationally backward propagation is more intensive since it involves two Fourier transform operations. However, unlike the previous case, the sampling interval on the receiver plane is the same as the sampling interval on the object plane and is not dependent on the distance between the planes or the wavelength. Hence backward propagation is more amenable for use in iterative methods where $f(x,y)$ and $g(x,y)$ have to be computed one from the other repeatedly. In view of this we shall consider only backward propagation in the rest of the work.

2.3 Need for Simulation Studies

As mentioned in the previous chapter the problem in imaging due to the following factors: (a) sampling, (b) truncation, (c) quantization and (d) noise. Given a fixed number of sensors there are various ways of configuring an array. It is possible to place them far apart and thus increase the extent of imaging or they could be kept closely so as to improve the sampling rate. The results in the two cases may be quite different. Again, the level of quantization is an important and crucial decision to be made.

If the quantization is high then, in general, the reconstructed image quality will be better, but will involve large overheads in terms of precise transducers, anolog to digital conversion and communication lines. Finally the problem of noise must be considered and suitable methods must be applied to reduce its effects.

In digital holography there is yet another important consideration and that is the measurement of parameters such as distance, wavelength and the spacing between samples. In applications such as underwater acoustic imaging (for which digital holography is used) the wavelength will be known quite accurately, but the measurement of distance may be inaccurate. In some other applications such as geophysical prospecting [37],[38] it is the wavelength that is the suspect. As we shall soon see, the effect of wrong measurement of parameters will significantly affect the quality of the reconstructed image.

In order to study each of the above mentioned problems we need to conduct experimental studies. But such a proposition is not feasible due to practical considerations. In the first place, in an experimental study we will have to consider many other extraneous factors and hence we will not be in a position to isolate the issues for study. Moreover an experimental set up is too costly and it is not possible to modify the setup at will, once a physical system is built. Hence we take recourse to simulation studies. But we do add a note of caution. In an experimental study we will come across problems that might have been overlooked in a simulation study and hence ultimately experimental studies are needed before an actual system is built.

2.4 Description of Simulation Studies

In this section we describe simulation studies to demonstrate the effect of (a) error in the measurement of parameters, (b) noise in phase and magnitude and (c) sparsity of samples on the quality of the reconstructed image. In what follows we will consider each of them separately. However, let us first give a brief description of our computer simulation setup.

The equation used for simulating the hologram is given by

$$f(i\Delta x, j\Delta y) = \sum_m \sum_n h(m\Delta x, n\Delta y)\; g(i\Delta x - m\Delta x,\; j\Delta y - n\Delta y) \qquad (2.10)$$

Here $h(m\Delta x, n\Delta y)$ is the discrete version of $h(x,y)$ given in (2.3). The steps in the reconstruction of an image from the field data $f(i\Delta x, j\Delta y)$ are :

(a) Compute the DFT of $f(i\Delta x, j\Delta y)$ as $F(m\Delta u, n\Delta v)$

(b) Divide $F(m\Delta u, n\Delta v)$ by $\exp(jkz(1-(\lambda m\Delta u)^2-(\lambda n\Delta v)^2)^{1/2})$

(c) Compute the inverse DFT of the result to obtain the object wavefield distribution.

A 64x64 pixel image shown in Fig.2.1(a) is used for our studies. The image matrix is appended with zeros to form a 128x128 point object field matrix which is used to generate a 128x128 point hologram. The default values of the parameters z, A and Δx are $z=2000.0$ units, $\lambda=0.25$ units and $\Delta x=0.5$ units. If all the received field data is used for image reconstruction we get back the original image as shown in Fig.2.1(b). Throughout the remaining studies only 64x64 points corresponding to the object region of the reconstructed image are shown.

24.1 Errors in Measurement of Parameters

A. Distance

Measurement of the distance z between object and receiver plane is usually not very accurate. Notice in (2.8) that any change in z changes linearly the phase function of $H(u,v)$ which effect is reflected in $G(u,v)$ and hence in $g(x,y)$. It has been well established that the phase of the Fourier transform of a real valued signal captures most of the information of the signal while the magnitude plays a relatively insignificant role [16],[68]. Let Δz denote the error between the actual and measured values of z. Now the Fourier transform $G(u,v)$ of $g(x,y)$, the object wavefield will contain the additional phase factor $\exp(jk\Delta z(1-(nu)^2-(\Delta v)^2)^{1/2})$. Hence the degradation due to error in the measurement of z depends on the absolute value of error and not on the relative error with respect to the actual distance. This implies that for imaging objects farther away the measurement of z will have to be more accurate to retain the same quality for the reconstructed image. We demonstrate this through simulation studies.

Fig.2.2 shows the reconstructed images when there is an absolute error of 2.0, 20.0 and 200.0 units when the actual distance between object and image plane is 2000.0,. 10000.0 and 20000.0 units. Notice that immaterial of the actual distance the reconstructed images appear identical for the same absolute error in distance.

B. Wavelength

In underwater acoustic imaging, where digital holography may be used, the excitation frequency is usually known accurately since it is under operator control. However the velocity of sound in water changes with depth and temperature [55] and hence there may be small errors in the computation of the wavelength. In other applications like seismic exploration the excitation frequency is known only approximately and estimation of the wavelength becomes a major issue. Notice in (2.8) that λ occurs in the denominator of the phase function of $H(u,v)$. Hence any error in the measurement of wavelength is going to affect the phase of $H(u,v)$ significantly. This implies that the quality of the image reconstructed will also be poor.

Simulation studies bear this out as can be judged from Fig.2.3. Fig.2.3(a)-Fig.2.3(d) show the reconstructed images when the error in wavelength ranges between 0.1% and +10%. For a large error (10%) in wavelength the reconstructed image is not intelliglible at all.

C. Spacing between Sensors

The spacing between sensors is usually known. But we still examine the effect of error in the measurement of Δx (the spacing between adjacent sensor elements) on the reconstructed image. Note that u and v are inversely related to Δx. Therefore for a small error in Δx there is a large change in the phase function of $H(u,v)$. Hence the quality of the reconstructed image can be expected to degrade significantly for a small error in the measurement of spacing. This is seen from Fig.2.4(a) where there is a +0.1% difference between the actual and estimated values of Δx. Fig.2.4(b)-Fig.2.4(d) show similar results, where the error between the actual and estimated values of Δx is 1%, 5% and 10% respectively.

These three studies show that the quality of the reconstructed images is very sensitive to errors in the measurement of parameters. This is because when there is an error in the measurement of parameters the actual system transfer function is different from the known one.

2.4.2 Noise and Error in Measurement of Signal

We now consider the effect of error in the measurement of signal and the effect of random noise introduced by the medium. While the former error can be to same extent taken care of by the use of sophisticated hardware, the latter - noise by medium - is beyond our control although we can attempt to reduce its effects. In what follows we will present results of simulation studies, to see the effect of error and noise in the received data on the reconstructed image.

A. Error in Measurement of Magnitude

Let $|f(x,y)|$ represent the magnitude of $f(x,y)$. Fig. 2.5(a) shows the reconstruction when the measured value of $|f(x,y)|$ has a random error of at most 10% of its true value. Fig.2.5(b) - Fig.2.5(d) show the results when the error is 25%, 50% and 75% respectively. Even for large errors (50% and 75%) in the measurement of magnitude the quality of the reconstructed image is still good.

B. Error in Measurement of Phase

Here we shall study the effect of improper measurement of phase of $f(x,y)$ on the reconstructed image. Fig.2.6(a) shows the result of reconstruction when the error in phase varies randomly between $\pi/16$ and $-\pi/16$. Fig.2.6(b) - Fig.2.6(d) show the result when the error is $\pi/8$, $\pi/4$ and $\pi/2$ respectively. For large errors ($\pi/4$ and $\pi/2$) in the measurement of phase, the quality of the reconstructed image is poor.

As a result of these two studies we see that noise in phase degrades the images more than noise in magnitude. Hence phase is more important than magnitude. However in any practical setup measurement of magnitude and phase are not made separately. Hence we shall consider the effect of error in the measurement of signal as a whole.

C. Noise

Let us now present the results of the study carried out to investigate the effect of noise in the received data on the reconstructed image. Gaussian distributed random noise was added to the received data and Fig.2.7 shows the result of reconstruction for different levels of noise.

2.4.3 Reconstruction from Sparse Data

In the studies mentioned earlier all the 128x128 data generated was used for reconstruction although the data itself may be noisy or the parameters may be known inaccurately. If only part of these samples are known then, even if the data were noise free, the reconstructed image quality will be poor. The iterative method of reconstruction using sparse data will be given in the next chapter. Here we shall present simulation studies of reconstructing images using sparse data by a straight forward application of the reconstruction procedure used until now. Where the sample values are not known a value of zero is assumed. Fig.2.8(a) shows the reconstructed image when every alternate sample (64x64 samples) is known. Fig. 2.8 (b)-Fig. 2.8 (d) show the result when only 32x32, 16x16 and 8x8 samples respectively are known. Thus we see that as the number of samples decrease there is a degradation in the quality of the reconstructed image.

2.4.4 Reconstruction from Phase and Magnitude

We consider here another form of partial data namely phase only and magnitude only. Fig.2.9(a) and Fig.2.9(b) show the result of using phase only and magnitude only respectively of the received data. Note that while the essential features of the original image are seen in the reconstruction from phase only the reconstruction from maginitude only is not intelligible. This reiterates our earlier conclusion that phase is more important than magnitude for the reconstruction of an image from digital holograms.

2.5 Inadequacy of Direct Methods

In this chapter we have focused our attention on digital holography and have discussed the problems that arise in a typical imaging setup. A brief description of the theory of imaging and two methods of reconstructing the image from the transformed signal was presented. It is seen from the studies conducted that direct methods of image reconstruction are inadequate to handle the problems of noise and sparse data. These problem are the subject of the rest of the thesis. We shall investigate the problem of sparsity of samples in the next chapter. In Chapter 4 we shall discuss some methods to overcome the problem of bounded error in measurement of the signal. Subsequently in Chapter 5, we shall consider Gaussian distributed random noise and suggest an iterative method to reduce the noise effects.

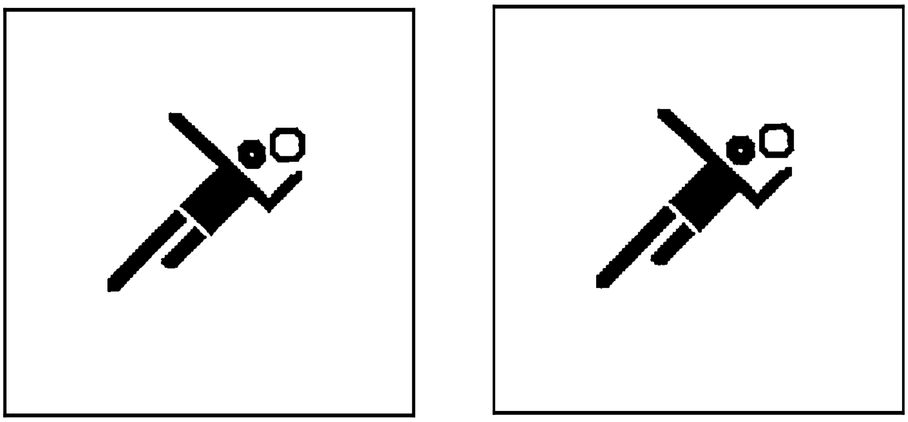

(a) (b)

Fig.2.1 Original and reconstructed image: (a) A 64x64 pixel image appended with zeros to form a 128x128 point data array. denoting the object field distribution. (b) Image reconstructed from the the sensor array data. In this case the reconstruction is exact. Note that the image part corresponding to the object is only the middle 64x64 points shown in the square.

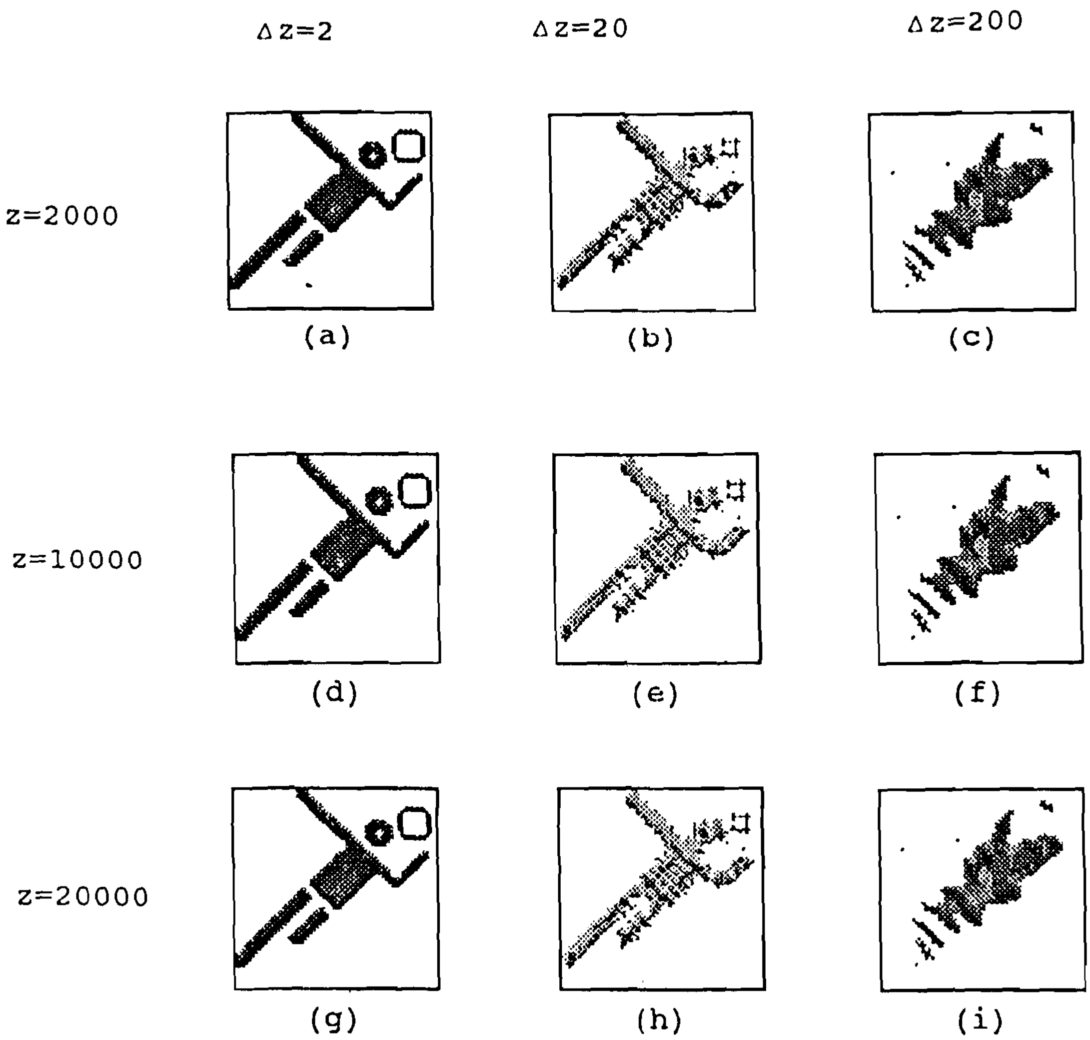

Fig.2.2 Effect of errors in the measurement of distance, z. The figures are given for three different distances between the object and the receiver planes and for three 'cases of errors. It is to be noted that generally the quality of the reconstructed image depends on the absolute error in the distance measurement.

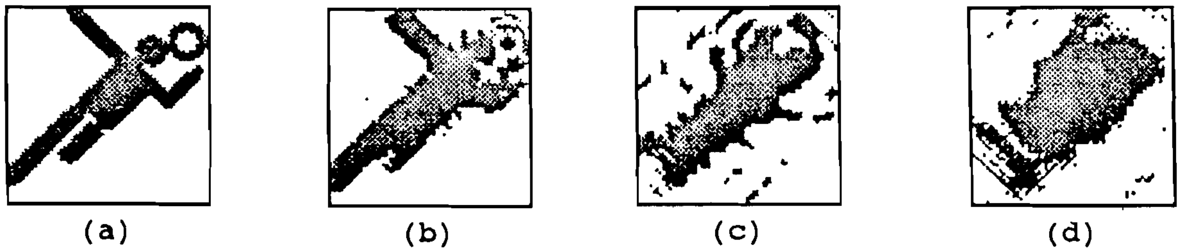

Fig. 2.3 Effect of errors in the measurement of wavelength, λ: (a) for 0.01% error in λ, (b) for 0.1% error in λ, (c) for 1% error in λ and (d) for 10% error in λ. Even for a small (0.01%) error in λ the degradation in the reconstructed image is significant.

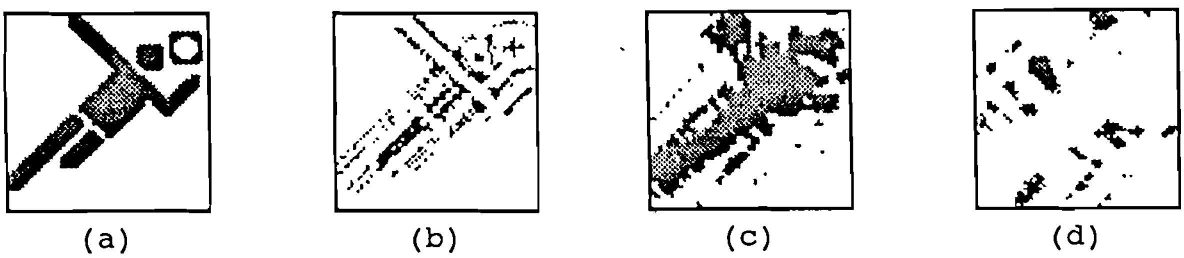

Fig. 2.4 Effect of random errors in the measurement of spacing $(\Delta x, \Delta y)$ between sensors for three different cases: (a) for 0.01% error in spacing, (b) for 0.1% error in spacing (c) for 1% error in spacing and (d) for 10% error in spacing. The error is assumed random within the limits specified. The figure shows that even for a small (0.1%) error in spacing causes significant degradation in the quality of the reconstructed image.

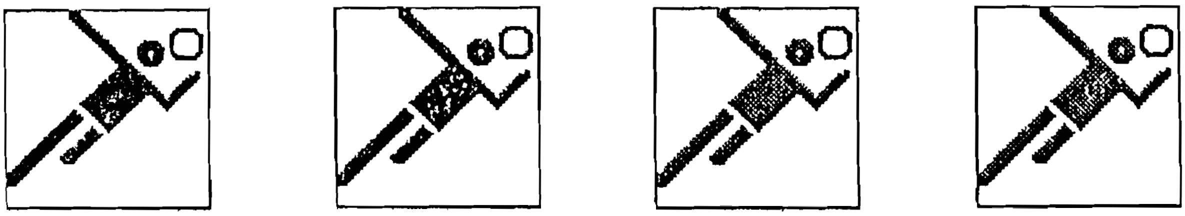

(a) (b) (c) (d)

Fig.2.5 Effect of random errors in magnitude of the received field for four different cases: (a) for maximum 5% error in magnitude, (b) for maximum 10% error in magnitude, (c) for maximum 25% error in magnitude and (d) maximum 50% error in magnitude. The error at each point is random within the limits specified. The figure shows that even large(50%) errors in magnitude do not seem to affect the quality of the reconstructed image significantly.

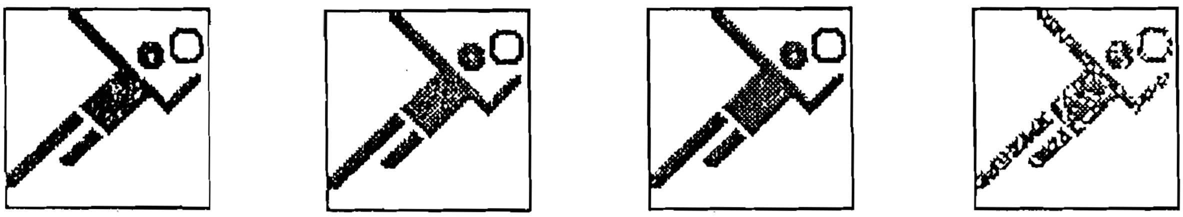

(a) (b) (c) (d)

Fig.2.6 Effect of random errors in phase of the received field for four different cases: (a) for phase errors of $\pm\pi/16$, (b) for phase errors of $\pm\pi/8$, (c) for errors of $\pm\pi/4$ and (d) for phase errors of $\pm\pi/2$. The error at each point is random within the limits specified.

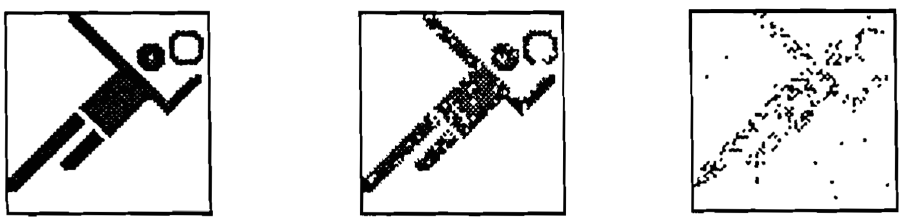

(a) (b) (c)

Fig.2.7 Effect of random noise in the measured complex field data for three different cases of signal to noise ratios(SNR): (a) for SNR=10 dB (b) for SNR= 0 dB and (c) SNR=-10 dB. Since both magnitude and phase are affected, there is a progressive degradation in the quality of the reconstructed image as SNR decreases.

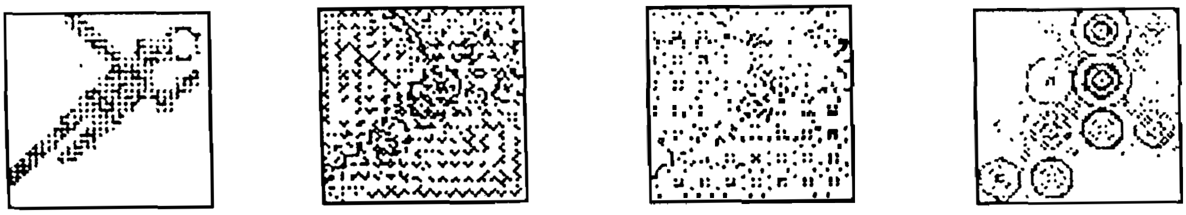

(a) (b) (c) (d)

Fig.2.8 Image reconstruction from sparse data for four different cases: (a) from **64x64** points of received data, (b) from 32x32 points of received data, (c) from **16x16** points of received data and (d) from 8x8 points of received data. The data is created by appropriate down-sampling and setting the values in between to zero. As expected, there is a systematic degradation as the number of samples of data are decreased.

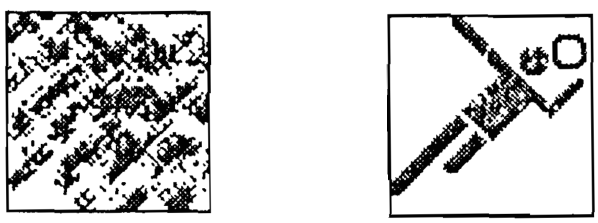

(a) (b)

Fig.2.9 Image reconstruction from partial data: (a) reconstruction from magnitude only and (b) reconstruction from phase only. The results show that significant features of the original image are preserved in the reconstruction from phase, indicating that phase is more important than magnitude.

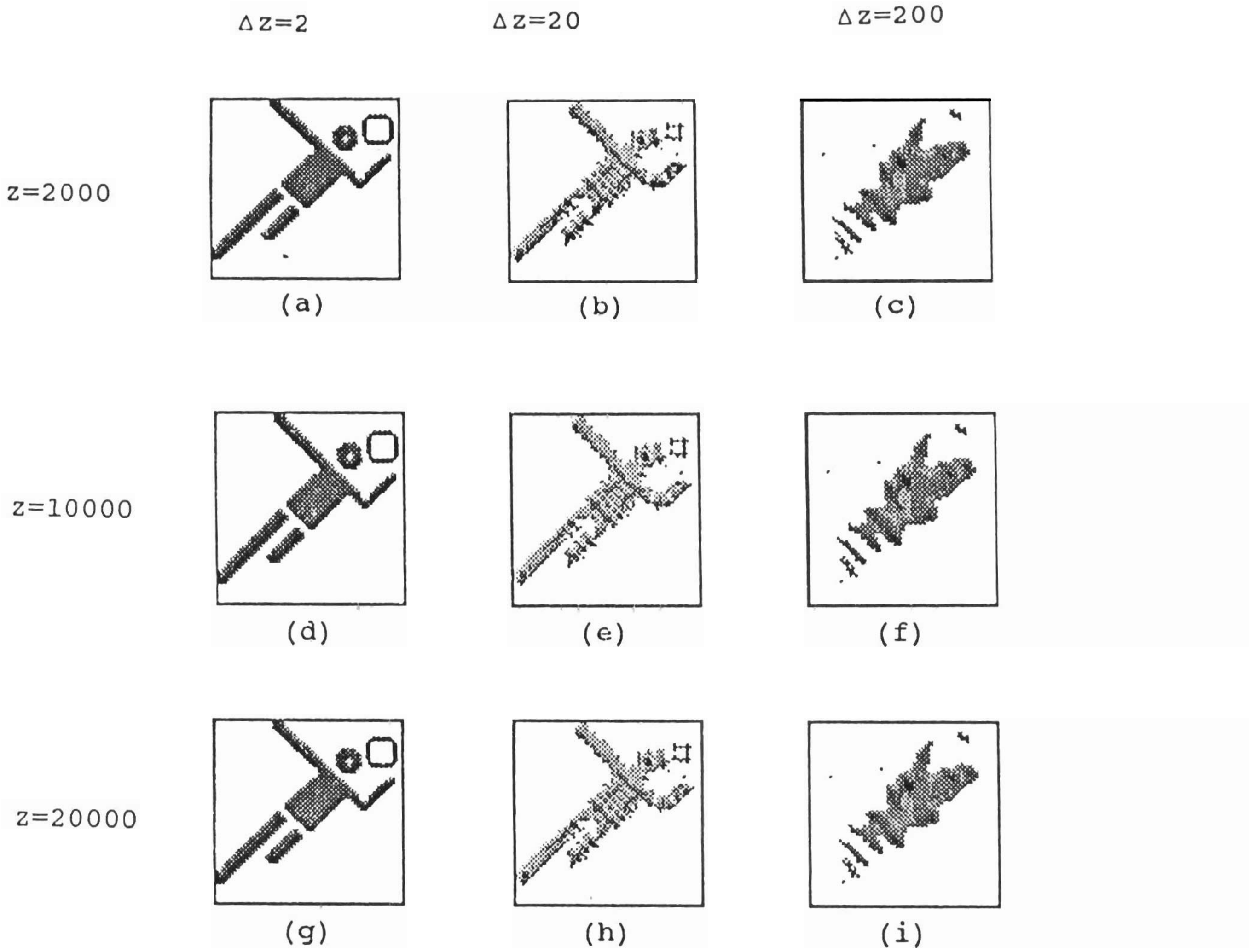

Fig.2.2 Effect of errors in the measurement of distance, z. The figures are given for three different distances between the object and the receiver planes and for three 'cases of errors. It is to be noted that generally the quality of the reconstructed image depends on the absolute error in the distance measurement.

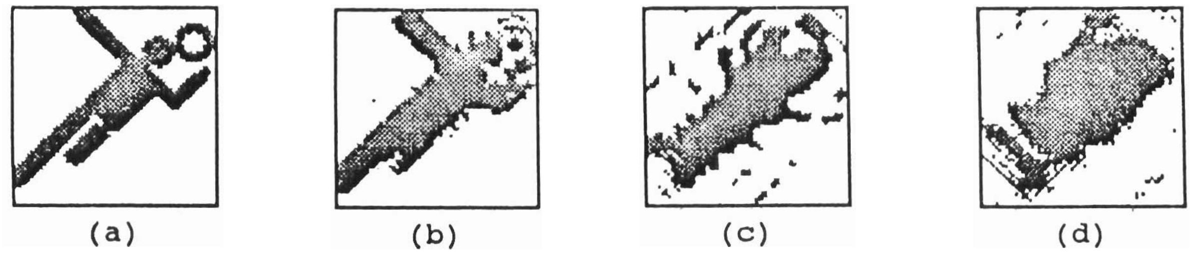

Fig. 2.3 Effect of errors in the measurement of wavelength, λ: (a) for 0.01% error in λ, (b) for 0.1% error in λ, (c) for 1% error in λ and (d) for 10% error in λ. Even for a small (0.01%) error in λ the degradation in the reconstructed image is significant.

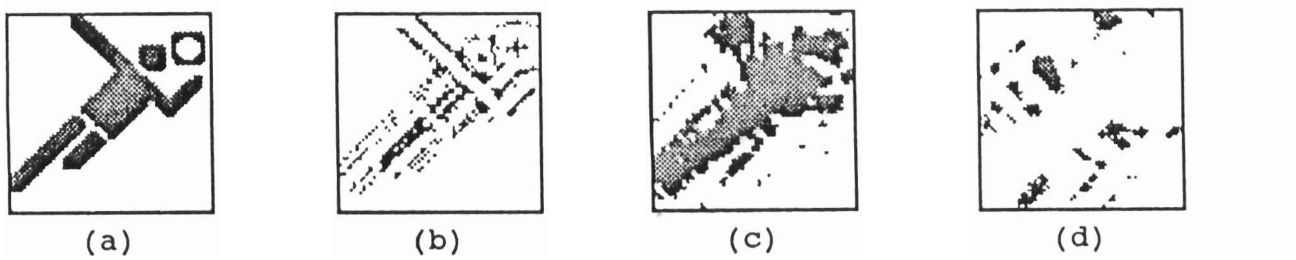

Fig. 2.4 Effect of random errors in the measurement of spacing $(\Delta x, \Delta y)$ between sensors for three different cases: (a) for 0.01% error in spacing, (b) for 0.1% error in spacing (c) for 1% error in spacing and (d) for 10% error in spacing. The error is assumed random within the limits specified. The figure shows that even for a small (0.1%) error in spacing causes significant degradation in the quality of the reconstructed image.

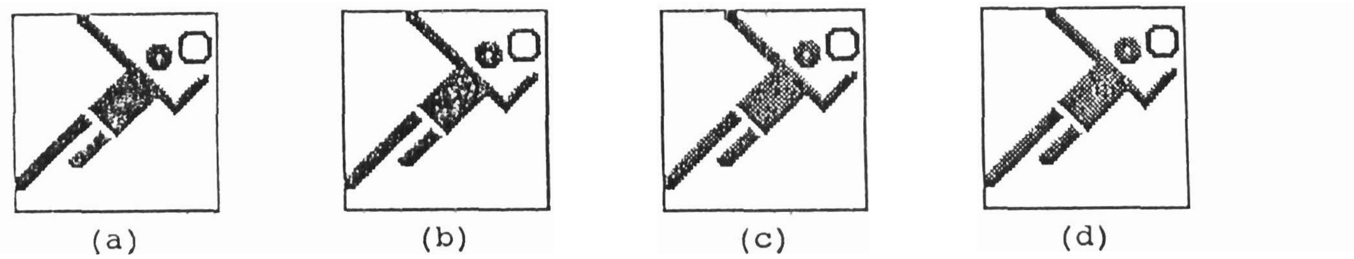

Fig.2.5 Effect of random errors in magnitude of the received field for four different cases: (a) for maximum 5% error in magnitude, (b) for maximum 10% error in magnitude, (c) for maximum 25% error in magnitude and (d) maximum 50% error in magnitude. The error at each point is random within the limits specified. The figure shows that even large(50%) errors in magnitude do not seem to affect the quality of the reconstructed image significantly.

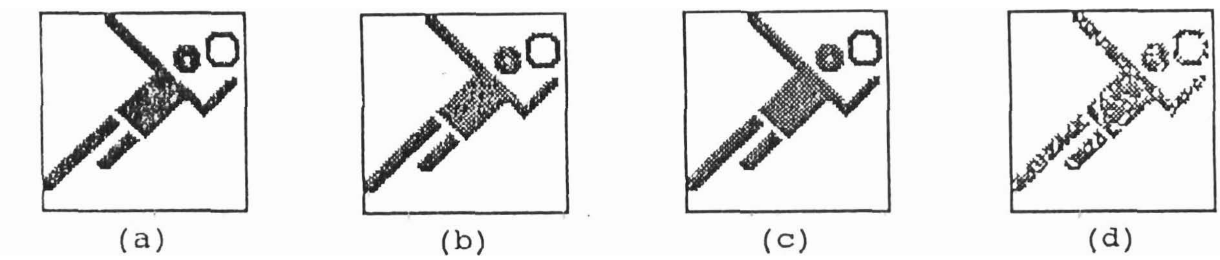

Fig.2.6 Effect of random errors in phase of the received field for four different cases: (a) for phase errors of $\pm\pi/16$, (b) for phase errors of $\pm\pi/8$, (c) for errors of $\pm\pi/4$ and (d) for phase errors of $\pm\pi/2$. The error at each point is random within the limits specified.

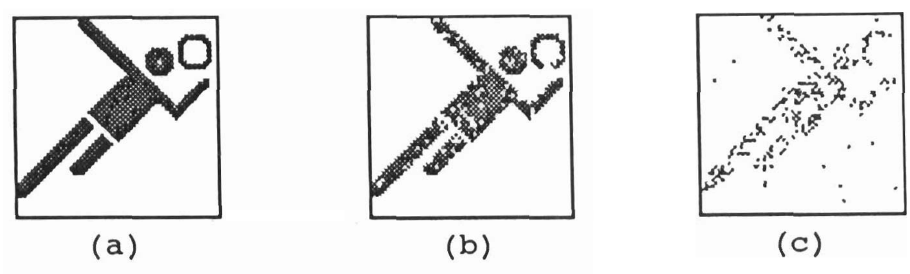

Fig.2.7 Effect of random noise in the measured complex field data for three different cases of signal to noise ratios(SNR): (a) for SNR=10 dB (b) for SNR= 0 dB and (c) SNR=-10 dB. Since both magnitude and phase are affected, there is a progressive degradation in the quality of the reconstructed image as SNR decreases.

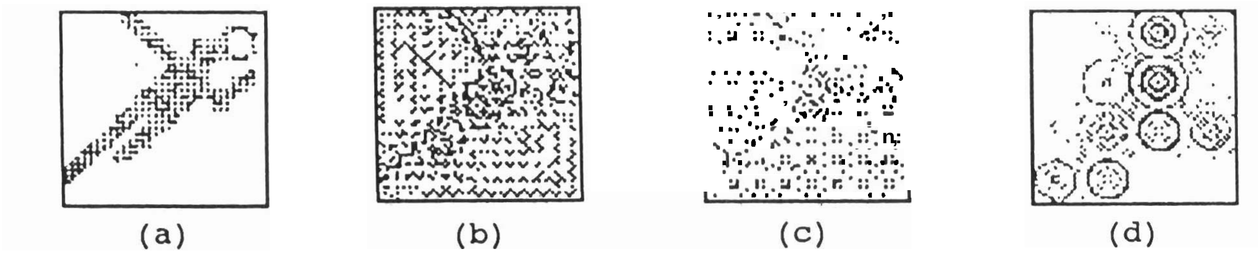

Fig.2.8 Image reconstruction from sparse data for four different cases: (a) from 64x64 points of received data, (b) from 32x32 points of received data, (c) from 16x16 points of received data and (d) from 8x8 points of received data. The data is created by appropriate down-sampling and setting the values in between to zero. As expected, there is a systematic degradation as the number of samples of data are decreased.

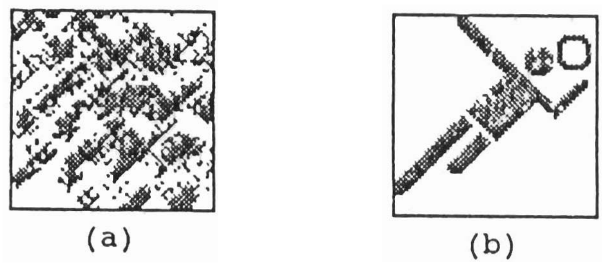

Fig.2.9 Image reconstruction from partial data: (a) reconstruction from magnitude only and (b) reconstruction from phase only. The results show that significant features of the original image are preserved in the reconstruction from phase, indicating that phase is more important than magnitude.

Chapter **3**

MULTISPECTRAL HOLOGRAMS

3.1 Previous Approaches to Sparse Data Problem

In the previous chapter we saw that as the number of sensors decreases the quality of the reconstructed image reduces sharply. In this chapter we suggest a way of overcoming this problem by collecting the data at multiple frequencies. We consider for the present noisefree data only. Noise considerations are treated in the subsequent two chapters.

Without additional information or data it is not possible to improve the resolution of the reconstructed images. Information regarding the domain of objects imaged may help in generating good quality images. It is desirable to describe formally the class of objects being imaged, since the search space of solutions for a given sensor array data would then be reduced. However, as of now, formal descriptions are available only for a very restricted class of objects [61] that do not have much relevance to any practical situation. It is not our aim to make yet another attempt in that direction. We hope to improve the quality of the reconstructed image by using additional data and the knowledge that the object is located within a certain known compact region, referred to as region of support. In other words, we assume that the wavefield distribution on the object plane is zero outside the known compact region of support. This assumption, though seldom true in any practical situation, is however a good approximation for most cases. Note that interpolation will not help in increasing the resolution.

Additional data required for better resolution can be obtained using synthetic aperture methods as in radar and sonar. The aim in these methods is to get data at a large number of sampling points by moving the object or sensor array relative to the other. An example of this type of imaging is computer tomography. Here the specimen to be imaged is made stationary and the sensor is moved along an arc or straight line and data is thus collected at many points using just one sensor. In nondestructive testing the specimen is moved relative to the stationary sensor array. The third method of synthetic aperture imaging is to move both object and sensor array relative to one another.

The other method of obtaining additional data, in digital holography especially, is to generate holograms of the same object using different excitation frequencies. Earlier attempts [19],[32],[45] using this approach were restricted to two or three holograms. In essence these methods computed a weighted sum of the images obtained from various frequencies, the weighting coefficients being chosen on the basis of some noise and signal statistics. In another approach using multiple frequencies the object field estimation is done by cross correlating the sensor array data obtained for multiple frequencies with the class of all images that are possible for a particular context [36]. Essentially, in the earlier approaches to image recovery from multiple frequency holograms, all manipulations were done on the image domain. Here we shall consider a way of using arbitrary number of holograms in an iterative procedure that integrates the process of imaging with image processing. Holograms thus obtained for the same object at multiple frequencies are henceforth referred to as multispectral holpgrams.

In Section 3.2 we shall state what we mean by a solution to the sparse data problem. We shall see that the need for multispectral holograms arises only because of poor sampling and truncation. In other words if data is sampled adequately over an infinite plane an exact reconstruction is theoretically possible, even for such data collected at only one frequency. We then present arguments to show that the size of the solution set may be expected to decrease as the number of frequencies for which the data is collected is increased. We propose to use an iterative procedure based on the method of POCS for image reconstruction from multispectral holograms. As mentioned in the previous chapter there are two methods of reconstructing an image from a hologram, namely the Fresnel/Fourier transform and the backward propagation method. We shall discuss the suitability of the backward propagation method compared to the Fresnel/Fourier transform method for the iterative procedure. Although the method of POCS for image reconstruction from multispectral holograms will be discussed in detail in Section 3.3, suffice here to state that it is similar in many respects to some of the well known iterative procedures for deconvolution, bandlimited interpolation,etc. We shall discuss two different ways of applying the POCS method namely the sequential and parallel method. We can show strong convergence for both these methods. Simulation studies presented in

Section 3.4 show that the quality of the reconstructed image improves significantly with the increase in the number of frequencies at which the holograms are collected. The main drawback of the proposed method is its inadequacy to handle noise. This is considered in the subsequent two chapters.

3.2 A Solution to the Sparse Data Problem

3.2.1 *Problem Statement*

The functions of interest in this study are elements of $L_{2X2}(\Omega)$ space of all two dimensional functions square integrable over Ω. The associated Hilbert space is the quotient space induced by the equivalence relation $\|g_1-g_2\| = 0$, where $g_1,g_2 \in L_{2X2}(\Omega)$. The problem is to compute $g(x,y) \in C_{fsc}$ such that

$$f_o(x,y) = g(x,y) * h(x,y) \tag{3.1}$$

for $f_o(x,y)$ known on $(x,y) \in I_p$ and $h(x,y)$ as given in (2.4). Here I_p is a compact set of points for which the data is known.

3.2.2 *Uniqueness of Solution*

Let us consider the case when all the data $f(x,y)$ is known, in the equation (2.1). Notice that according to (2.2), (2.7) and (2.8) hologram formation may be viewed as an ideal low pass filter. We can show that if the solution set consists of bounded, piecewise continuous functions with compact regions of support, then the solution is unique. An exact solution may not be possible on account of noise. In such cases it can be shown that a quasisolution is unique. The latter result will be discussed in Chapter 5. Here we consider the noise free case only.

For ease of notation let us consider the one dimensional problem first. This may be posed as follows: Let

$$f(x) = g(x) * h(x). \tag{3.2}$$

Let $H(\omega)$, the Fourier transform of $h(x)$, vanish outside some compact subset of the real line. In other words, $H(\omega) = 0$, for $\omega \notin B_W$, where B_W is some compact subset of the real line, and $H(\omega)$ is piecewise continuous and bounded in B_W. Let the solution set be

$$C_{fsc} = \{g(x) : g(x) = 0,\ x \notin C_p, \text{ and } g(x) \text{ is piecewise continuous}\}, \tag{3.3}$$

where C_p is a compact subset of the real line. It is required to compute $g(x)$ given $f(x)$. Using convolution theorem we can write

$$F(\omega) = G(\omega) \cdot H(\omega), \tag{3.4}$$

where $F(\omega)$, $G(\omega)$ and $H(\omega)$ denote the Fourier transforms of $f(x)$, $g(x)$ and $h(x)$ respectively. Since $H(\omega)$ is bandlimited, $F(\omega)$ is also restricted to the same band as $H(\omega)$. Hence,

$$G(\omega) = F(\omega)/H(\omega), \quad \text{for} \quad \omega \in B_W. \tag{3.5}$$

Since $g(x)$ has finite support its Fourier transform is analytic[34] and hence by analytic continuation $G(\omega)$ can be computed uniquely.

This result can be extended to the two dimensional case. Thus if $g(x,y)$ is a piecewise continuous function belonging to $L_{2X2}(\Omega)$ space with compact regions of support then its Fourier transform is analytic and the solution to (2.1) is unique.

3.2.3 Use of Additional Data

We have of course assumed that $f(x,y)$ and $h(x,y)$ are known completely. In practice this is not the case since $f(x,y)$ is sampled and known only over a finite set of points. Hence, even in the noise free case there may be many $g(x,y)$ having the said finite region of support such that $f(x,y) = g(x,y) * h(x,y)$, for $(x,y) \in I_p$, the set of sampling points. That is if g_1 and g_2 are two solutions then $\|g_1 - g_2\|$ need not necessarily be zero. In this section we shall see how more data can be collected for the same number of sampling points by changing the frequency of excitation. Prior to that we must show that collecting more data aids in reconstructing a better quality image in that the computed solution using more data is likely to be closer to the desired solution than otherwise.

Let

$$C_{fo} = \{ g(x,y) : f_o(x,y) = g(x,y)*h(x,y), \text{ for } f_o(x,y) \text{ known on } (x,y) \in I_p \}. \tag{3.6}$$

Suppose n holograms are collected for various wavelengths λ_1, λ_2, ..., λ_n. Let $f(x,y;\lambda_i)$ denote the hologram for a wavelength Xi. Define

$$C_{fi} = \{ g(x,y) : g(x,y)*h(x,y;\lambda_i) = f(x,y;\lambda_i), \text{ for } (x,y) \in I_p \} \tag{3.7}$$

Let $C_i = C_{fi} \cap C_{fsc}$. We will show later that every bounded subset of C_{fsc} is compact. We assume that the desired solution is bounded and hence belongs to a bounded subset of C_{fsc}. Without loss of generality we shall refer to the bounded subset of C_{fsc} containing the solution, as C_{fsc} itself. Since C_{fsc} is compact and any closed subset of a compact set is also compact, C_i is compact. Let $g_n(x,y)$ be the solution computed from n holograms and $g_{n+1}(x,y)$ be the solution obtained from n+l holograms. Let

$C'_n = \bigcap_{i=1}^{n} C_i$. Hence $g_n(x,y) \in C'_n$ and $g_{n+1}(x,y) \in C'_{n+1}$. Let $g_o(x,y)$ be the desired solution and $Pr(\|g_o(x,y)-g_n(x,y)\|>\epsilon)$ denote the probability that $\|g_o(x,y)-g_n(x,y)\|>\epsilon$ for some $\epsilon>0$, and $Pr(\|g_o(x,y)-g_{n+1}(x,y)\|>\epsilon)$ the probability that $\|g_o(x,y)-g_{n+1}(x,y)\|>\epsilon$.

Since each of the sets C_i is compact, the diameter of the set C'_n denoted as $D(C'_n)$ is finite. Here diameter of a set C is defined as

$$\underset{g_1,g_2 \in C}{\mathrm{Max}} \|g_1(x,y) - g_2(x,y)\|. \tag{3.8}$$

Also, since $C'_n \supseteq C'_{n+1}$, it follows that $D(C'_{n+1}) \leq D(C'_n)$, and hence $Pr(\|g_o(x,y)-g_n(x,y)\|>\epsilon) \geq Pr(\|g_o(x,y)-g_{n+1}(x,y)\|>\epsilon)$. Thus as the number of holograms increases one would expect to arrive at a solution that is closer to the desired solution. Note also that $f(x,y)$ is not linearly dependent upon the wavelength. Hence by varying the wavelength we obtain two linearly independent sets of data. While this may not necessarily be true if the number of samples is finite it is obvious that if the number of samples is much more than the number of frequencies for which the data is known then the data obtained for one frequency will be independent of that obtained for another.

At this point we need to mention why we do not consider changing other parameters practical. The parameters that could be altered in an imaging setup are wavelength, distance and sampling rate. changing distance or the sampling rate is same as synthetic aperture imaging mentioned earlier. This means that we have to move the sensor array relative to the object', which is difficult to implement in practice.

3.2.4 Suitability of Backward Propogation

We have just seen that if data is collected at multiple frequencies, we can hope to reduce the size of the solution set and thus improve the quality of the reconstructed image. As was mentioned in the previous chapter there are two methods of image reconstruction from digital holograms namely **Fresnel/Fourier** transform and backward propogation. In this section we shall see which of the two methods is more useful for image reconstruction from multispectral holograms.

In the **Fresnel/Fourier** trasform the resolution of the reconstructed image depends upon the wavelength used and is given by (2.5) which is reproduced below:

$$\Delta x = \lambda z/N\Delta x_o \qquad \Delta y = \lambda z/N\Delta y_o \tag{3.9}$$

Hence the resolution on the reconstruced image varies with wavelength. Therefore to **combine** the data from different frequencies, every reconstructed image must be transformed into one with a common base band resolution. Transforming an image of one resolution into another of a different resolution is computationally intensive. Moreover it is not suitable for use in an iterative procedure for reasons that we shall now discuss. For correct computation of phase the sampling rate must be $(\lambda z/N)^{1/2}$. In other words for a given sampling interval and distance there is only one frequency that can be used to compute the phase exactly. In an application like underwater acoustic imaging it is not feasible to change the sampling rate since the sensors are fixed on an array. Thus it is not possible to use **Fresnel/Fourier** transform to reconstruct an image from holograms obtained by changing the wavelength. The same argument holds for reconstructing an image from multiple holograms obtained by varying the distance between object and image plane.

In backward propogation the imaging system can be treated as a linear shift invariant system and the sampling rate is the resolution on the reconstructed image. This resolution depends on the wavelength only in so far as it specifies the best resolution possible for the reconstructed image. Note however that the physical sampling rate need not be a limitation on the resolution of the reconstructed image. We may assume the presence of phantom sensors where sampled data is not available. The signal on these phantom sensors may be computed using data collected at other frequencies. Thus backward propogation is more suitable for iterative computation since (a) the resolution is independent of wavelength within a broad range of operation and (b) the resolution can be improved by increasing the number of frequencies.

3.3 POCS Method of Computing a Solution

In this section we shall discuss the POCS method of computing a solution. Recall that the problem of reconstructing an image from sparse data reduces to finding a common element of $C_{fsc} \cap C_{f1} \cap C_{f2} \cap \cdots \cap C_{fn}$. These sets as we know are closed convex sets. Hence the POCS method of computing a solution can be applied. POCS is an iterative method and the computation performed at the k-th iteration is given by

$$g_k(x,y) = P_{fsc} T_{f1} T_{f2} \cdots T_{fn} g_{k-1}(x,y), \qquad (3.10)$$

where $T_{fi} = 1+s_{fi}(P_{fi}-1)$, P_{fi} is the projection onto C_{fi} and $0<s_{fi}<2$. For reasons of faster convergence we could choose s_{fi}

such that $s_{fi}>1$. However such a choice must be made judiciously and yields faster convergence only in the initial stages of computation. $g_o(x,y)$, the initial estimate of the solution is usually chosen such that it belongs C_{fsc}. The computation of the projection onto C_{fsc} is trivial and has been given in Chapter 1. The computation of the projection operator P_{fi} is a little more involved and is discussed in the next subsection. To show strong convergence of our iterative procedure it is enough if we show that C_{fsc} is precompact. This is discussed in Section 3.3.2. Later we shall also see how the computation involved at every iteration can be speeded up in a multiprocessor system by applying the operators in parallel rather than in sequence. We can show that the solution set is the same whether the operators are applied in parallel or in sequence.

3.3.1 Computation of Projection Operator

Given $f_o(x,y)$ known at the set of points I_p and a function $g(x,y)$ it is required to compute $g_p(x,y)$ as a solution of

$$\text{Min } \|g(x,y) - g_o(x,y)\| \tag{3.11}$$

such that

$$g_o(x,y) * h(x,y) = f(x,y), \qquad \text{for } (x,y)\in I_p. \tag{3.12}$$

Since $\|.\|$ is always positive, minimising it is same as minimising its squared value. Hence consider

$$\iint_{-\infty}^{\infty} |g(x,y) - g_p(x,y)|^2 \, dx\, dy \tag{3.13}$$

By Parseval's relation, the above expression can be written as

$$1/(2\pi) \iint_{-\infty}^{\infty} |G(u,v) - G_p(u,v)|^2 \, du\, dv \tag{3.14}$$

where $G(u,v)$ and $G_p(u,v)$ represent the Fourier transforms of

$g(x,y)$ and $g_p(x,y)$ respectively. Let $F(u,v)$ denote the Fourier transform of $f(x,y) = g(x,y)*h(x,y)$ and $F_p(u,v)$ the Fourier transform of $f_p(x,y) = g_p(x,y)*h(x,y)$. Now

$$G(u,v)=F(u,v)/H(u,v), \qquad \text{for } (u,v)\in B_w \tag{3.15}$$

and

$$G_p(u,v)=F_p(u,v)/H(u,v), \qquad \text{for } (u,v)\in B_w \tag{3.16}$$

where $B_w = \{(u,v): u^2+v^2 \leq 1/\lambda^2\}$.

Hence (3.14) may be written as

$$1/(2\pi)\iint_{B_w}|G(u,v)-G_p(u,v)|^2\, dudv + 1/(2\pi)\iint_{\bar{B}_w}|G(u,v)-G_p(u,v)|^2\, dudv$$

$$= 1/(2\pi)\iint_{B_w}|F(u,v)/H(u,v) - F_p(u,v)/H(u,v)|^2\, du\, dv \;+$$

$$1/(2\pi)\iint_{\bar{B}_w}|G(u,v) - G_p(u,v)|^2\, du\, dv \tag{3.17}$$

To minimise the second term we let

$$G_p(u,v) = G(u,v), \qquad \text{for } (u,v)\in\bar{B}_w \tag{3.18}$$

Thus we are left with

$$1/(2\pi) \iint_{B_w} |F(u,v)/H(u,v) - F_p(u,v)/H(u,v)|^2\, du\, dv$$

Since $|H(u,v)| = 1$, the above expression can be written as

$$1/(2\pi) \iint_{B_w} |F(u,v) - F_p(u,v)|^2\, du\, dv$$

Again, using Parseval's theorem the expression can be wriiten as

$$\iint_{-\infty}^{\infty} |f(x,y) - f_p(x,y)|^2\, dx\, dy$$

Since f and f_p are bandlimited functions, the expression can be reduced to the following form :

$$\sum_{i=-\infty}^{\infty}\sum_{j=-\infty}^{\infty} |f(i\Delta x,j\Delta y) - f_p(i\Delta x,j\Delta y)|^2$$

Now by the statement of the problem,

$$f_p(i\Delta x,j\Delta y) = f_o(i\Delta x,j\Delta y), \qquad \text{for } (i,j)\in I_p. \tag{3.19}$$

Hence to minimise the expression we let

$$f_p(i\Delta x,j\Delta y) = f(i\Delta x,jay), \qquad \text{for } (i,j)\notin I_p \tag{3.20}$$

Notice that $F(u,v)$ can be computed from $f(x,y)$ and hence $G_p(u,v)$ can be computed using (3.16) and (3.18). Thus $g_p(x,y)$ can be computed from' $G_p(u,v)$.

3.3.2 *Compactness of* C_{fsc}

The set C_{fsc} first mentioned in Chapter 2 is defined formally, for the one dimensional case. Then we shall go on to show that C_{fsc} is precompact. This result will then be extented to two dimensions. We shall begin with the definition of a compact set.

Definition [63]: A set C is said to be compact if every sequence in C contains a subsequence that converges to a limit in C. A set is said to be relatively compact if its closure is compact and is known as a precompact set if any bounded subset of it is compact.

Note that boundedness is a necessary condition for compactness and is sufficient for any finite dimensional space. For example $L^2(s)$ space is not a finite dimensional space and hence boundedness is not a sufficient condition for compactness. Here S is the entire real line. The following result which is a restricted form of the Frechet-Kolmogrov theorem [63] states the necessary and sufficient conditions for $B \subset L^2(S)$ to be precompact.

Theorem 3.1 [63]: A set $B \subset L^2(S)$ is precompact if $\sup_B \|x\| < \infty$ and, for every $x \in B$,

$$\lim_{t \to 0} \|x(t+s) - x(s)\| = 0 \qquad \text{uniformly,}$$

and $\lim_{a\to\infty} \int_{|s|>a} |x(s)|^2 \, ds = 0$ uniformly.

In order to show compactness of C_{fsc}, let us first define the set. Let K be a compact subset of S and K_1, K_2, ... K_n be collection of pairwise disjoint relatively compact subsets whose union is K and each of whose Lebesgue measure [69] is nonzero. C_{fsc} is defined as the set of all functions x(s), continuous in each K_i, i = 1,...n, and zero elsewhere.

To show that C_{fsc} is precompact we can apply Theorem 3.1. Consider any bounded $x(s)\in C_{fsc}$. The first criterion of the above theorem holds, since x(s) is, by definition, bounded. The second criterion can be shown as follows.

$$\lim_{t\to 0} \int_{S} |x(t+s)-x(s)|^2 \, ds = \lim_{t\to 0} \sum_{i=1}^{n} \int_{K_i} |x(t+s)-x(t)|^2 \, ds \quad (3.21)$$

Since in K°_i, the interior of K_i, x(s) is continuous

$$\lim_{t\to 0} \sum_{i=1}^{n} \int_{K^\circ_i} |x(t+s)-x(t)|^2 ds = 0 \quad (3.22)$$

Hence (3.21) may be written as

$$\lim_{t\to 0} \int_{S} |x(t+s)-x(s)|^2 \, ds = \lim_{t\to 0} \sum_{i=1}^{n} \int_{K_i-K^\circ i} |x(t+s)-x(t)|^2 ds \quad (3.23)$$

Now as the measure of the set $K_i-K^\circ_i$ is zero and x(t+s)-x(t) is bounded the last expression tends to zero. Thus the second condition is fulfilled. The third condition of Theorem 3.1 holds by definition of C_{fsc}.

Thus in the one dimensional case C_{fsc} is precompact. It is easy to see that all the results from Theorem 3.1 can be extended to any finite dimensional field.

3.3.3 *Convex Combination of Nonexpansive Operators*

In this section we wish to show that a convex combination of nonexpansive operators is nonexpansive. This result is useful to develop distributed algorithms for a multiprocessor environment. Earlier we saw that sparse data of the hologram $f(x,y;\lambda_i)$ known on a set I_p for a wavelength λ_i defines a convex set C_i of functions $g(x,y)$ that could have given rise to the known data. Hence if we have the data for n frequencies then it is possible to compute a $g(x,y)$ belonging to each C_i by the method of POCS. Here the operators P_{fi} are applied in succession. In a multiprocessor environment it would be advantageous if all operators P_{fi} (or T_{fi}) are applied in parallel and the results combined in a suitable fashion so that the desired solution is obtained. This, we show, can be done by a convex combination of the result of each of these operators. We begin with some definitions.

Definition [18]: T is a nonexpansive operator if

$$\|Tx - Ty\| \le k\,\|x - y\|, \tag{3.24}$$

where k is a real positive number such that 1 T is a contraction mapping if $k < 1$.

Definition: x is said to be a fixed point of an operator T if $T(x)=x$.

Theorem 3.2: Let $T_1, T_2, \ldots T_n$ be a collection of nonexpansive operators from $C \to C$, where C is a closed convex set in a Hilbert space H. Let,

$$T = a_1T_1 + a_2T_2 \ldots + a_nT_n \tag{3.25}$$

where $a_1+a_2 \ldots +a_n = 1$ and $a_1, a_2 \ldots a_n$ are all greater than zero. T is a nonexpansive operator from $C \to C$. Furthermore if T_i for some i, $1 \le i \le n$, is a contraction mapping, then so is T.

Proof:

$$\|Tx-Ty\| = \|a_1T_1x +\ldots+ a_nT_nx - (a_1T_1y +\ldots+ a_nT_ny)\| \quad (3.26)$$

$$\leq a_1\|T_1x-T_1y\| +\ldots+ a_n\|T_nx-T_ny\| \quad (3.27)$$

$$\leq a_1\|x-y\| +\ldots+ a_n\|x-y\| \quad (3.28)$$

$$\leq \|x-y\| \quad (3.29)$$

If T_i is a contraction mapping, then (3.28) becomes a strict inequality and the second part of the result follows.

(End *of proof)*

3.3.4 Nature of the Solution

Let us consider the nature of the solutions provided by the two operators $P_{fsc}T_1T_2\ldots T_n$ and $P_{fsc}(a_1T_1+a_2T_2+\ldots+a_nT_n)$, where $a_1, a_2, \ldots, a_n$ denote a set of real numbers satisfying the constraints specified in Theorem 3.2. The two operators may not necessarily have the same fixed points. However if the set C'_n is nonempty, then we can show that the set of fixed points of the two operators is identical and is precisely the set C'_n. It has been shown earlier that the set of fixed points of the operator $P_{fsc}T_1T_2\ldots T_n$ is the set C'_n. Our aim is to show that the set of fixed points of $P_{fsc}(a_1T_1+a_2T_2+\ldots+a_nT_n)$ is also C'_n. It is obvious that C'_n is a subset of the fixed points of $P_{fsc}(a_1T_1+a_2T_2+\ldots+a_nT_n)$ since every $g\in C'_n$ is also a fixed point of $P_{fsc}(a_1T_1+a_2T_2+\ldots+a_nT_n)$. The containment in the other direction can be shown as follows: Let g_1 be fixed point of $P_{fsc}(a_1T_1+a_2T_2+\ldots+a_nT_n)$ and $g_2\in C'_n$. Consider $\|g_2-g_1\|$. Since g_2 is also a fixed point of $P_{fsc}(a_1T_1+a_2T_2+\ldots+a_nT_n)$,

$$\|g_2-g_1\| \quad \|P_{fsc}(a_1T_1+a_2T_2+\ldots+a_nT_n)g_2 - P_{fsc}(a_1T_1+a_2T_2+\ldots+a_nT_n)g_2\| \quad (3.30)$$

Again, since P_{fsc} is a linear operator the above equation can be written as

$$\|g_2-g_1\| = \|a_1(P_{fsc}T_1g_2-P_{fsc}T_2g_1)+\ldots+a_n(P_{fsc}T_ng_2-P_{fsc}T_ng_1)\| \tag{3.31}$$

$$\leq a_1\|(P_{fsc}T_1g_2-P_{fsc}T_1g_1)\|+\ldots+a_n\|(P_{fsc}T_ng_2-P_{fsc}T_ng_1)\| \tag{3.32}$$

$$\leq a_1\|g_2-g_1\| + \cdots + a_n\|g_2-g_1\| \tag{3.33}$$

$$= \|g_2-g_1\| \tag{3.34}$$

(3.31) follows from triangular inequality and (3.32) follows from the fact that $P_{fsc}T_i$ is a nonexpansive operator. Hence we derive

$$a_1\|(P_{fsc}T_1g_2-P_{fsc}T_1g_1)\|+ \ldots +a_n\|(P_{fsc}T_ng_2 - P_{fsc}T_ng_1)\|$$
$$= a_1\|g_2-g_1\|+ \ldots +a_n\|g_2-g_1\| \tag{3.35}$$

Now $P_{fsc}T_ig_2 = g_2$ for $1\leq i\leq n$, since $g_2\in C_n'$. Hence

$$a_1\|g_2-P_{fsc}T_1g_1\|+ \ldots + a_n\|g_2 - P_{fsc}T_ng_1\|$$
$$= a_1\|g_2-g_1\|+ \ldots +a_n\|g_2-g_1\| \tag{3.36}$$

Since the above equation holds for any choice of $\{a_i\}$, we deduce that, for $i = 1, 2, \ldots, n$,

$$\|g_2-P_{fsc}T_ig_1\| = \|g_2-g_1\| \tag{3.37}$$

If $g_1\notin C_n'$, then $\|g_2-P_{fsc}T_ig_1\|<\|g_2-g_1\|$. Hence by contradiction $g_1\in C_n'$. Thus $g_1\in C_n'$. Since g_1 is an arbitrary fixed point of $P_{fsc}(a_1T_1+a_2T_2+\ldots +a_nT_n)$ it follows that every fixed point of $P_{fsc}(a_1T_1+a_2T_2+\ldots +a_nT_n)$ also belongs to C_n'. This implies that the fixed points of $P_{fsc}(a_1T_1+a_2T_2+\ldots+a_nT_n)$ are just the fixed points of $P_{fsc}T_1T_2\ldots T_n$. Notice however that this result does not hold if C_n' is empty.

3.3.5 Strong Convergence of POCS Method

Theorem 1.4 assures strong convergence if there exists at least one subsequence that converges strongly. Consider the operator $P_o P_1 P_2 \ldots P_n$, where P_1, P_2, $\ldots P_n$ are as discussed earlier and P_o is the projection onto a precompact convex set. Now the result of every iteration of the POCS method is bounded and belongs to a precompact set. By definition any bounded sequence in a precompact set has a convergent subsequence and hence the method of POCS assures strong convergence if the result of every iteration belongs to a precompact set.

We have shown earlier that C_{fsc} is compact and in all our iterative schemes we apply the operator P_{fsc} last. Hence strong convergence is guaranteed. However since we are dealing with a digital computer for all our computation we are forced to consider only finite dimensional spaces. In such a situation weak convergence implies the strong convergence.

3.4 Image Reconstruction from Multispectral Holograms

3.4.1 *Termination of the Iterative Procedure*

The termination of an iterative procedure in a practical implementation can be done in several ways. The simplest way is to decide the number of iterations a priori. This is not advisable in most cases as the number of iterations required for an acceptible solution may vary with the initial data. One method often used in numerical analysis is to stop when the result of two successive iterations does not change much. In other words let x_k be the result of the k-th iteration. The iterations stop when $e_k = \|x_k - x_{k-1}\| < \epsilon$, where ϵ is some predetermined value. It is advisable to normailse e_k by dividing it by $\|x_k\|$, provided $\|x_k\|$ does not tend to zero.

For inverse problems such as signal reconstruction it is required to compute $f=Tg$. An iterative procedure like POCS may not compute an exact solution in a finite number of iterations. Hence it is necessary to decide a priori the level of accuracy of the solution. The accuracy of the solution is measured as the normalised mean square error between the computed solution and the known data. More formally the error at the k-th iteration is given by

$$e_k = \Big(\sum_{x,y \in I_p} |f(x,y) - h(x,y) * g_k(x,y)|^2 \Big) / \sum_{x,y \in I_p} |f(x,y)|^2 \qquad (3.38)$$

In the simulation studies to follow the iterative procedure was terminated when e_k attained a value of 0.05 or less.

3.4.2 Sparse Data

To show the need for multispectral holograms in a practical situation we shall first conduct studies for sparse number of samples. The simulation setup is as mentioned in the previous chapter. The object field distribution used for the studies is shown in Fig.2.1. The distance between object and sensor planes is 2000.0 units. The distance between adjacent samples along both axes is 0.5 units. We shall consider four sampling rates namely when the hologram is available on (a) 64x64 points, (b) 32x32 points,' (c) 16x16 points and (d) 8x8 points. For each of these cases it is possible to configure the samples in different ways. We consider (a) offset data, (b) down sampling, (c) extrapolation and (d) random sampling. These terms will be defined shortly.

Let the 128x128 square mesh of equally spaced sampling points be indexed as i,j = -64, -63, ..., 63. We shall consider the down sampled case first. When there are 64x64 elements in the array the sampling points are indexed as i,j = -64, -62, ..., 62 (in steps of two). The result of the iterative reconstruction procedure is shown in Fig.3.1(a). We shall now consider the case when only 32x32 samples are known. The values the indices take are i,j = -62, -58, ..., 62 (in steps of four). The result of applying the iterative procedure is show in Fig.3.1(b). For 16x16 samples the elements of I_p take indices i,j = -60,- 52,...60, (in steps of eight). The result of applying the iterative procedure is shown in Fig.3.1(c). When there are 8x8 samples the values the indices take are i,j= -56,-40, ...,56. The result of the iterative procedure is shown in Fig.3.1(d).

We shall consider offset data next. By offset data for 64x64 samples we refer to a collection of samples wherein the indices are given as i,j = -64,-63, ..., -1. This then constitutes the set I_p of sampling points. Using these sampling points and applying the POCS procedure as described earlier the reconstructed image is shown in Fig.3.1(e).[1] For 32x32 the elements of I_p take indices i,j = -32,-31,...,-1. The results of the iterative reconstruction procedure is shown in Fig.3.1(f). When there are just 16x16 samples the indices are i,j = -16, -15, ..., -1. The result of the iterative reconstruction procedure is given in Fig.3.1(g). For 8x8 array, the values the

....

1. See Algorithm 3.1 for the pseudo code of image reconstruction from digital hologram using finite support constraint.

indices take are $i,j = -8, -7, ..., -1$. The result of the reconstruction is shown in Fig.3.1(h)

By extrapolation with 64x64 samples we mean that the indices of the elements of the set I_p are chosen as, $i,j = -32, -31, ... 31$. The result of applying the POCS procedure in this case is shown in Fig.3.1(i). We now consider extrapolation with 32x32 samples. Here the elements of I_p take indices $i,j = -16, -15, ..., 15$. If there are just 16x16 samples the elements of I_p take indices $i,j= -8,-7,...,7$. When there are just 8x8 elements the values the indices take are $i,j=-4,-3,...,3$. Fig.3.1(j), Fig.3.1(k) and Fig.3.1(l) show the result of applying the iterative procedure for 32x32, 16x16 and 8x8 samples respectively.

Finally let us consider random sampling. In Fig.3.1(m) is shown the result of using 4096 randomly chosen samples in the image reconstruction procedure. In Fig.3.1(n) is shown the image obtained by using 1024 randomly chosen samples. In Fig.3.1(o) the result shown is obtained by using 256 samples. And in Fig.3.1(p) the result shown is obtained by using 64 samples.

The results of these experiments show that, as the number of samples is reduced the reconstructed images are very poor in quality. Moreover when the data is sparse, down sampling and random sampling appear to be more promising. Notice also that although offset data is just another form of extrapolation, the result of using offset data is better than that of "extrapolation". These tentative conclusions will be seen to hold for multispectral hologram data as well. In the next section we shall show that by collecting data at multiple frequencies it is possible to reconstruct a good quality image even if the number of sampling points is a mere 16x16.

3.4.3 Simulation Studies for Multispectral Hologram

There are two ways of combining data from multiple holograms. The first method is to apply the operators in sequence and the second is to apply them in parallel and obtain a convex combination of the results. The second approach is useful only in a multiprocessor system and hence all our studies are based on the sequential approach.[2] Moreover notice that if the convex sets intersect the set of fixed points in both cases are the same.

As mentioned earlier, it is likely that as the number of frequencies increases, the computed solution will be closer to the desired solution. Here we conduct simulation studies to show the effectiveness of the proposed method to combine data from multispectral holograms. First we shall present the results using 64x64 sampling points for offset data, down sampling, extrapolation and random sampling, using two, four, eight and sixteen wavelengths. The next study will be on an array of 32x32 elements. Following that we shall present the results obtained using a 16x16 array of elements. Finally we shall consider a 8x8 array. The terms offset data, down sampling, extrapolation and

....

2. See Algorithm 3.2 for the pseudo code of the sequential image reconstruction procedure from multispectral digital holograms and Algorithm 3.3 for the pseudo code of the parallel image reconstruction procedure from multispectral digital holograms

random sampling have been defined earlier. The wavelengths used are 0.25 and 0.26 units when two wavelengths are used. When four frequencies are used the wavelengths are 0.25, 0.26, 0.27 and 0.28 units. When eight frequencies are used the wavelengths in addition to the four mentioned are 0.29, 0.30, 0.31, and 0.32. When sixteen frequencies are used the wavelengths chosen are 0.25, 0.255, ..., 0.325. Fig.3.2 to Fig.3.5 show the results of using multiple frequencies on a 64x64, 32x32, 16x16 and 8x8 array respectively.

A few remarks regarding the results are in order here. Notice first that as for the single frequency case the results of down sampling and random sampling are indeed better than those for offset data and extrapolation. If we consider hologram formation as some sort of a Fourier transform, then, in down sampling or random sampling the distribution of the samples is spread evenly over the entire frequency range. In extrapolation there is little sampling on the high frequency region. In offset data the sampling is spread over all frequencies but in a narrow region. Hence offset data yields results in between down sampling and extrapolation.

Another interesting feature of Fig.3.2 is that as the number of frequencies is increased from four to sixteen in the down sampled or randomly sampled case the quality of the reconstructed image does not show significant improvement. In a subsequent chapter we shall see that if the data is noisy there is a significant improvement as the number of frequencies is increased from four to eight for a 64x64 array.

3.5 Tradeoff between Computational and Receiver Complexity

In this chapter we saw that if all the data is available then there exists a unique solution for the problem of computing $g(x,y)$ given $f(x,y)$ and $h(x,y)$. We have seen that if the samples are sparse the quality of the reconstructed image is poor and degrades as the number of samples reduces. One method of increasing the amount of data for the same sampling array is by obtaining holograms for different wavelengths. Multispectral holograms, as we call them, can be used in an iterative algorithm for improving the quality of the reconstructed image. We proved the convergence of the iterative procedure used for image reconstruction. We also saw that there are two ways of combining the data namely the sequential and parallel method and showed that the two methods have essentially the same solution. Simulation studies were conducted for image reconstruction from multispectral holograms using the sequential method. The results show that by using multiple frequencies an intelligible 64x64 image can be reconstructed using just 8x8 sensors. However there is a tradeoff in that the number of frequencies for which the data is collected must be increased. Also the amount of computation required for an acceptible solution increases as the number of holograms is increased. Rather than using a large array, we could use a small array and increase the number of frequencies. Every increase in the size of the array increases the circuit complexity almost exponentialy as it is necessary to synchronise each one of the sensors to a common synchronising element. Increasing the number of frequencies is not as complex as increasing the number of sensors.

Let us now discuss some of the limitations of the proposed procedure. An implicit assumption in our work is that $g(x,y)$, the field distribution on the object plane is independent of the wavelength. This is not strictly true although the variation is not much if the wavelengths are close. Actual field tests must be conducted to find out how much the dependency is. An interesting issue that we have not been able to address satisfactorily is the optimum interval between adjacent frequencies. Finally, notice that the method is applicable for noise free data or more precisely if C_n' is nonempty. The next two chapters address the problem when such a condition does not hold.

Initialise:

(1) $g(x,y)$ = constant, for (x,y) in region of support,

= 0, otherwise.

Repeat

(2) Compute $G(u,v)$ the Fourier transform of $g(x,y)$

(3) For all (u,v) do

If $u^2+v^2 \le 1/\lambda^2$ then

$F(u,v) = G(u,v)*\exp(jkz(1-(\lambda u)^2-(\lambda v)^2)^{1/2})$

else $F(u,v) = 0$

endif

(4) Compute $f'(x,y)$ the inverse Fourier transform of $F(u,v)$

(5) Replace $f'(x,y) = f(x,y)$ for $(x,y) \in I_p$

(6) Compute $F''(u,v)$ the Fourier transform of $f'(x,y)$

(7) For all (u,v) do

If $u^2+v^2 \le 1/\lambda^2$ then

$G'(u,v) = F(u,v)\exp(-jkz(1-(\lambda u)^2-(\lambda v)^2)^{1/2})$

else

$G'(u,v) = G(u,v)$

endif

(8) Compute $g'(x,y)$ the inverse Fourier transform of $G(u,v)$

(9) $g(x,y) = g'(x,y)$ for (x,y) in region of support

= 0 otherwise

until satisfactory solution obtained.

Algorithm 3.1: The POCS procedure to reconstruct an image with finite support from hologram data $f(x,y)$ known at a set of points $(x,y) \in I_p$

Initialise:

(1) $g_o(x,y)$ = constant, for (x,y) in region of support,

= 0, otherwise.

(2) k = l

Repeat

(3) For i = 1 to n, (* n denotes number of frequencies *)

do steps 4 to 6

(4) Compute $f_k(x,y;\lambda_i) = g_{k-1}(x,y)*h(x,y;\lambda_i)$

as in Algorithm 3.1 (Steps 2-5).

(5) Compute $g_k(x,y)$ from $f_k(x,y;\lambda_i)$

as in Algorithm 3.1 (Steps 6-9).

(6) k = k+l

until satisfactory solution obtained.

Algorithnz3.2: The sequential POCS procedure to reconstruct an image using multispectral hologram data $f(x,y;\lambda_i)$ known for n different frequencies.

Initialise:

(1) $g_o(x, y)$ = constant, for (x, y) in region of support,

= 0, otherwise.

(2) $k = 1$

Repeat

(3) For $i = 1$ to n, (* n denotes number of frequencies *)

do steps 4 to 7

(4) Compute $f_k(x,y;\lambda_i) = g_{k-1}(x,y)*h(x,y;\lambda_i)$

as in Algorithm 3.1 (Steps 2-5).

(5) Compute $g(x,y;i)$ from $f_k(x,y;\lambda_i)$

as in Algorithm 3.1 (Steps 6-9).

(6) $k = k+1$

(7) $g_k(x,y) = 0.9(a_1 g(x,y;1)+...+a_n g(x,y;n)) + 0.1 g_{k-1}(x,y)$

until satisfactory solution obtained.

Algorithm 3.3: The parallel POCS procedure to reconstruct an image using multispectral hologram data $f(x,y;\lambda_i)$ known for n different frequencies.

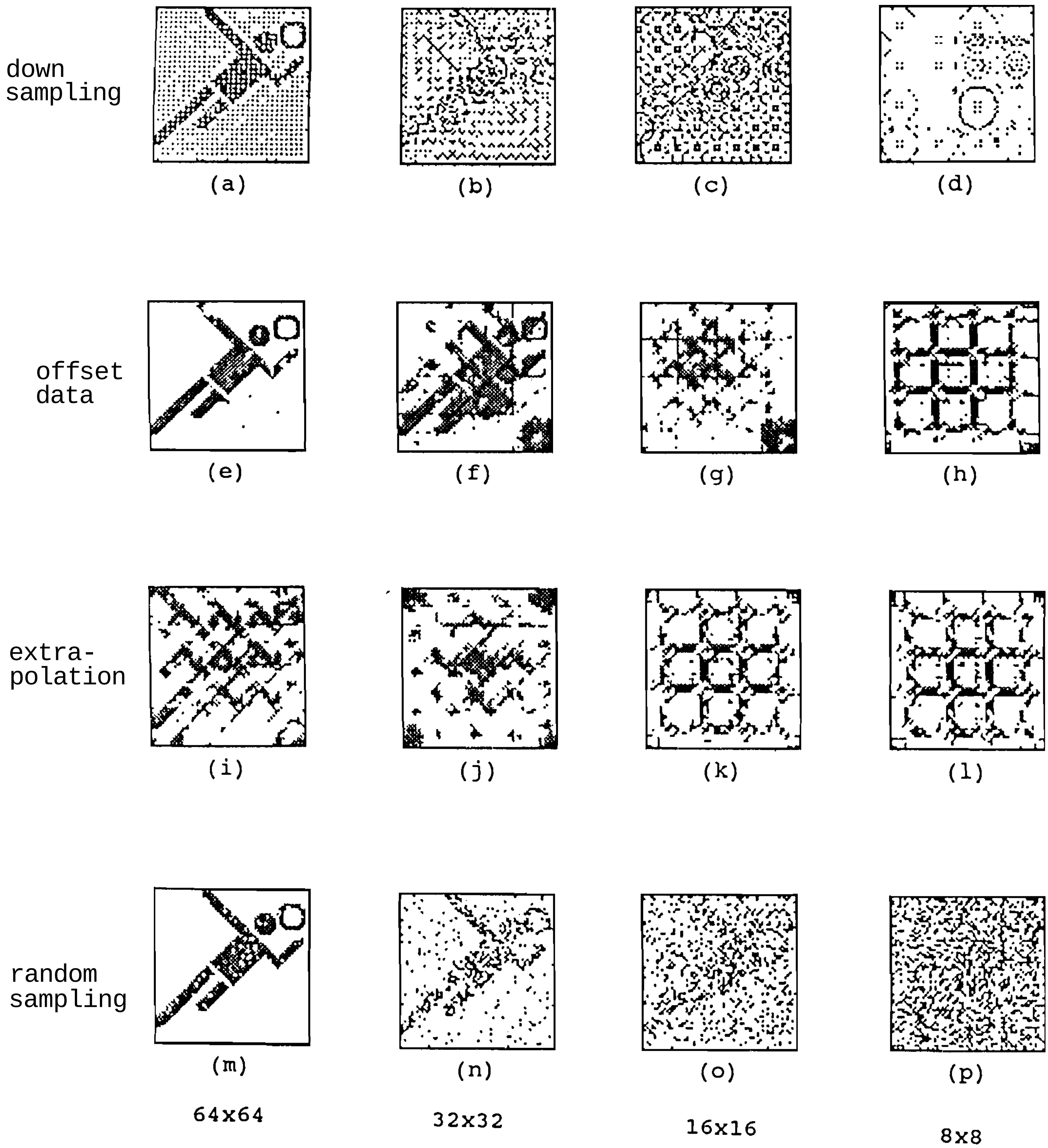

Fig.3.1 Effect of poor sampling of the received data on the reconstructed image. The complete received data consists of 128x128 samples. The figure shows the image reconstructed for four different types of sampling and for four sets of under sampled values. The unknown sample values are set to zero.

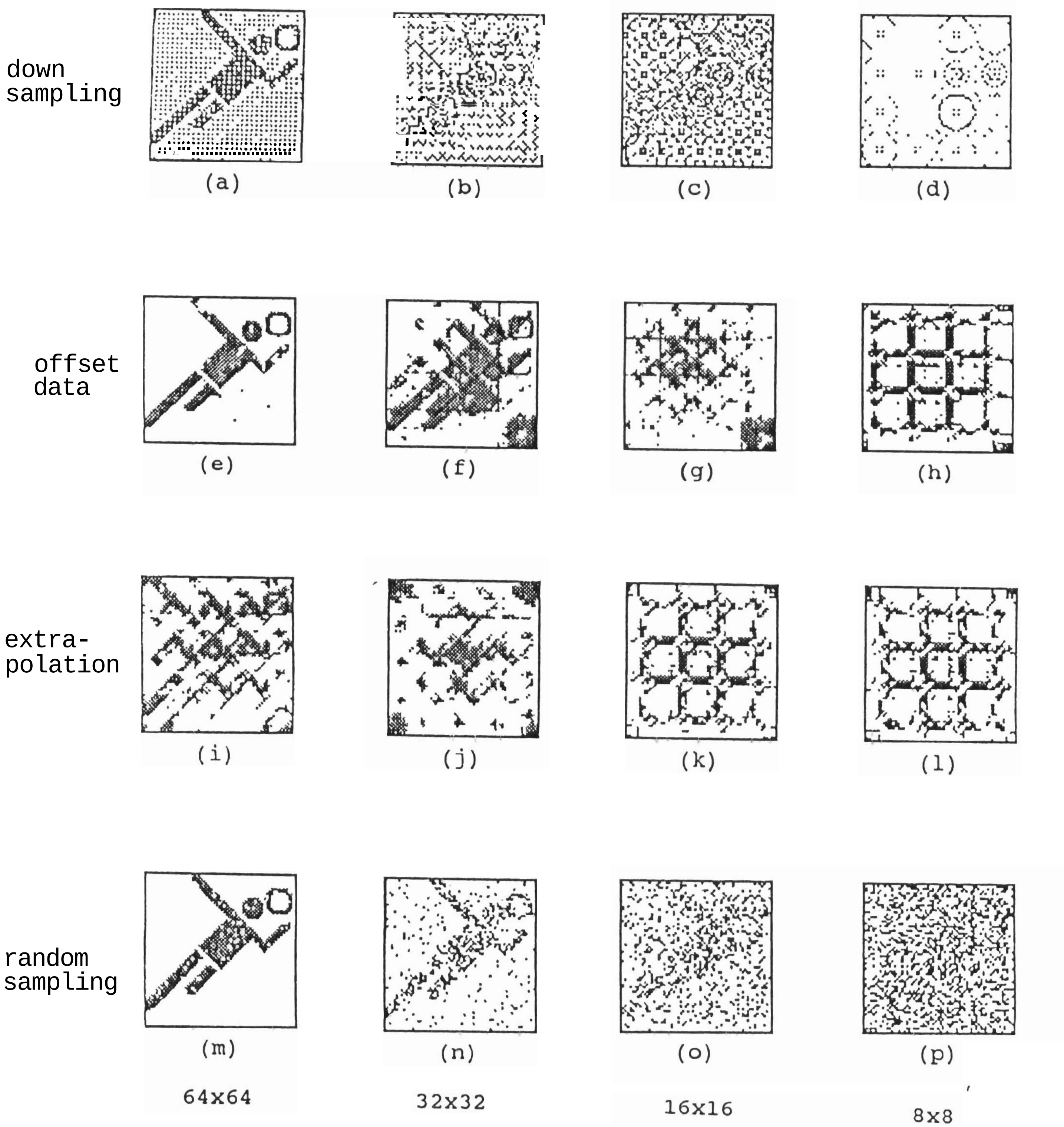

Fig.3.1 Effect of poor sampling of the received data on the reconstructed image. The complete received data consists of 128x128 samples. The figure shows the image reconstructed for four different types of sampling and for four sets of under sampled values. The unknown sample values are set to zero.

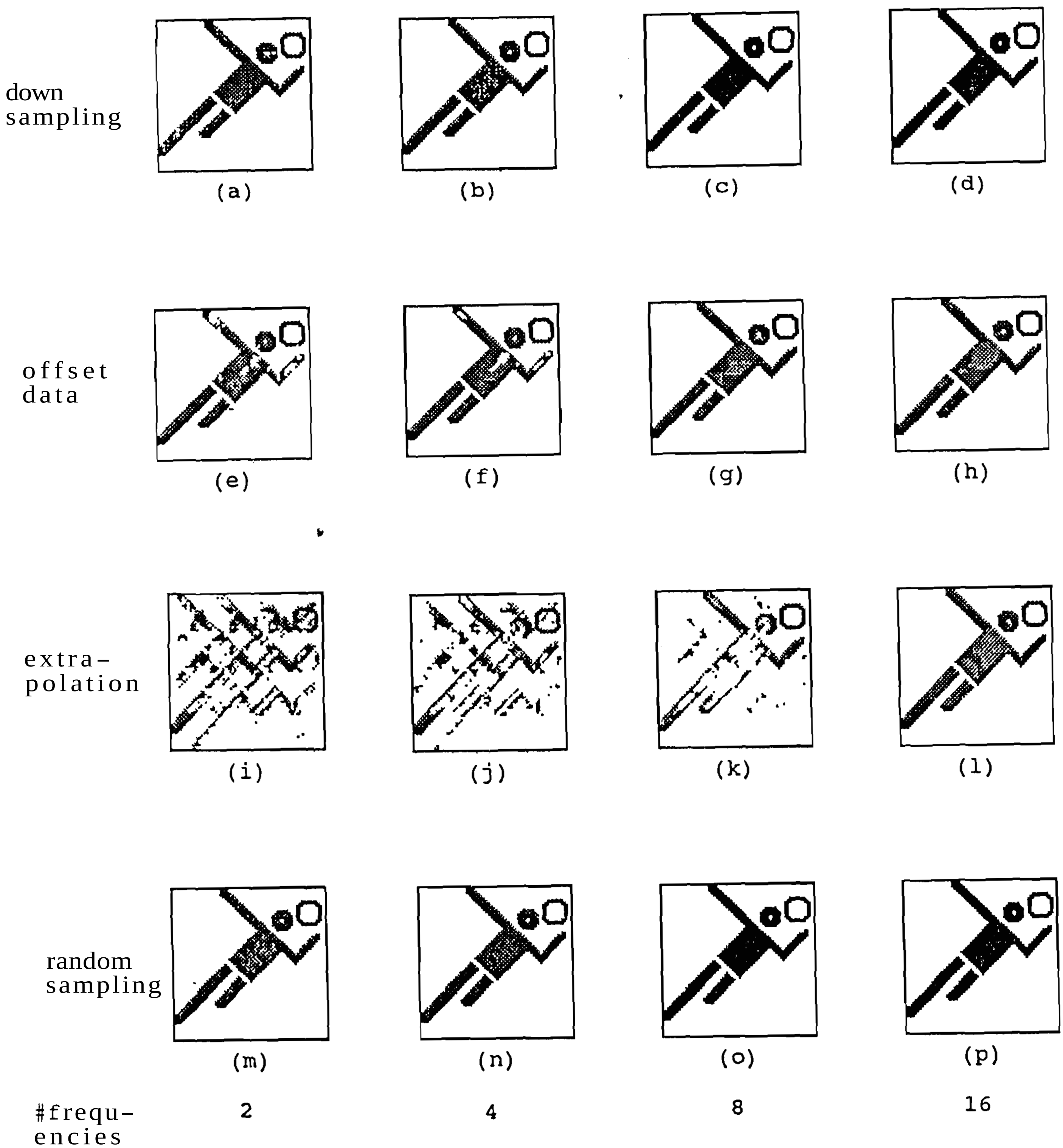

Fig.3.2 Effect of multiple frequency data on the image reconstructed from sparse receiver array. The data consists of 64x64 samples. The figure shows the image reconstructed for four types of sampling and four cases of multiple frequencies.

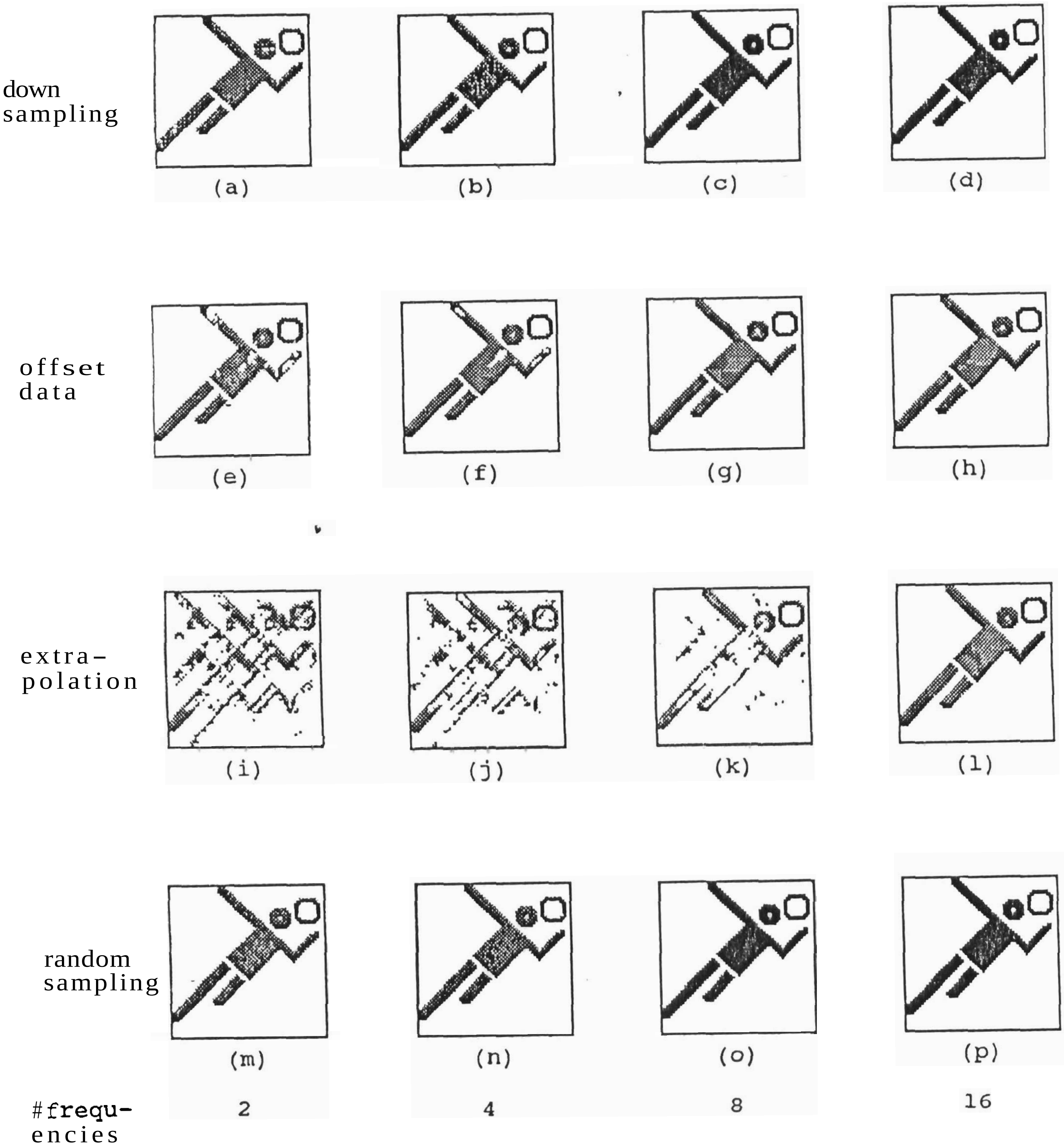

Fig.3.2 Effect of multiple frequency data on the image reconstructed from sparse receiver array. The data consists of **64x64** samples. The figure shows the image reconstructed for four types of sampling and four cases of multiple frequencies.

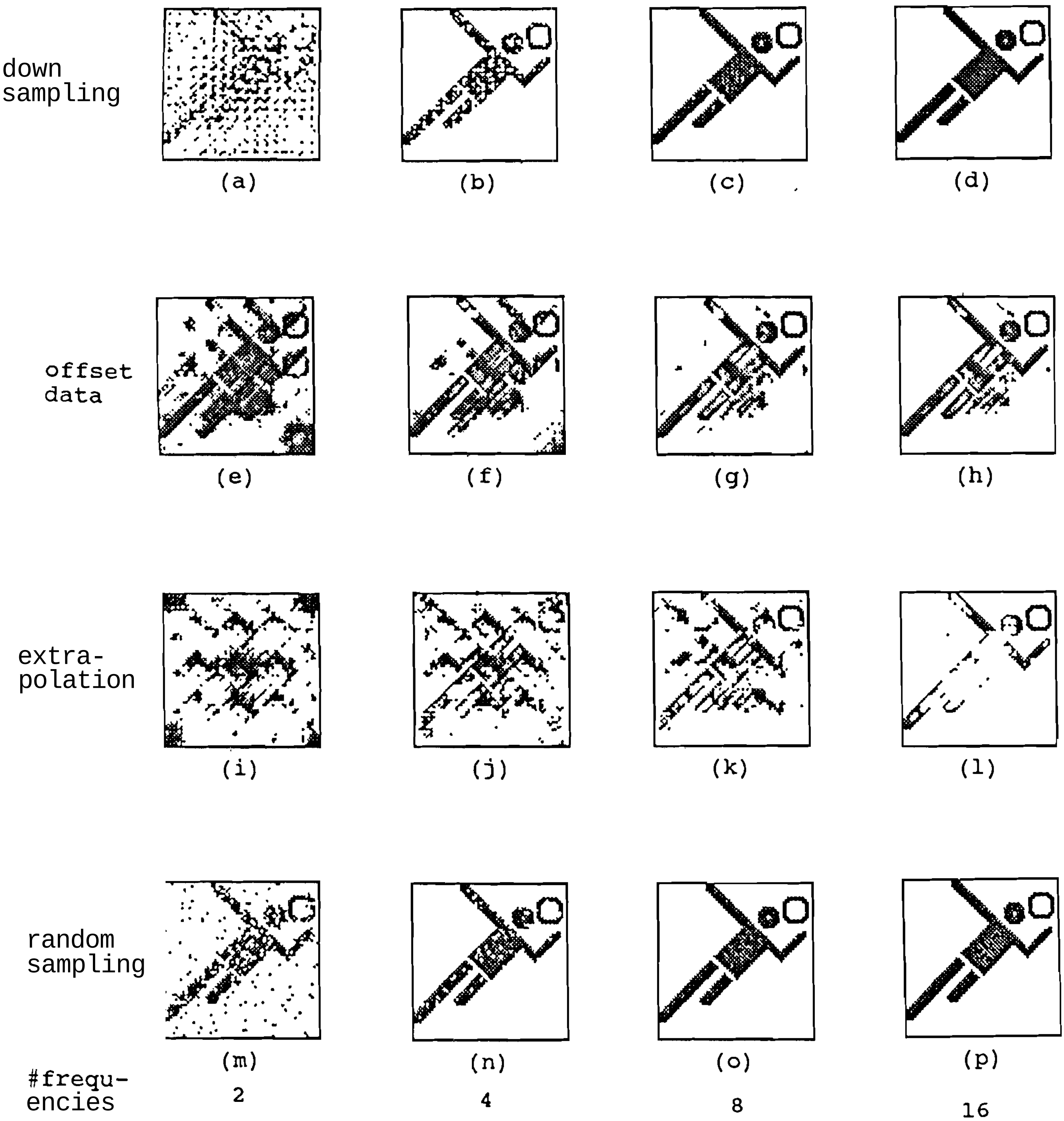

Fig.3.3 Effect of multiple frequency data on the image reconstructed from sparse receiver array. The data consists of 32x32 samples. The figure shows the image reconstructed for four types of sampling and four cases of multiple frequencies. The quality of the image reconstructed improves as the number of frequencies are increased.

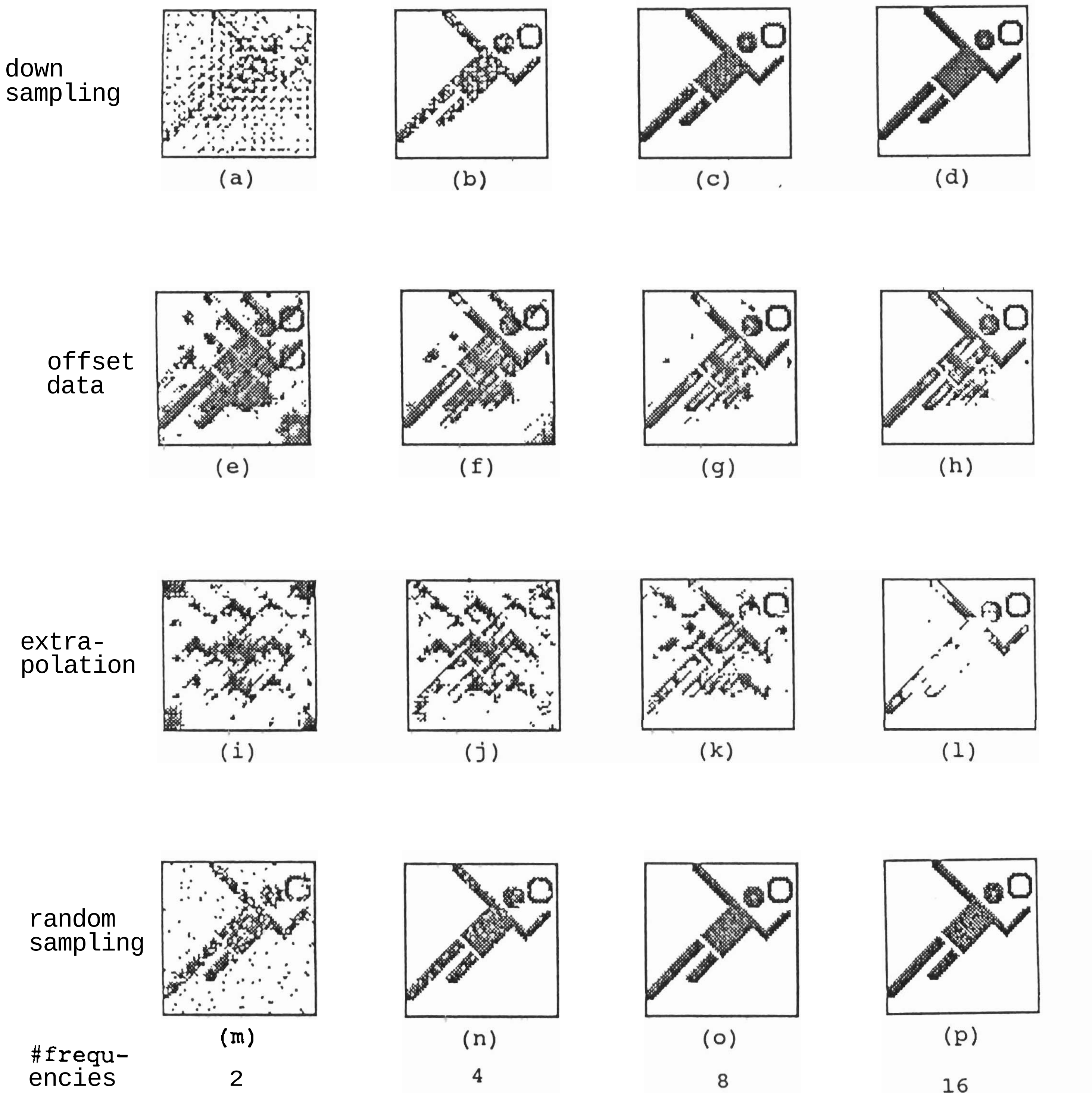

Fig.3.3 Effect of multiple frequency data on the image reconstructed from sparse receiver array. The data consists of 32x32 samples. The figure shows the image reconstructed for four types of sampling and four cases of multiple frequencies. The quality of the image reconstructed improves as the number of frequencies are increased.

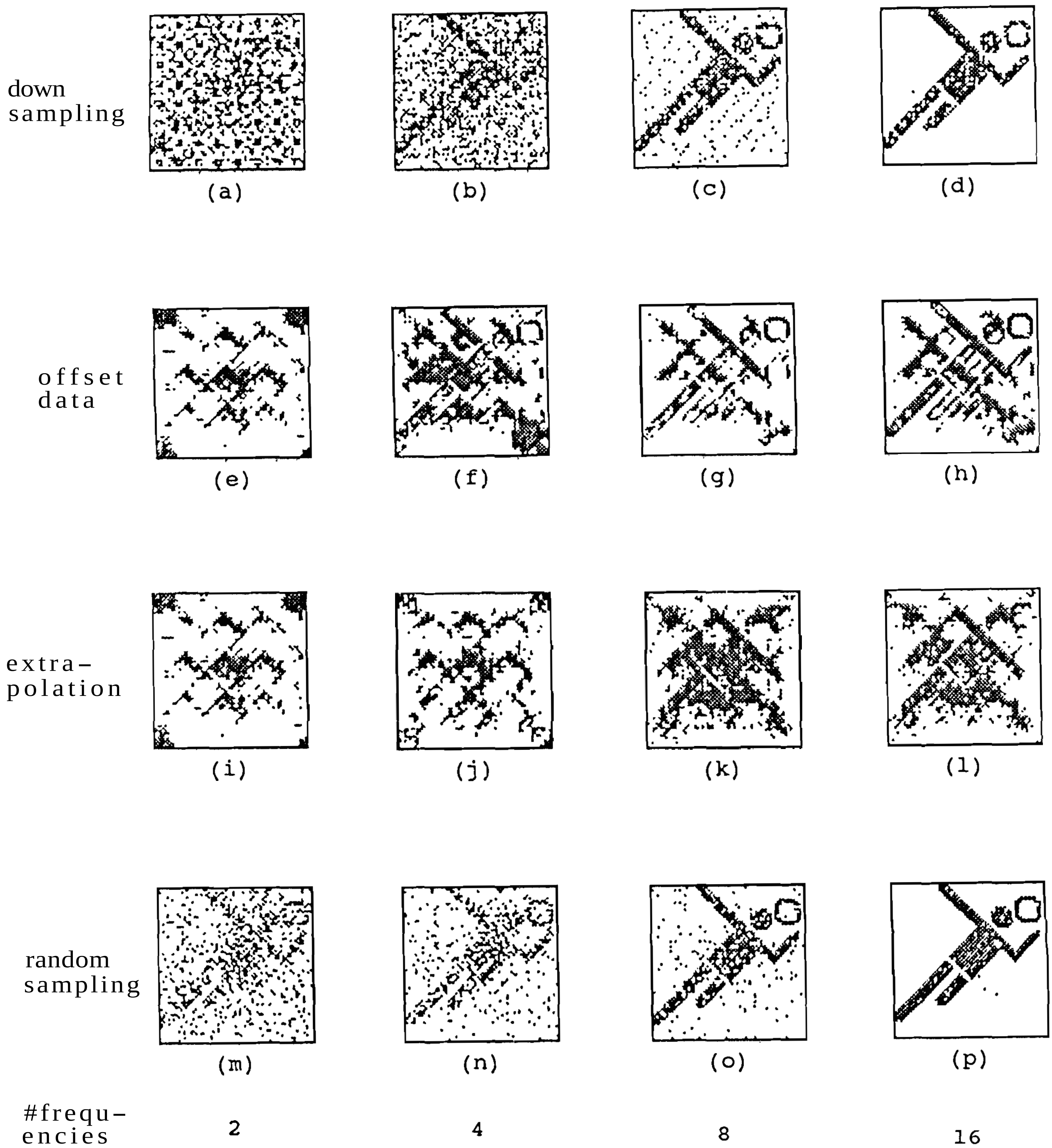

Fig.3.4 Effect of multiple frequency data on the image reconstructed from sparse receiver array. The data consists of **16x16** samples. The figure shows the image reconstructed for four types of sampling and four cases of multiple frequencies.

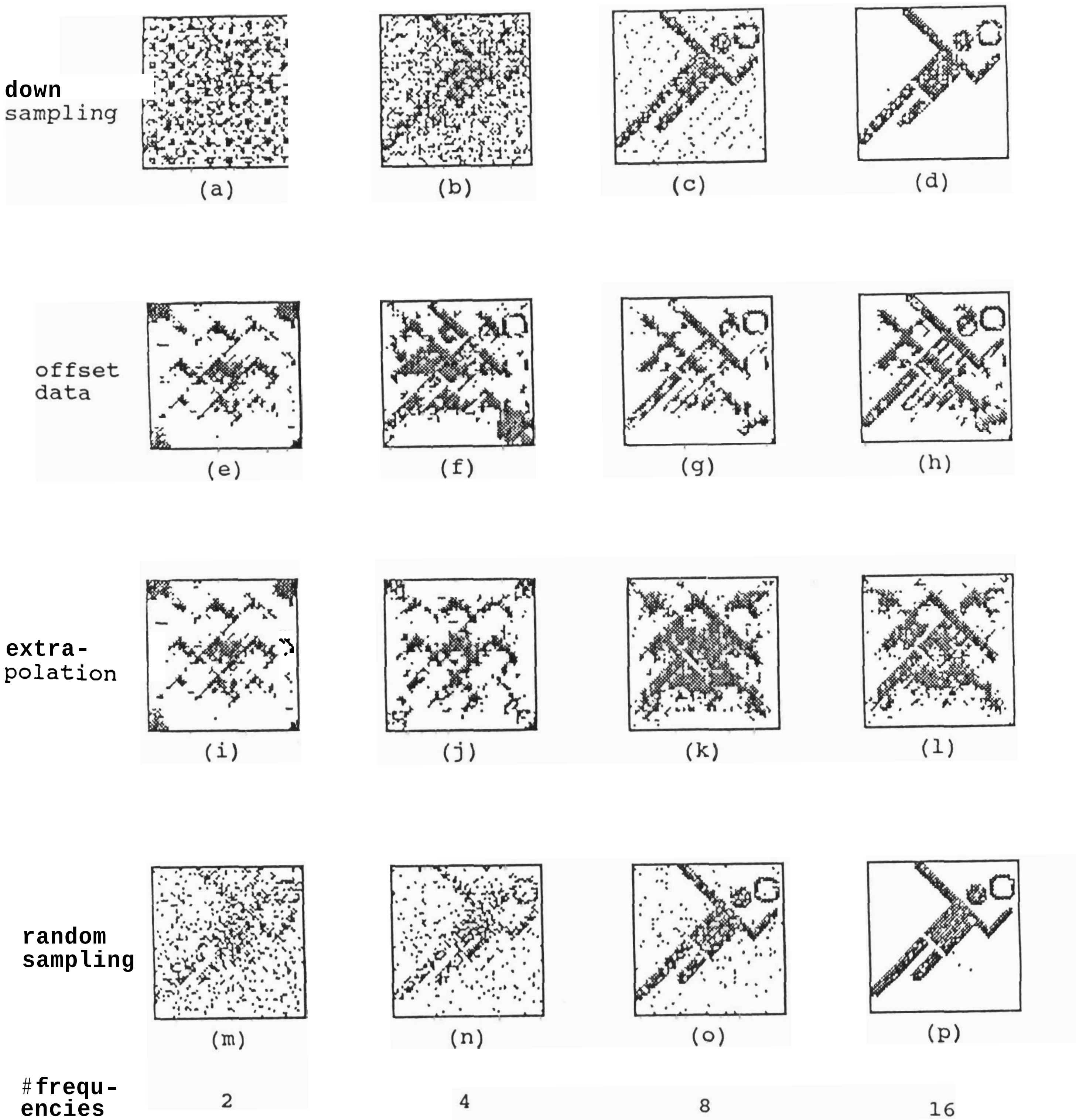

Fig.3.4 Effect of multiple frequency data on the image reconstructed from sparse receiver array. The data consists of 16x16 samples. The figure shows the image reconstructed for four types of sampling and four cases of multiple frequencies.

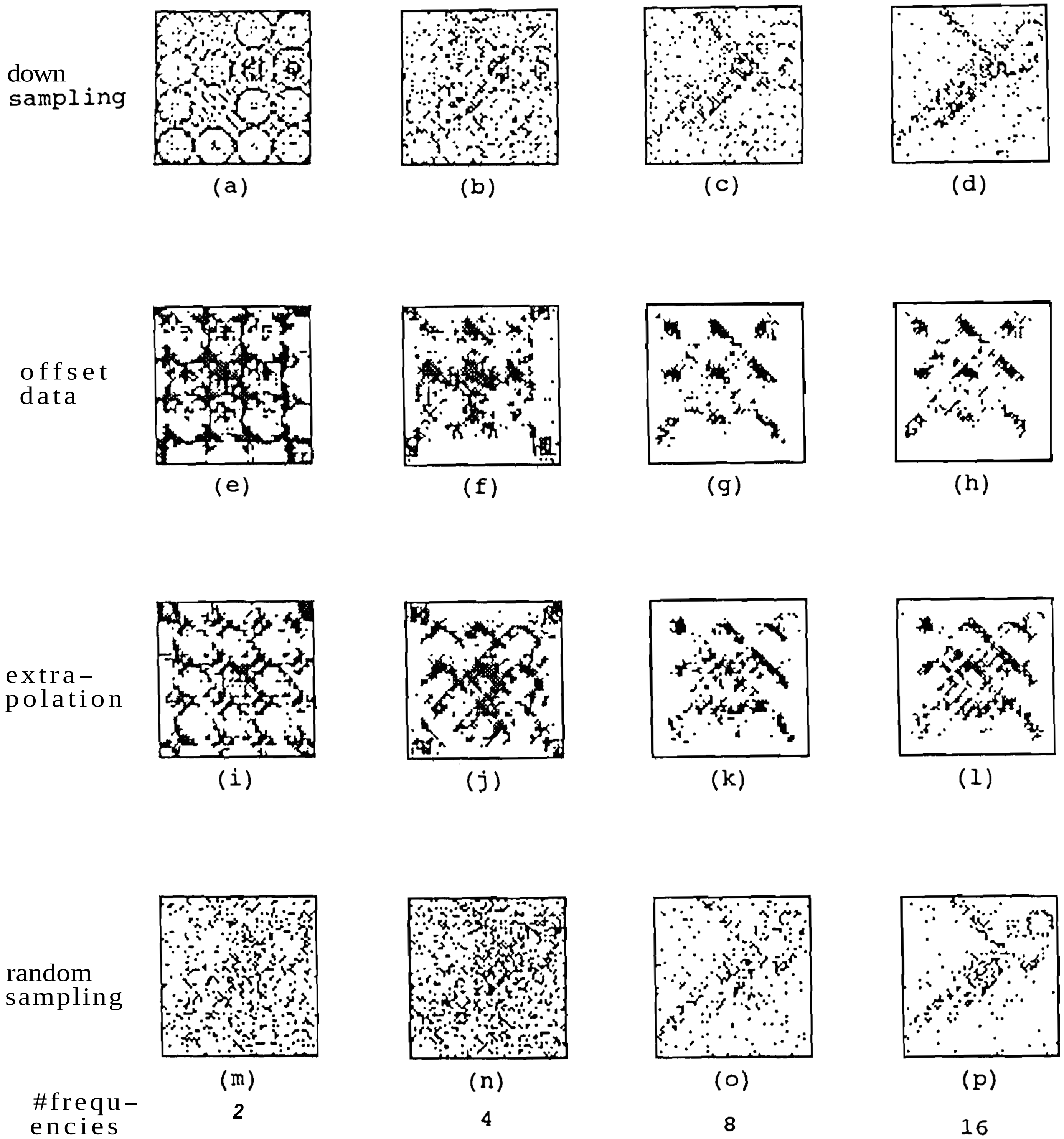

Fig.3.5 Effect of multiple frequency data on the image reconstructed from sparse receiver array. The data consists of 8x8 samples. The figure shows the image reconstructed for four types of sampling and four cases of multiple frequencies. The figure shows that even for very low sampling rate **it is** possible to get a good image provided the number of frequencies are large(16).

Chapter 4

IMAGING WITH NOISE

4.1 Ill-Posedness arising due to Absence of Solution

We saw in the previous chapter that collecting data at multiple frequencies helps in improving the quality of the reconstructed image. Application of the methods proposed earlier to noisy data is not straightforward since we have not proved convergence for such data. In this chapter we attempt to apply the method of POCS by altering the constraints of the problem. Unlike in the previous chapter, where we try to reconstruct an image that matches with the known data exactly, here we attempt to compute an image that matches with the known data to within a certain degree. The drawback of the method proposed here is that certain constants defining the degree of accuracy of the reconstructed signal must be known precisely a priori. In the next chapter we shall discuss a method that does not require the knowledge of these parameters. A comparative study of the results obtained by the methods proposed in this chapter and those proposed in the next are given in Chapter 5.

Imaging with noise is an ill-posed problem as there may exist no object field distribution with known constraints that could have given rise to the known initial data. The problem of noise in image reconstruction has been studied extensively [1],[9]. To reduce the effects of noise in the reconstructed signal one needs to have extra information regarding the signal and some characteristics of the noise. In Section 1.4 some methods of noise filtering were discussed. Most of the noise filtering methods were based on regularisation techniques, which attempt to compute an optimal solution of some sort using noise and signal statistics. These techniques are not applicable for the problem of image reconstruction from digital holograms as the only **information** available a **priori** is the extent of the object and not noise or signal statistics. Moreover the application of the regularization techniques for image reconstruction from digital holograms is not obvious.

Our approach in this chapter is to adapt the method of POCS described in Chapter 1 for the problem of image reconstruction in the presence of bounded noise in the digital holograms. The assumptions we make here are:

(a) the extent of the field of the object is compact and

(b) the noise is bounded.

Note that for noisy data the convex sets defined by the known data and C_{fsc} (the set of all signals with finite support) may have no common element. A graphical illustration of the effect of noise on the solution set is shown in Fig.4.1. The set of all signals satisfying the known data moves away from the set C_{fsc} if the data is noisy. Hence it is not possible to ignore the noise and apply the POCS method directly as for the noise free case since convergence is not assured when the intersection of the convex sets is empty. To force an intersection we may expand C'_{fo} by relaxing the constraint that the reconstructed signal matches the known data exactly. As shown in Fig.4.1, if the expansion is too small, intersection of the convex sets may still not be possible. If the expansion is too large then a wide variety of solutions are possible and hence an arbitrary solution from among the set of all possible solutions may not be satisfactory. Hence the bound on the separation between the reconstructed signal and the known data must be known precisely.

Formally, if $f(x,y)$ is the known data and R is a linear transformation operator, then our aim is to find $g(x,y)$ such that $\rho(f(x,y), Rg(x,y)) \leq b$. Here ρ is a distance measure and 'b' is a known constant. In general, it is in vain to compute $g(x,y)$ such that $\rho(f(x,y), Rg(x,y)) < b$, since, if we did, we will be computing a solution that is more accurate than the original data itself. In fact it has been argued elsewhere [60] that for 'best' results we must compute $g(x,y)$ such that $\rho(f(x,y), Rg(x,y)) = b$. If the set of all solutions $g(x,y)$ such that $\rho(f(x,y), Rg(x,y)) \leq b$, which is henceforth referred' to as the "feasible solution set", is convex, and if C_{fsc} and the feasible solution set have nonempty intersection, then the POCS method can be applied. A feasible solution set is convex if the distance measure satisfies the triangular inequality. We shall come across some distance measures that are not strictly metrics but which define convex feasible solution sets.

In the next section we shall describe some feasible solution sets for the Fredholm's equation of the first kind. These sets are shown to be closed and convex. The method of computing the projection operators for these sets are discussed. In Section 4.3 we show how these results can be applied to the problem of image reconstruction from digital holograms. In Section 4.4 we shall discuss the implications and limitations of the methods proposed here to the general problem of signal recovery.

4.3 Feasible Solutions for the Fredholm's Equation

The Fredholm's equation of the first kind is given by (see Equation (1.10))

$$f(y) = \int_a^b h(x,y)g(x)\, dx = Rg(x), \tag{4.1}$$

where $h(x,y)$ is a continuous function in both x and y, and $f(y)$ is defined in the interval $[c,d]$. Let R denote the Fredholm's operator. Note that for ease of notation we restrict our discussion to one dimensional signals. The results of our discussion are applicable in a straight forward way to all finite dimensional signals. It is required to define a distance measure ρ on the space of functions f(y) such that a feasible solution set defined by the measure has practical significance. Some of the common metrics that we shall use later are given below:

$$\rho_C(f_1,f_2) = \operatorname{Sup}|f_1(y) - f_2(y)| = \|f_1-f_2\|_C \tag{4.2}$$

$$\rho_{L1}(f_1,f_2) = \int|f_1(y) - f_2(y)|\, dy = \|f_1-f_2\|_{L1} \tag{4.3}$$

and

$$\rho_{L2}(f_1,f_2) = \left(\int|f_1(y)-f_2(y)|^2\, dy\right)^{1/2} = \|f_1-f_2\|_{L2}. \tag{4.4}$$

The following functional is not a metric although it can be used to define a closed convex feasible solution set,

$$\rho_\theta(f_1,f_2) = \sup_y \rho_\phi(\phi_1(y),\phi_2(y)), \tag{4.5}$$

where $\phi(y)$ may be defined by

$$f(y) = |f(y)|\exp(j(\phi(y))). \tag{4.6}$$

Note that $\phi(y)$ refers to the wrapped phase function of $f(y)$ and ρ_ϕ is the smallest positive difference between $\phi_1(y)$ and $\phi_2(y)$. More formally if $0 \le \phi_1(y),\ \phi_2(y) \le 2\pi$ then

$$\rho_\phi(\phi_1(y),\phi_2(y)) = \phi_1(y)-\phi_2(y), \quad \text{for } 0<\phi_1(y)-\phi_2(y)\leq\pi,$$
$$= \phi_2(y)-\phi_1(y), \quad \text{for } 0<\phi_2(y)-\phi_1(y)<\pi. \quad (4.7)$$

The feasible solution sets that are defined by the functionals just mentioned are given in Equations (4.8) - (4.11) below.

$$C_d = \{g(x): \rho_C(f,Rg) \leq d\}, \quad (4.8)$$

where $f(y)$ and d are given.

$$C_r = \{g(x): \rho_{L2}(f,Rg) \leq r\}, \quad (4.9)$$

where f(y) and r are given.

$$C_t = \{g(x): \rho_{L1}(f,Rg) \leq t\}, \quad (4.10)$$

where $f(y)$ and t are given.

$$C_\theta = \{g(x): \rho_\theta(f,Rg) \leq \theta\}, \quad (4.11)$$

where $f(y)$ and θ are given and $\theta<\pi/2$.

We claim the following:

Lemma 4.1: C_d, C_r, C_t and C_θ are closed convex sets.

Proof: In what follows we shall prove only the convexity of the sets mentioned. To prove their closure we make use of the fact that if $R:C_A\to C_B$ is a linear operator in a Hilbert Space and C_B is closed then C_A is also closed. This result which is a corollary to the open mapping theorem can be proved by contradiction as follows. Let C_A be not closed. There exists a $g\in\bar{C}_A$ such that every open set containing 'g' has at least one element belonging to C_A. This implies that $Rg\notin R(C_A) = C_B$ and every neighbourhood of $Rg \in R(\bar{C}_A)$ contains an $Rg_o \in R(C_A)$. Hence $R(\bar{C}_A)$ is not open, implying that $R(C_A)$ is not closed which is a contradiction. Let us now consider each of the sets individually.

(i) Let $g_1(x)$ and $g_2(x)$ belong to C_d. Hence

$$\rho_C(f,Rg_1) \leq d \quad (4.12)$$

and

$$\rho_C(f,Rg_2) \leq d. \tag{4.13}$$

Consider

$$g_3(x) = ag_1(x) + (1-a)\ g_2(x), \tag{4.14}$$

where $0<a<1$. To prove the convexity of C_d it is required to show that $\rho_C(f,Rg_3) \leq d$. Due to the linearity of R we can write

$$Rg_3 = aRg_1 + (1-a)Rg_2 \tag{4.15}$$

Hence

$$\rho_C(f,Rg_3) = \|a(f-Rg_1) + (1-a)(f-Rg_2)\|_C, \tag{4.16}$$

$$\leq a\|f-Rg_1\|_C + (1-a)\|f-Rg_2\|_C, \tag{4.17}$$

$$\leq ad + (1-a)d = d. \tag{4.18}$$

(4.17) follows from triangular inequality and (4.18) from the given assumptions of the Lemma. Notice that $R(C_d)$ is a closed ball in the C metric and is a closed set devoid of interior points in L^2 metric. In other words no open ball about any element of $R(C_d)$ is a proper subset of $R(C_d)$. From the reasoning given at the beginning of the proof C_d is also closed.

(ii) The convexity of C_r can be proved in a similar way. Let $g_1(x)$ and $g_2(x)$ belong to C_r. Hence

$$\rho_{L2}(f,Rg_1) \leq r \tag{4.19}$$

and

$$\rho_{L2}(f,Rg_2) \leq r. \tag{4.20}$$

Consider $g_3(x) = ag_1(x) + (1-a)g_2(x)$ where $0<a<1$. To prove the convexity of C_r it is required to show that $\rho_{L2}(f,Rg_3) \leq r$. Due to the linearity of R we can write

$$Rg_3 = aRg_1 + (1-a)Rg_2 \tag{4.21}$$

Hence

$$\rho_{L2}(f,Rg_3) = \|a(f-Rg_1) + (1-a)(f-Rg_2)\|_{L2}, \quad (4.22)$$

$$\leq a\|f-Rg_1\|_{L2} + (1-a)\|f-Rg_2\|_{L2}, \quad (4.23)$$

$$\leq ar + (1-a)r = r. \quad (4.24)$$

(4.23) follows from triangular inequality and (4.24) from the given assumptions of the Lemma. Notice that $R(C_r)$ is a closed ball in the L^2 metric.

(iii) Let $g_1(x)$ and $g_2(x)$ belong to C_t. Consider $g_3(x) = ag_1(x) + (1-a)g_2(x)$ where $0<a<1$. To prove the convexity of C_t it is required to show that $\rho_t(f,Rg_3) \leq t$. Due to the linearity of R we can write

$$Rg_3 = aRg_1 + (1-a)Rg_2 \quad (4.25)$$

Hence

$$\rho_t(f,Rg_3) = \|a(f-Rg_1) + (1-a)(f-Rg_2)\|_{L1}, \quad (4.26)$$

$$\leq a\|f-Rg_1\|_{L1} + (1-a)\|f-Rg_2\|_{L1}, \quad (4.27)$$

$$\leq at + (1-a)t = t. \quad (4.28)$$

(4.27) follows from triangular inequality and (4.28) from the given assumptions of the lemma. Notice that $R(C_t)$ is a closed ball in the L^1 metric. It is a closed set in L^2 metric.

(iv) To prove convexity of C_θ consider

$$g_3(x) = ag_1(x) + bg_2(x), \quad (4.29)$$

where $g_1(x)$ and $g_2(x)$ belong to C_θ and 'a' and 'b' are real positive numbers. Now

$$Rg_3 = aRg_1 + bRg_2. \quad (4.30)$$

In other words

$$|Rg_3|\exp(j\phi_3) = a|Rg_1|\exp(j\phi 1) + b|Rg_2|\exp(j\phi 2). \quad (4.31)$$

Now

$$\rho_\phi(\phi_f,\phi_3) \leq \mathrm{Max}(\rho_\phi(\phi_f,\phi_1),\rho_\phi(\phi_f,\phi_2)), \tag{4.32}$$

$$\leq 8. \tag{4.33}$$

Thus $g_3 \in C_\theta$ and C_θ is a linear subspace. To show the closedness of C_θ notice that the set of all f' such that $\rho_\phi(\phi_f,\phi_{f'}) \leq \theta$ is a closed cone. Hence C_θ is also a closed convex cone.

(End of *Proof*)

4.3 Computation of the Projection Operator

We shall now see how the projection onto these sets are computed. Recall that the operation $R^{-1}Qg(x)$ is defined as follows:

$$g_o(x) = R^{-1}Qg(x), \tag{4.34}$$

if,

$$\|g_o(x) - g(x)\| = \underset{g'(x)}{\mathrm{Min}} \|g'(x) - g(x)\|, \tag{4.35}$$

and

$$Rg'(x) = Q_R Qg(x), \tag{4.36}$$

where Q_R is the projection onto the range of R. Notice that $g_o(x)$ is the projection of $g(x)$ onto the set

$$C_g = \{g'(x): Rg'(x) = Q_R Qg(x)\}. \tag{4.37}$$

The projection is unique if C_g is a closed convex set. As discussed in the previous section, since R is a linear bounded nonzero operator C_g is a closed convex set. Let us now consider the computation of the projection onto the sets C_d, C_r, C_t and C_θ respectively. As in Chapter 1 we shall consider only those operators R for which the problem of

$$\underset{g_1 \in C}{\mathrm{Min}} \|g-g_1\|$$

can be reduced to the problem of

$$\min_{Rg_1 \in R(C)} \|Rg - Rg_1\| .$$

(i) Let P_d denote the projection operator onto the set C_d. Let f(x) represent the known data and let $g(x)$ be the function whose projection on C_d needs to be computed. It is required to find $g_p(x)$ such that

$$\min_{g_o(x)} \|g(x) - g_o(x)\| = \|g(x) - g_p(x)\| \tag{4.38}$$

and

$$\|f(x) - Rg_p(x)\|_C = d. \tag{4.39}$$

From Kuhn–Tucker [29] conditions we know that the optimal solution must satisfy either of the following two conditions:

$$|f(y) - Rg(x)| \leq d, \tag{4.40}$$

or

$$|f(y) - Rg_p(x)| = d. \tag{4.41}$$

In the first case the condition turns out to be redundant. In the second case $\|g(x) - g_p(x)\|$ can be minimised if

$$Qg_p(x) = a\, Rg(x) + (1-a)\, f(y), \tag{4.42}$$

where

$$a = d/|Rg(x)-f(y)|. \tag{4.43}$$

In the first instance, we have

$$Rg_p(x) = R\, g(x). \tag{4.44}$$

In short

$$\begin{aligned} Qg(x) &= Rg(x), && \text{for } |f(y)-Rg(x)| \leq d, \\ &= aRg(x) + (1-a)f(y), && \text{otherwise.} \end{aligned} \tag{4.45}$$

The projection is simply $R^{-1}Qg(x)$.

(ii) Let P_r denote the projection operator onto C_r. By arguments similar to those just presented, we can write

$$P_r g(x) = g(x), \qquad \text{for } \|f(y) - Rg(x)\| \le r,$$
$$= R^{-1}(a\ Rg(x) + (1-a)\ f(y)), \text{ otherwise} \qquad (4.46)$$

where

$$a = r/\|f(y)-Rg(x)\|. \qquad (4.47)$$

(iii) For continuous signals the projection onto the set C_t is very involved. To simplify matters let us consider the discrete situation. Here the set C_t may be defined as:

$$C_t = \{ g: \Sigma|f-Hg| \le t\}, \qquad (4.48)$$

where H is a matrix operator. The projection of $Hg \notin H(C_t)$ onto $H(C_t)$ is computed as shown in Fig.4.2 for the two dimensional case. For an arbitrary but finite number of dimensions, we can derive

$$Qg[i] = af[i] + (1-a)Hg[i], \qquad (4.49)$$

where

$$a = e/(|f[i]-Hg[i]|), \qquad \text{for } i \in K,$$
$$= 1, \qquad \text{otherwise.} \qquad (4.50)$$

K is defined as

$$K = \{i: |f[i]-Hg[i]|>e\} \qquad (4.51)$$

and 'e' is given by

$$|K|e = \sum_{i\in K} |f[i]-Hg[i]| - t. \qquad (4.52)$$

$|K|$ denotes the cardinality of the set K. The above result is easily proved using the proof by contradiction technique. It holds for the continuous case also with summation replaced by integration and cardinality replaced by the Lebesgue measure [69].

(iv) Let P_θ denote the projection operator onto C_θ. It is required to compute $g(x)$ such that

$$\|g(x) - g_p(x)\| = \min_{g_o(x)} \| g(x) - g_o(x)\| \tag{4.53}$$

and

$$\rho_\theta(f, Rg) \leq \theta. \tag{4.54}$$

The method of computing the projection onto C_θ is illustrated graphically in Fig.4.3. In the figure $Rg(x)$ is projected onto the line whose phase is $\phi_f + 8$. It is seen from the figure that for $Rg(x)$ as shown $Qg(x)$ can be given by

$$Qg(x) = Rg(x) \cos(\phi_f(y)-\phi_{Rg}(y)+\theta) \exp(j(\phi_f(y)-\phi_{Rg}(y)+\theta)) \tag{4.55}$$

$Qg(x)$ is the point in the shaded area that is closed to $Rg(x)$. Now, if $Rg(x)$ is on the opposite side of ϕ_f then we have,

$$Qg(x) = Rg(x) \cos(\phi_f(y)-\phi_{Rg}(y)-\theta) \exp(j(\phi_f(y)- \phi_{Rg}(y)-\theta)) \tag{4.56}$$

Moreover if $|\phi_f(y) - \phi_{Rg}(y)| > \theta+\pi/2$ then $Qg(x)$ can be given by

$$Qg(x) = 0. \tag{4.57}$$

Summing up, we have

$$\begin{aligned} Qg(x) &= Rg(x), && \text{for } |\phi_{Rg}(y) - \phi_f(y)| \leq \theta, \\ &= 0, && \text{for } |\phi_f(y) - \phi_{Rg}(y)| > \theta+\pi/2, \\ &= Rg(x)\cos(\phi_f(y)-\phi_{Rg}(y)-\theta) \exp(j(\phi_f(y)-\phi_{Rg}(y)-\theta)), \\ & && \text{for } \phi_f(y) - \phi_{Rg}(y) > \theta \\ &= Rg(x)\cos(\phi_{Rg}(y)-\phi_f(y)+\theta) \exp(j(\phi_f(y)-\phi_{Rg}(y)+\theta)), \\ & && \text{for } \phi_f(y) - \phi_{Rg}(y) < -\theta. \end{aligned} \tag{4.58}$$

In this section we have considered the computation of the projection onto various convex feasible solution sets. In the next section we shall see the relevance of these sets the problem of image reconstruction from digital holograms.

4.4 Image Reconstruction from Noisy Holograms

4.4.1 *Significance* of C_d, C_r, C_t and C_θ

The previous section dealt with a very general operator namely the Fredholm's operator. Here we shall consider the computation of the feasible solution to the problem of image reconstruction from noisy digital holograms. In particular we will consider image reconstruction from bounded error. Notice that the sets C_r, C_d, C_t, and C_θ can be defined for the convolution operation since convolution is only a special case of Fredholm's operator. After a brief discussion of what these sets mean in practice we shall go on to describe the iterative procedures in each of these cases.

Consider the set C_d first. Errors may arise in practice in the measurement of signals due to several factors. In many situations there is an inherent limitation on the accuracy of the measuring device. Here we aim to reconstruct an image that agrees with the known data to the extent described by the accuracy of the measuring devices. Moreover the reconstructed image must also have a finite region of support. A noniterative procedure for computing such a solution is not obvious. However, an iterative procedure for computing a solution satisfying the two constraints may converge very slowly. In the next subsection we shall give a detailed account of the iterative procedure.

C_r is the set of all solutions that could have given rise to the known field distribution to within an error energy of r. In many instances it is possible to estimate the level of noise energy. In fact this statistic is often used to model the noise as a Gaussian distributed random process with zero mean and known variance. In computing a solution that belongs to C_r the value of 'r' must be known accuartely. In general, if r is known an attempt should be made to compute a solution such that $\|f-h*g\|=r$. This equality can not be ensured in the POCS method. However, it is possible to compute g such that $\|f-h*g\|\leq r$. The iterative procedure to compute such a solution is given in Section 4.5.2.

C_t is the set of all functions $g(x)$ such that is within a distance 't' from 'f' in the L^1 metric. This set is not of much interest to us and was given merely to cite yet another example of using a metric for defining a feasible solution set.

In [25] and [42] the problem of signal reconstruction from phase for digital holography has been treated at length. In Chapter 6 we shall deal exclusively with the problem of noise in phase. If the error in the phase is bounded, then C_θ denotes the set of all object field distributions that could have given rise to a receiver field distribution whose phase function is within an error of 'θ' to $\phi(x,y)$.

Before we go on to specific problems of image reconstruction in the presence of bounded noise, we will recall the definition of the operator $R^{-1}Q(g(x,y))$ for our problem, since it is required in computing every one of the projection operators. Let

$$g_p(x,y) = R^{-1}Q(g(x,y)). \tag{4.59}$$

Now

$$\begin{aligned} G_p(u,v) &= G(u,v), && \text{for } u^2+v^2 > 1/\lambda^2, \\ &= F(u,v), && \text{otherwise,} \end{aligned} \tag{4.60}$$

where $G_p(u,v)$ and $G(u,v)$ are the Fourier transforms of $g_p(x,y)$

and $g(x,y)$ respectively and $F(u,v)$ is the Fourier transform of,

$$f(x,y) = Q(g(x,y)). \tag{4.61}$$

$g_p(x,y)$ may be computed from $G_p(u,v)$. Notice that for each of the sets C_r, C_d and C_ϕ we can consider sparse data and use multispectral holograms. $Q(g(x,y))$ will be defined separately for each one of the projection operators onto these set including the case of multispectral holograms.

4.4.2 Bounded Magnitude of Noise

In this section we shall describe an iterative procedure for image reconstruction from digital holograms in the presence of bounded noise. Let

$$f(x,y) = h(x,y) * g(x,y) + n(x,y) \tag{4.62}$$

where $h(x,y)$ is as given in Chapter 2, and $|n(x,y)| \leq d$. It is required to compute a two dimensional signal $g(x,y) \in C_{fsc}$ such that

$$|f(x,y) - h(x,y) * g(x,y)| \leq d. \tag{4.63}$$

In other words we wish to compute a $g(x,y) \in C_{fsc} \cap C_d$, where C_d is now defined as

$$C_d = \{g(x,y): |f(x,y) - h(x,y) * g(x,y)| \leq d\}. \tag{4.64}$$

This can be done by the method of POCS. The function computed at the k-th iteration is given by

$$g_k = P_{fsc} T_d g_{k-1}, \tag{4.65}$$

where

$$T_d = 1 + s_d(P_d - 1), \tag{4.66}$$

and the initial estimate $g_o \in C_{fsc}$. The sequence $\{g_k\}$ converges strongly since the result of every iteration belongs to C_{fsc}.

If $f(x,y)$ is known only at a sparse set of sampling points, the method would require some minor modifications which is discussed below. Define

$$C_{di} = \{g(x,y): |g(x,y)*h(x,y;\lambda_i)-f(x,y;\lambda_i)| \le d, \text{ for } (x,y)\in I_p\} \tag{4.67}$$

$Q(g(x,y))$ is given by

$$\begin{aligned} Qg(x,y) &= h(x,y)*g(x,y), && \text{for } (x,y)\in I_p, \\ &= (1-a)f(x,y;\lambda_i) + ah(x,y;\lambda_i)*g(x,y), && \text{otherwise,} \end{aligned} \tag{4.68}$$

where

$$\begin{aligned} a &= 1, && \text{for } |g(x,y)*h(x,y;\lambda_i) - f(x,y;\lambda_i)| \le d, \\ &= d/|g(x,y)*h(x,y;\lambda_i) - f(x,y;\lambda_i)|, && \text{otherwise.} \end{aligned} \tag{4.69}$$

Thus the projection operation can also be performed if we use (4.68). This means that we can now use multispectral holograms. The computation to be performed at the k-th iteration is given by

$$g_k = P_{fsc}T_{d1}T_{d2}\cdots T_{dn}g_{k-1}, \tag{4.70}$$

where g_k is image function computed at the k-th iteration, n is the number of holograms and $T_{di} = 1 + s_{di}(P_{di}-1)$, for $0<s_{di}<2$. P_{di} is the projection onto the set C_{di}.

The POCS method merely converges to a solution and will not in most cases attain the desired solution in a finite number of iterations. Hence a condition to terminate the iterative procedure must be formulated a priori. Terminating the iterative procedure after a fixed finite number of iterations is clearly not advisable. In our work we propose to terminate the iterative procedure when the reconstructed signal satisfies the known data at 95% of the points. To be more explicit, let

$$I_k = \{(x,y): (x,y)\in I_p \text{ and } |f(x,y)-h(x,y)*g(x,y)| \le d\}. \tag{4.71}$$

Let $|I_k|$ denote the cardinality of the set I_k. The iterative procedure is terminated when $|I_k|/|I_p|$ attains a value 0.95 or more. For multispectral holograms we use the ratio $|I_{ki}|/(n|I_p|)$ where

$$I_{ki} = \{(x,y): (x,y)\in I_p \text{ and } |f(x,y;\lambda_i)-h(x,y;\lambda_i)*g(x,y)| \le d\}. \tag{4.72}$$

4.4.2. *Bounded Noise Energy*

Let

$$f(x,y) = h(x,y)*g(x,y) + n(x,y) \tag{4.73}$$

where $h(x,y)$ is as given in (2.2) and $\|n(x,y)\| \le r$. Here the norm refers to the root mean squared value. The problem here is to compute $g(x,y)$ such that $\|f(x,y)-h(x,y)*g(x,y)\| \le r$. As before our intention is to compute a solution by the method of POCS. The operator to be applied at each iteration is $P_{fsc}P_r$ where P_r has been defined in Section 4.2.3. Although the simulation studies are presented in the next chapter let us give here a brief description of the actual procedure.

Without loss of generality we consider only multispectral holograms. For a given $f(x,y;\lambda_i)$, define

$$C_{ri} = \{g(x,y): \sum_{(x,y)\in I_p} |g(x,y)*h(x,y;\lambda_i) - f(x,y;\lambda_i)|^2 \le r^2\}. \tag{4.74}$$

The projection onto the set C_{ri} is computed as follows: Let

$$\begin{aligned} Qg(x,y) &= h(x,y;_i)*\, g(x,y), \quad &&\text{for } (x,y) \notin I_p, \\ &= (1-a)\,f(x,y;\lambda_i) + a h(x,y;\lambda_i)*g(x,y), &&\text{otherwise.} \end{aligned} \tag{4.75}$$

where

$$\begin{aligned} a &= 1, \quad &&\text{for } r_o \le r, \\ &= r/r_o, &&\text{otherwise.} \end{aligned} \tag{4.76}$$

Here

$$r_o^2 = \sum_{(x,y)\in I_p} |g(x,y)*h(x,y;\lambda_i) - f(x,y;\lambda_i)|^2. \qquad (4.77)$$

Thus the projection P_{ri} can be computed from $Q\{g(x,y)\}$. The computation to be performed at the k-th iteration is given by:

$$g_k = P_{fsc}\, T_{r1}\, T_{r2} \cdots T_{rn}\, g_{k-1} \qquad (4.78)$$

where g_k is image function computed at the k-th iteration,

$$T_{ri} = 1 + s_{ri}(P_{ri} - 1) \qquad (4.79)$$

$0<s_{ri}<2$ and P_{ri} is the projection onto the set C_{ri}. As usual $g_o(x,y)$ will be a constant function in C_{fsc}. A detailed description of the above iterative procedures for the single and multiple frequency holograms is given in Algorithm 4.3 and Algorithm 4.4.

4.6 Need for a Method That Does Not Rely on a Priori Parameters

This chapter brought out the use of the POCS method in signal reconstruction in the presence of noise. We considered the Fredholm's equation of the first kind and described some examples of convex sets and their projection operators. We then applied the results to the problem of image reconstruction from noisy digital holograms. These methods are applicable when the noise is bounded by some known value. However if the estimated values for the bounds are lower than the actual values, then the method of POCS may not converge. To avoid this situation we may attempt to make a very conservative estimate of the bound. In this case the variance of the estimate of the solution may be large, which is again an undesirable situation. Hence we need a procedure that converges to a common point of a collection of convex sets if there exists one. Moreover it should converge even if there exists no common point. Such a procedure is given in the next chapter. Simulation studies were conducted to study the effectiveness of the proposed procedure for imaging with noise. The results are presented in the next chapter, where we shall give a comparative study of the methods proposed in this chapter and the next.

```
Initialise:
(1)    g_o(x,y)  =  constant,    for (x,y) in region of support,
                 =  0,           otherwise.
(2)    k  = 1
Repeat
(3)    Compute f'(x,y) = g_{k-1}(x,y)*h(x,y)
                  as in Algoritm 3.1 (Steps 2-5).
(4)    For all (x,y)∈I_p do {* Compute projection onto C_d *}
           If (|f'(x,y)-f(x,y)|≤d) then
               f_k(x,y) = f'(x,y)
           else
               a = d/|f'(x,y)-f(x,y)|
               f_k(x,y) = af'(x,y) + (1-a)f(x,y)
           end if
(5)    Compute g_k(x,y) from f_k(x,y)
                  as in Algorithm 3.1 (Steps 6-9)
(6)    k = k + 1
until satisfactory solution obtained.
```

Algorithm 4.1: The POCS procedure to reconstruct an image with finite support from hologram data $f(x,y)$ known at a set of points $(x,y)\in I_p$ subject to bounded noise magnitude.

Initialise:

(1) $g_o(x,y)$ = constant, for (x,y) in region of support,
= 0, otherwise.

(2) k = 1

Repeat

(3) For i = 1 to n, (* n denotes number of frequencies *)
do steps 4 to 7

(4) Compute $f'(x,y) = g_{k-1}(x,y) * h(x,y;\lambda_i)$
as in Algoritm 3.1 (Steps 2-5)

(5) Compute $f_k(x,y)$ from $f'(x,y)$
as in Algorithm 4.1 (Step 4)

(6) Compute $g_k(x,y)$ from $f_k(x,y)$
as in Algorithm 3.1 (Steps 6-9)

(7) k = k + 1

until satisfactory solution obtained.

Algorithm 4.2: The POCS procedure to reconstruct an image using multispectral hologram data $f(x,y;\lambda_i)$ known for n different frequencies subject to bounded magnitude of noise

```
Initialise:
(1)    go(x,y) = constant,    for (x,y) in region of support,
               = 0,           otherwise.
(2)    k = 1
Repeat
(3)    Compute f'(x,y) = gk-1(x,y)*h(x,y)
                    as in Algoritm 3.1 (Steps 2-5)
(4)    squared-error = 0
(5)    For all (x,y)∈Ip do (* Compute total error energy *)
               squared-error= squared-error+|f'(x,y)-f(x,y)|^2
(6)    If (squared-error ≥ r^2) then
               a = r/√(squared-error)
               For all (x,y)∈Ip do
                    fk(x,y) = (1-a)·f'(x,y) +  a·f(x,y)
       endif
(7)    Compute gk(x,y) from fk(x,y)
                    as in Algorithm 3.1 (Steps 6-9)
(8)    k = k + 1
until satisfactory solution obtained.
```

Algorithm 4.3: The POCS procedure to reconstruct an image with finite support from hologram data $f(x,y)$ known at a set of points $(x,y)\in I_p$ subject to bounded noise energy constraint.

Initialise:

(1) $g_o(x,y)$ = constant, for (x,y) in region of support,
= 0, otherwise.

(2) k = 1

Repeat

(3) For i =1 to n, (* n denotes number of frequencies *)
do steps 4 to 9

(4) Compute $f'(x,y;\lambda_i) = g_{k-1}(x,y)*h(x,y;\lambda_i)$
as in Algorithm 3.1 (Steps 2-5)

(5) squared-error = 0

(6) For all $(x,y)\in I_p$ do (* Compute total error energy *)
squared-error= squared-error+$|f'(x,y)-f(x,y)|^2$)

(7) If (squared_error≥ r^2)
then
a = r/√(squared-error)
For all $(x,y)\in I_p$ do
$f_k(x,y) = (1-a)\cdot f'(x,y) + a\cdot f(x,y)$

endif

(8) Compute $g_k(x,y)$ from $f_k(x,y)$
as in Algorithm 3.1 (Steps 6-9)

(9) k = k + 1

until satisfactory solution obtained.

Algorithm 4.4: The POCS procedure to reconstruct an image with finite support from multispectral hologram data $f(x,y)$ known at a set of points $(x,y)\in I_p$ subject to bounded noise energy constraint.

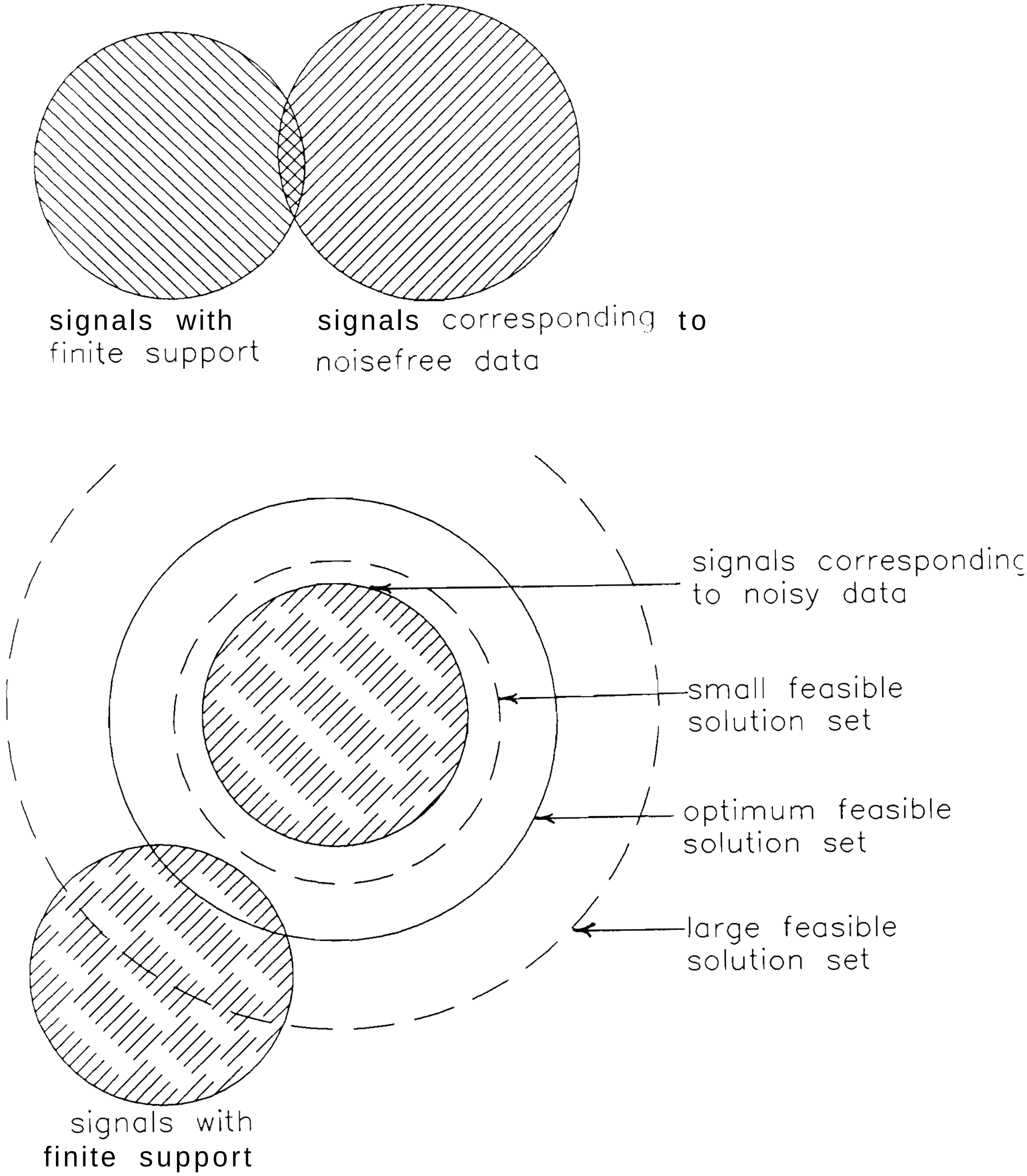

Fig.4.1 Effect of noise on the solution set.

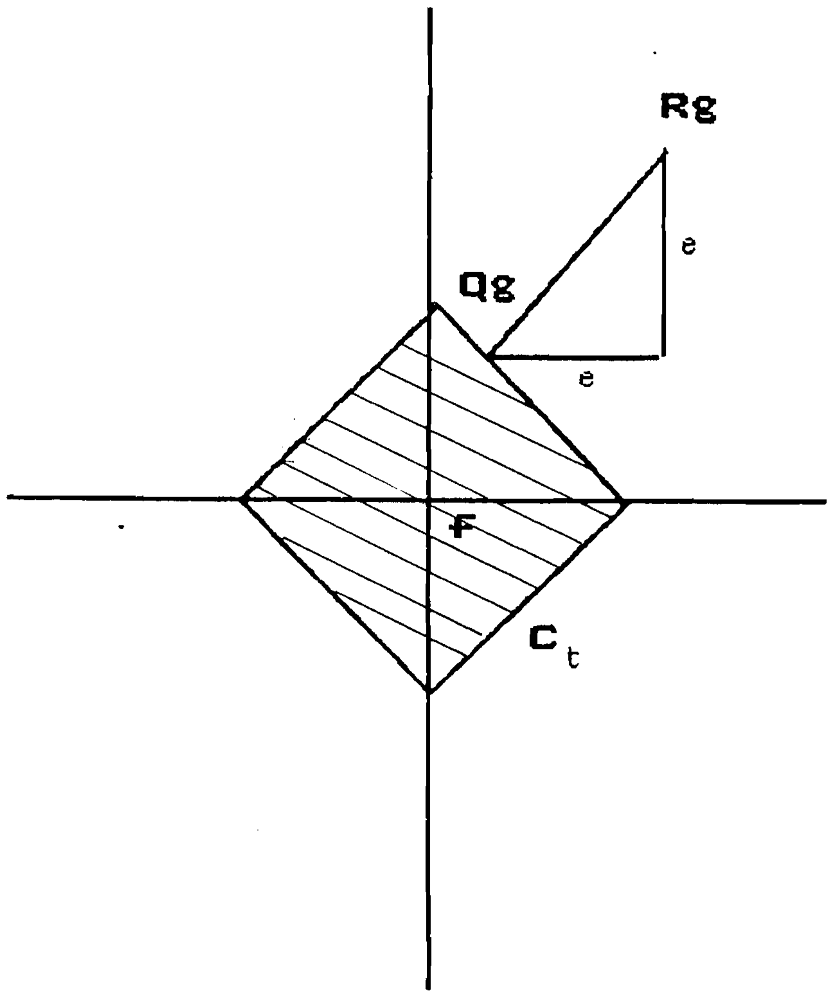

Fig.4.2 Projection onto C_t. The hatched region denotes the set set $\mathbf{H}(C_t)$ and $\mathbf{Qg}$ is the projection of Rg onto C_t. Note that the magnitude difference between Qg and $\mathbf{Rg}$ is 'e' in every dimension. In other words, if N denotes the number of dimensions

$$Ne = \Sigma|\mathbf{Hg}[n]-\mathbf{f}[n]| \quad - t.$$

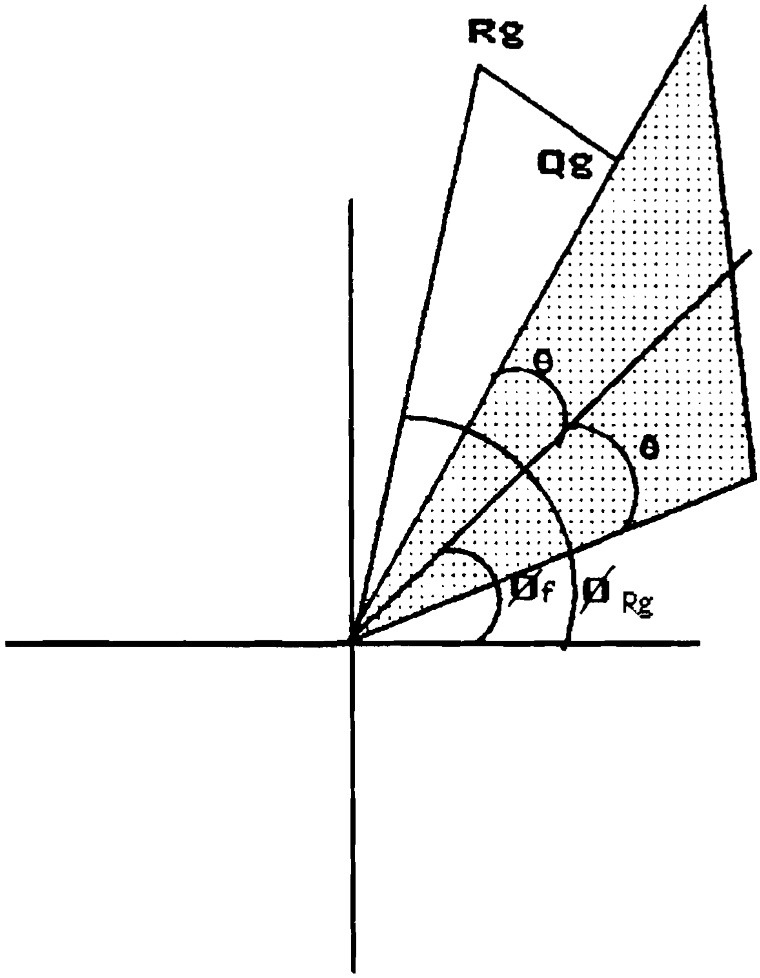

Fig. 4.3 Projection onto C_ϕ. The hatched region denotes the set C_ϕ. The point closest to Rg in C_ϕ is Qg. Hence Qg may be given by

$$Qg = |Rg| \cos(\phi_{Rg} - (\phi_f + i)) \exp(j(\phi_f + i)).$$

Chapter 5

IMAGE RECONSTRUCTION BY THE METHOD OF PROJECTION ONTO NONINTERSECTING CONVEX SETS

5.1 Need for an Alternative to POCS

In Chapter 4 an attempt was made to reconstruct a feasible solution from the available noisy data. The drawback of this method is that accurate knowledge of some particular statistic of the signal is required. In this chapter we develop another method of computing a solution to the problem of image reconstruction from digital holograms in the presence of noise. This method does not require any a **priori** statistics. Simulation studies were conducted to compare the effectiveness of the proposed solution with the feasible solution. Although a precise characterisation of the proposed solution is not known, simulation studies show that sometimes it yields better results than the feasible solution.

The process of hologram formation of a finite aperture signal can be viewed as a linear mapping from the set of signals with finite support to the set of bandlimited signals. In other words if R represents the hologram forming operator then $R:C_{fsc}\rightarrow B_p$ is a mapping from C_{fsc}, the set of signals with finite support to B_p, the set of bandlimited signals. Consider the equation

$$f(x,y) = Rg(x,y) + n(x,y). \tag{5.1}$$

It is required to compute $g(x,y)$ from $f(x,y)$ given the operator R. Here $n(x,y)$ is some noise function. It is obvious that on account of noise $f(x,y)$ may not belong to B_p. Hence it would be inappropriate to look for a $g(x,y)$ such that $f(x,y) = R\, g(x,y)$.

Our first attempt at reducing the effect of noise would be to remove that component of noise that is not limited to within the known band. This can be done by bandlimiting $f(x,y)$ to obtain $f'(x,y)$. In Chapter 3 we showed that if $f(x,y)$ is noisefree then there exists a unique $g(x,y) \in C_{fsc}$ such that $f(x,y) = Rg(x,y)$. This is because the Fourier transform of $g(x,y)$ is an analytic function and the Fourier transform of $f(x,y)$ can be extended by analytic continuation uniquely. If $f(x,y)$ is noisy then its Fourier transform may not be analytic within the prescribed band. Thus the Fourier transform of $f(x,y)$ cannot be extended analytically. However we can show that if we consider only a bounded subset of C_{fsc} then there exists a unique function $g(x,y)$ such that $\|f-Rg\|$ is minimised.

Let us now see why the method of POCS cannot be applied to compute such a solution. Recall that in Chapter 3 we formulated the problem of image reconstruction in the noisefree case as: Find $g(x,y) \in C_{fo} \cap C_{fsc}$ where

$$C_{fo} = \{g(x,y): f(x,y) = R\, g(x,y)\}. \tag{5.2}$$

When the given data is noisy there may exist no solution to the problem. Thus $C_{fsc} \cap C_{fo}$ may be empty. In such a situation the method of POCS is not guaranteed to converge. In fact simulation studies indicate that the method indeed diverges. Some other attempts to solve the problem of signal reconstruction from noisy data are based on regularisation techniques, which we have seen in Chapter 1. No work has been reported in literature extending these techniques to the problem of image reconstruction from multispectral holograms. An extension of these techniques to this problem is not obvious either. In Chapter 4 an attempt was made to compute a feasible solution which is so defined that at least one exists. The POCS method can be applied for computing a feasible solution if the feasible solution set is closed and convex. The drawback of this method is that accurate knowledge of some particular statistic of the signal is required. For example it is assumed that the noise magnitude is bounded by a value 'd' or that the noise energy is bounded by a value 'r'. If the estimated value of 'd' or r is higher than the true value, then the variance of the estimate of the solution g(x,y) may be large and the result is unsatisfactory. If the value of 'd' or r is in reality more than the estimated value then the POCS method may not converge at all as the feasible solution set defined by these values may not intersect with C_{fsc}. To overcome this problem we propose here a method that does not require the knowledge of these values. Moreover, as we shall soon show through simulation studies, the method presented in this chapter yields comparable performance even when such accurate statistics are available. However although the method can be proved to converge, convergence to a feasible solution set cannot be assured.

The rest of this chapter is organised as follows: In the next section we shall describe the theory of the method of Projection Onto NonIntersecting Convex Sets (PONICS), which is based on a theorem on the fixed point of nonexpansive operators. The method of PONICS was proposed earlier in a different form in [32] and [73] for signal synthesis and signal reconstruction. In

Section 3 we shall discuss the application of the method for image reconstruction from digital holograms. In Section 4 simulation studies for the methods presented here and in the previous chapter are described. A comparison of the two methods shows the effectiveness of PONICS for signal reconstruction in the presence of noise.

5.2 Projection Onto Nonintersecting Convex Sets (PONICS)

5.2.1 Theoretical Background

The method of PONICS is based on a theorem on the computation of the fixed point of a nonexpansive operator. Prior to stating the method we shall first state a few results required to show the validity of the proposed method. Recall that the projection onto a closed convex set is a nonexpansive operator and so is the operator $P_{fsc}T_{f1}T_{f2}\cdots T_{fn}$ defined in Chapter 3. Moreover the POCS method aims at computing the fixed point of $P_{fsc}T_{f1}T_{f2}\cdots T_{fn}$ and the method is applicable if $C_{fsc} \cap C_{fi}$ is nonempty. The following theorem suggests a method of computing the fixed point even if that condition does not hold.

Theorem 5.1: Let T be a nonexpansive mapping from $C \to C$ with a nonempty set of fixed points where C is a closed convex subset of a Hilbert space H. Let $T_s = s + (1-s)T$, where $0<s<1$. $\{T_s^N(x)\}$ converges weakly to a fixed point of T. Moreover the convergence is strong if at least one of the subsequences converges strongly.

Definition: T is called an asymptotically regular operator at x if

$$\lim_{N\to\infty} \|T^N x - T^{N+1} x\| = 0$$

Let C denote a closed convex set that is a subset of a Hilbert space H. T is said to be asymptotically regular at C, or simply asymptotically regular, if it is asymptotically regular at all $x \in C$. Notice that asymptotic regularity and convergence are related concepts. In fact convergence implies asymptotic regularity though the converse is not always true. Consider for example the sequence generated by, $x_N = 1 + 1/2 + 1/3 + \ldots + 1/N$. Although the sequence $\{x_N\}$ is asymptotically regular, it does not converge to a finite limit. The following theorem states a sufficient condition for a continuous operator to be asymptotically regular.

Theorem5.2: [18] Let a continuous operator $T: C \to C$ have a nonempty set of fixed points and choose s in $(0,1)$, then the mapping

$$T_s(x) = s(x) + (1-s)T(x) \tag{5.3}$$

(a) is a mapping from $C \to C$,

(b) has the same fixed points as T and

(c) is asymptotically regular.

The above theorem holds for a nonexpansive operator also since any nonexpansive operator is also continuous. As stated earlier asymptotic regularity does not imply convergence. The following theorem states the conditions for asymptotic regularity to imply convergence.

Theorem 5.3 [71]: Let $T: C \to C$ be an asymptotically regular nonexpansive operator with closed convex domain $C \subset H$ and let its set of fixed points F be nonempty. Then for any $x \in C$ the sequence $\{T^N(x)\}$ converges weakly to an element of F. Moreover the convergence is strong if and only if at least one of the subsequences converges strongly.

Proof of Theorem 5.1 : From Theorem 5.2 we know that T_s is asymptotically regular at all points in C and has the same fixed points as T. Applying Theorem 5.2 the desired result follows. (End *of Proof)*

From the above three theorems and using the result that a nonexpansive operator on a convex bounded set has at least one fixed point [43], the following corollary to Theorem 5.1 follows.

Corollary 5.4 : Let $T: C \rightarrow C$ be a nonexpansive operator with closed convex bounded domain $C \subset H$. Then for any $x \in C$ the sequence $\{T_s^N(x)\}$ converges weakly to an element of F. Moreover the convergence is strong if and only if at least one of the sub-sequences converges strongly. Here

$$T_s = s + (1-s)T \tag{5.4}$$

Consider the conditions required by the above result and the condition required by method of POCS. In the first case boundedness of the set C is necessary while in the method of POCS convergence is assured to a common element of a collection of closed convex sets none of which need be bounded. While in theory boundedness implies a severe restriction, in practice we deal only with bounded sets although the exact bound is not known. Hence boundedness is not necessarily a serious limitation. Let us now see how to make use of Corollary 5.4 to develop an iterative method for signal reconstruction in the presence of noise.

Consider the operator $P = P_1P_2$, where P_1 and P_2 are projection operators onto convex sets C_1 and C_2 respectively. P is a nonexpansive operator from $C_1 \rightarrow C_1$, since P_1 and P_2 are nonexpansive operators and any finite concatenation of nonexpansive operators is also nonexpansive. If C is a bounded set then there exists at least one fixed point in C_1 for the operator P. Moreover the sequence $\{P_s^N(x)\}$ converges to a fixed point of P. Here $P_s=1+s(P-1)$, where $0<s<1$. Note that C_1 and C_2 may have no element in common. This argument can be extended to an arbitrary number of sets. Let $P=P_1P_2...P_n$, where $P_1, P_2, .., P_n$ are projection operators onto closed convex sets $C_1, C_2, ..., C_n$. P is a nonexpansive operator from $C_1 \rightarrow C_1$. Again if C_1 is bounded then the sequence $\{P_s^N(x)\}$ converges to a fixed point of P for all $x \in C_1$. Here P_s is understood in the sense as mentioned before. Thus even though the sets $C_1, C_2, ..., C_n$ have no element in common there exists a fixed point of the operator $P_1P_2...P_n$ which can be computed by the above mentioned method. We shall henceforth refer to it as the method of projection onto nonintersecting convex sets or PONICS for short. Although the method of PONICS assures convergence, nothing has been said so far about the nature of the solution. In the method of POCS, convergence is to an arbitrary common element of $C_1, C_2, ..., C_n$. In case there are no common elements, PONICS will still converge to a solution. In other words we are at a loss to state in precise terms the computational problem that the method solves. Although the method is ambiguous in its aim we will show through simulation studies that it indeed helps in computing an acceptable solution to the problem of image reconstruction from multispectral digital holograms. If only two convex sets are involved the method of PONICS computes a quasisolution. This is shown in the next section.

5.2.2 Quasisolutions

If there are only two convex sets a quasisolution can be defined and as we shall soon see the method of PONICS computes a quasisolution. Also, in certain cases the quasisolution is unique. The following result which states the conditions for the existence and uniqueness of a quasisolution is a corollary to Theorem 1.3.

Lemma 5.5: If for a given Fredholm's operator R, g=0 is the only solution to the equation $Rg=0$ on a compact set G_o then a quasisolution to the equation $f=Rg$ on G_o for given f is unique and depends continuously on the initial data.

In other words, even if there exists other $g\notin G_o$ such that $Rg=0$, the uniqueness of a quasisolution is assured if there exists only one $g\in G_o$, which is identically zero, satisfying the equation $Tg=0$. It was pointed in Chapter 3 that C_{fsc} is precompact and that for any deconvolution problem such as image reconstruction from digital holograms, if the impulse response is nonzero in any finite band then g=0 is the only solution in C_{fsc} for $h*g=0$. Recall that image reconstruction from digital holograms is a deconvolution problem where the system transfer function is a low pass filter. Let us now show that the method of PONICS computes a quasisolution.

Consider the operator $Q = 1 + s(P_{fsc}P_{fo}-1)$ operating on the set C_{fsc}, where P_{fsc} and P_{fo} are defined earlier. We wish to show that the fixed point of $P_{fsc}P_{fo}$ to which the sequence $\{Q_s^N\}$ converges satisfies the following condition:

$$\|g'-P_{fo}g'\| = \min_{\substack{g_1 \in C_{fsc} \\ g_2 \in C_{fo}}} \|g_1 - g_2\| \tag{5.5}$$

where g' is a fixed point of $P_{fsc}P_{fo}$. This is shown as follows: By definition of the projection operator,

$$\|g'-P_{fo}g'\| = \|g'-C_{fo}\|. \tag{5.6}$$

Also since $P_{fsc}P_{fo}g'=g'$, we can write

$$\|P_{fsc}P_{fo}g' - P_{fo}g'\| = \|P_{fo}g'-C_{fsc}\|. \tag{5.7}$$

That is,

$$\|g'-C_{fo}\| = \|P_{fo}g - C_{fsc}\| \tag{5.8}$$

Now let $g_1 \in C_{fsc}$ and $g_2 \in C_{fo}$ be two elements such that

$$\|g_1-g_2\| = \min_{\substack{g_1' \in C_{fsc} \\ g_2' \in C_{fo}}} \|g_1' - g_2'\| \tag{5.9}$$

It is obvious that $g_2=P_{fo}g_1$ and $g_1=P_{fsc}g_2$. In other words $g_1=P_{fsc}P_{fo}g_1$. We now wish to show that the pair g_1 and g_2 is either unique or if there exists another function g' such that $P_{fsc}P_{fo}g' = g'$, then $\|g_1-g_2\| = \|g'-P_{fsc}P_{fo}g'\|$. Let

$$u = P_{fo}g_1 - g_1, \tag{5.10}$$

$$v = g_1 - g', \tag{5.11}$$

$$w = g_1 - P_{fo}g', \tag{5.12}$$

$$x = g' - P_{fo}g', \tag{5.13}$$

$$Y = P_{fo}g' - P_{fo}g_1, \tag{5.14}$$

and $$z = g' - P_{fo}g_1. \tag{5.15}$$

Notice that

$$x + y = z, \tag{5.16}$$

$$u + y = -w, \tag{5.17}$$

$$u + v = -z, \tag{5.18}$$

and $$x + v = w. \tag{5.19}$$

Taking the squared norm of both sides of the above four equations we derive

$$\|x\|^2 + \|y\|^2 + 2 \operatorname{Re} \langle x,y\rangle = \|z\|^2, \tag{5.20}$$

$$\|u\|^2 + \|y\|^2 + 2 \operatorname{Re} \langle u,y\rangle = \|w\|^2, \tag{5.21}$$

$$\|u\|^2 + \|v\|^2 + 2 \operatorname{Re} \langle u,v\rangle = \|z\|^2, \tag{5.22}$$

$$\|x\|^2 + \|v\|^2 + 2 \operatorname{Re} \langle x,v\rangle = \|w\|^2. \tag{5.23}$$

From the Lemma 1.5, we know that $\langle x,y\rangle$, $\langle u,y\rangle$, $\langle u,v\rangle$, and $\langle x,y\rangle$ are all greater than zero. Hence we derive

$$\|x\|^2 + \|y\|^2 \leq \|z\|^2, \tag{5.24}$$

$$\|u\|^2 + \|y\|^2 \leq \|w\|^2, \tag{5.25}$$

$$\|u\|^2 + \|v\|^2 \leq \|z\|^2, \tag{5.26}$$

$$\|x\|^2 + \|v\|^2 \leq \|w\|^2. \tag{5.27}$$

Adding (5.24) and (5.26), and (5.25) and (5.27) we derive

$$\|x\|^2 + \|y\|^2 + \|u\|^2 + \|v\|^2 \leq 2\|z\|^2, \tag{5.28}$$

$$\|x\|^2 + \|y\|^2 + \|u\|^2 + \|v\|^2 \leq 2\|w\|^2. \tag{5.29}$$

From the "parallelogram law", we derive

$$2\|x\|^2 + 2\|y\|^2 = \|x+y\|^2 + \|x-y\|^2 \geq \|z\|^2. \tag{5.30}$$

That is,

$$2\|x\|^2 + 2\|y\|^2 \geq \|z\|^2. \tag{5.31}$$

Similarily,

$$2\|u\|^2 + 2\|v\|^2 \geq \|z\|^2, \tag{5.32}$$

$$2\|x\|^2 + 2\|v\|^2 \geq \|w\|^2, \tag{5.33}$$

and $$2\|u\|^2 + 2\|y\|^2 \geq \|w\|^2. \tag{5.34}$$

Adding (5.31) and (5.32), and (5.33) and (5.34) we derive,

$$\|x\|^2 + \|y\|^2 + \|u\|^2 + \|v\|^2 \geq \|z\|^2, \tag{5.35}$$

$$\|x\|^2 + \|y\|^2 + \|u\|^2 + \|v\|^2 \geq \|w\|^2. \tag{5.36}$$

From the Equations (5.28) and (5.29), and (5.35) and (5.36) we derive

$$2\|z\|^2 = 2\|w\|^2 = \|u\|^2 + \|v\|^2 + \|x\|^2 + \|y\|^2. \tag{5.37}$$

It trivially follows from the above equations that

$$\langle x,y\rangle = \langle u,v\rangle = \langle x,v\rangle = \langle u,y\rangle = 0 \tag{5.38}$$

Subtracting (5.23) from (5.22), we get

$$\|u\|^2 = \|x\|^2, \tag{5.39}$$

which is the desired result.

We have just seen how a quasisolution can be computed. The uniqueness of a quasisolution follows if we can show that g=O is the solution to $h*g=0$. In the next section we shall see a method of speeding up the convergence to a fixed point of $P_{fsc}P_{fo}$.

5.2.3 Modified Method of POCS

In this section we shall show that the operator $1 + a_o(P_{fsc}P_{fo}-1)$ for $0<a_o<2$ can be used to converge to a fixed point of $P_{fsc}P_{fo}$. Using a value of $a_o>1$ will help to speed up convergence in the initial stages of the iterative procedure. Consider the operator $T_{fo}=1+s_{fo}(P_{fo}-1)$, where $0<s_{fo}<2$. Recall that T_{fo} is a nonexpansive operator and that the fixed points of $P_{fsc}P_{fo}$ and $P_{fsc}T_{fo}$ are same and are just the common elements of C_{fsc} and C_{fo}.

We will now show that if for the unbounded set C_{fsc} the set of fixed points of $P_{fsc}P_{fo}$ is nonempty then the set of fixed points of $T_{fsc}P_{fo}$ is identical to the set of fixed points of

$P_{fsc}P_{fo}$ even if C_{fsc} and C_{fo} have no common element. Consider the operator $P_{fsc}T_{fo}$. Since $P_{fsc}T_{fo}$ is a nonexpansive operator we can use $Q=1+s(P_{fsc}T_{fo}-1)$, where $0<s<1$, to converge to a fixed point of $P_{fsc}T_{fo}$. We wish to show that $Q_s=1+a_o(P_{fsc}P_{fo}-1)$ for $a_o=s \cdot s_{fo}$. This may be shown as follows. For any $g \in C_{fsc}$,

$$g + s(P_{fsc}T_{fo}g - g) = g + s(P_{fsc}(g + s_{fo}(P_{fo}g - g)) - g) \tag{5.40}$$

Since P_{fsc} is a linear operator and for $g \in C_{fsc}$, $P_{fsc}g = g$, the above equation reduces to

$$g + (P_{fsc}T_{fo}g - g) = g + s(P_{fsc}g + P_{fsc}s_{fo}(P_{fo}g - g) - g), \tag{5.41}$$

$$= g + ss_{fo}P_{fsc}(P_{fo}g - g), \tag{5.42}$$

$$= g + ss_{fo}(P_{fsc}P_{fo}g - g). \tag{5.43}$$

From the above equation the desired result trivially follows. Let us now show that the fixed points of $P_{fsc}P_{fo}$ and $P_{fsc}T_{fo}$ are identical. We shall attempt to do so by showing that the fixed points of $P_{fsc}P_{fo}$ and Q_s are same. That the fixed points of $P_{fsc}P_{fo}$ are also fixed points of Q_s is obvious. To show the converse consider g', a fixed point of Q_s. Now,

$$g' = Qg' = g' + a_o(P_{fsc}P_{fo}g' - g'). \tag{5.44}$$

Hence

$$a_o(P_{fsc}P_{fo}g' - g') = 0. \tag{5.45}$$

Since $a_o \neq 0$, it follows that g' is also a fixed point of $P_{fsc}P_{fo}$. Thus the fixed points of $P_{fsc}P_{fo}$ and Q_s are identical. In other words $\{Q_s^N(g)\}$ converges to a fixed point of $P_{fsc}P_{fo}$. If we choose $a_o=1$, $Q_s=P_{fsc}P_{fo}$, which is the operator usually applied for the noisefree case. We have just shown that $P_{fsc}P_{fo}$ can be applied for the noisy case also and that it converges to a quasisolution. We conclude this section by showing that the fixed points of $P_{fsc}T_{fo}$ and $P_{fsc}P_{fo}$ are identical. In the next section we shall see how the methods discussed in this chapter can be applied to the problem of image reconstruction from digital holograms in the presence of noise.

5 3 Image Reconstruction from Multispectral Digital Holograms

The problem of image reconstruction from digital holograms may be stated as follows. Let

$$f(x,y;\lambda_i)=h(x,y;\lambda_i)*g(x,y) + n_i(x,y), \qquad \text{for } i=1,2,...,n \tag{5.4 6}$$

where

$f(x,y;\lambda_i)$ is the hologram known at a fixed set of points I_p for a wavelength Xi,

$h(x,y;\lambda_i)$ is the impulse response at a wavelength λ_i,

$g(x,y)$ is the object field distribution that is independent of wavelength,

$n_i(x,y)$ is some noise function.

It is required to compute $g(x,y)\in C_{fsc}$ given $f(x,y;\lambda_i)$ at $(x,y)\in I_p$ and for wavelengths $\lambda_1, \lambda_2, ..., \lambda_n$. Notice that the problem as stated is ill-posed as there may exist no solution. As a simplification consider the case of only one hologram.

It was shown in the previous section that if $f(x,y;\lambda_i)$ is known completely then it is possible to compute a quasisolution belonging to C_{fsc}. However if $f(x,y;\lambda_i)$ is known only at a finite set of points, then $g(x,y)=0$ is not the only solution to $h(x,y)*g(x,y) = 0$ for $(x,y)\in I_p$. Hence the quasisolution is not unique. However an arbitrary quasisolution can be computed by applying the method of PONICS. We shall describe how this may be done. Let

$$C_{fo} = \{g(x,y): f(x,y) = h(x,y)^* g(x,y), \quad \text{for } f(x,y) \text{ given on } (x,y)\in I_p\}. \qquad (5.47)$$

C_{fo} would be null if $f(x,y)$ is noisy and is known over the entire receiver plane. In that case we should use $f'(x,y)$, the projection of $f(x,y)$ onto the set of bandlimited functions, in the definition of C_{fo}. If the cardinality of I_p is finite then C_{fo} is nonempty. Since the solution set is a subset of C_{fsc}, we can apply the operator $P_{fsc}P_{fo}$ iteratively on any $g\in C_{fsc}$. Notice that C_{fo} is a closed convex set.

If the hologram data is known for n different wavelengths $\lambda_1, \lambda_2, \ldots, \lambda_n$, then our aim would be to generate a sequence belonging to C_{fsc} and depends on the initial data. However we are not in a position to give a precise characterisation of the point to which it converges.

There are in general two ways of producing such a sequence corresponding to the sequential and parallel methods. In the parallel method we apply the operator

$$R_{par} = 1 + sP_{fsc}(s_1T_{f1} + s_2T_{f2} + \ldots + s_nT_{fn}) \qquad (5.48)$$

where

$$T_{fi} = 1 + s_{fi}(P_{fi} - 1), \quad 0<s_{fi}<2 \qquad (5.49)$$

and

$$s_1 + s_2 + \ldots + s_n = 1. \qquad (5.50)$$

Since T_{fi} is a nonexpansive operator, using Theorem 3.1 we can show that $s_1T_{f1} + s_2T_{f2} + \ldots + s_nT_{fn}$ is a nonexpansive operator and thus it is seen that the sequence $\{R^N_{par}(g)\}$, $g\in C_{fsc}$ will converge to a fixed point of $P_{fsc}(s_1T_{f1}+s_2T_{f2}+...+s_nT_{fn})$. In the sequential method the operator applied at every iteration is,

$$R_{seq} = 1 + sP_{fsc}(T_{f1} + T_{f2} + ... + T_{fn}) \quad (5.51)$$

Although we are not formally able to characterise the nature of the solution given by either of these two operators R_{par} is appealing intuitively as s_1, s_2, ..., s_n can be suitably chosen to reflect the relative emphasis of each of the known data on the solution. The sequential method gives unknown relative importance to each of the known data. In the next section we shall present simulation studies to show the efficacy of the method of PONICS.

5.4 Simulation Studies

5.4.1 *Overview*

The purpose of simulation study is threefold namely (i) to show the convergence of the PONICS method, (ii) to compare the computation involved for signal reconstruction in the presence of bounded noise magnitude by the method of POCS and PONICS and (iii) to compare the effectiveness of the parallel and sequential methods of PONICS. Accordingly the simulation studies are organised in two parts: (i) comparison of the method of PONICS and POCS for image reconstruction in the presence of uniformly distributed noise and (ii) comparison of the sequential and parallel methods of PONICS for image reconstruction in the presence of uniformly distributed noise.

Let us consider the method of POCS to compute a feasible solution. First we shall consider bounded noise energy. Here the method of POCS can be applied. But we can show that applying the method of PONICS will result in practically the same solution.

Consider the case of just one hologram data. If the set C_r (defined in Equation (4.10)) and C_{fsc} intersect, both the method of POCS and the method of PONICS will converge to an element of $C_r \cap C_{fsc}$. In the method of PONICS we take a projection onto C_{fo} which is a subset of C_r. Thus the projection onto C_{fo} will result in an interior element of C_r. Hence convergence to an element of $C_{fsc} \cap C_r$ will be faster. Notice that it is simple to verify whether the solution belongs to $C_{fsc} \cap C_r$ or not. Thus the method of PONICS can be applied with the termination criterion being that the solution belong to $C_{fsc} \cap C_r$. Notice that convergence can be speeded up in the method of POCS by using $T_r = 1 + s_r(P_r - 1)$, $0 < s_r < 2$, instead of P_r. Here s_r must be chosen such that $T_r(g(x,y))$ must belong to an element of C_r where r is the actual value of noise energy. Thus using the operator T_r it is possible to apply the method of POCS with a small margin of error on the estimated value of noise energy. However the method of PONICS does not require the value of r at all except for terminating the iterative procedure. Hence we shall not consider the POCS method for image reconstruction in the presence of bounded noise energy.

The other type of feasible solution involves the use of the information that the magnitude of the noise is bounded. Here we shall consider both the POCS and the PONICS method. Consider the case when only one hologram data is available. Let $f(x,y)$ be the given field distribution and $fo(x,y)$ a function such that $\|f(x,y) - f_o(x,y)\|_C \leq d$. Notice that L^2 distance between $f(x,y)$ and $f_o(x,y)$ may be unbounded. Moreover the set $\{g(x,y)\colon h(x,y) * g(x,y) = f_o(x,y)\}$ is a subset of C_d (defined in Equation (4.9)).

Hence C_d is an unbounded set. An arbitrary element $g \in C_{fsc} \cap C_d$ may be far removed from the actual solution, in terms of the l^2 norm. In other words the variance of the estimate of the solution will be large. On the other hand, using the method of PONICS we can compute a quasisolution. However the result may not necessarily belong to C_d. Yet as we see later the method of PONICS converges faster to a point that is close to the desired solution.

For multispectral noisy holograms the PONICS method has both a sequential and parallel implementation. Recall from Chapter 3 we saw that for the noisefree multispectral data the sequential and parallel methods have the same solution set. For noisy data however no such statement can be made. Hence simulation studies were carried out for noisy data comparing both the methods. But the results did not bring out any appreciable difference between the two methods.

5.4.2 Comparison of the Method of POCS and PONICS

In this subsection we shall consider uniformly distributed noise. Uniformly distributed noise is in reality random noise with bounded magnitude. We shall compare the POCS and PONICS method of image reconstruction. Before we go on to describe the results let us first describe the criterion used for terminating the iterative procedure. A fixed number of iterations decided a priori is unsatisfactory as it cannot reveal the tradeoff between accuracy of the desired result and the computational complexity. Of the many error criteria that could have been used to judge how far the current solution is from the actual, the one that was simplest to compute is chosen. The error criterion has been described in Chapter 4. In the actual implementation some minor modifications were introduced. Let us describe the procedure proposed earlier first.

The iterative procedure may be terminated when the Figure Of Merit (FOM),

$$|I_f|/|I_p| \leq k_d. \tag{5.52}$$

Here $|I_f|$ and $|I_p|$ refer to the cardinality of the sets I_f and I_p respectively. I_f is defined as

$$I_f = \{ (x,y): |f(x,y) - h(x,y)*g(x,y)| \leq d, \text{ for } (x,y)\in I_p \} \tag{5.53}$$

Here 'd' is a known maximum bound on the magnitude of noise. For multispectral holograms the figure of merit is $(\Sigma|I_{fi}|)/(n|I_p|)$, where n is the number of frequencies and I_{fi} is the set I_f for a wavelength λ_i. In other words,

$$I_{fi} = \{ (x,y): |f(x,y;\lambda_i) - h(x,y;\lambda_i)*g(x,y)| \leq d, (x,y)\in I_p\} \tag{5.54}$$

Keeping in line with the simulation studies conducted earlier, we chose k_d=0.95. The difficulty encountered was that the number of iterations required to obtain this accuracy was quite large and hence the iterations were terminated when the number of iterations times the number of frequencies reached 50. Yet another relaxation was made to terminate the iterative procedure when the figure of merit defined above did not improve over successive iterations.

Fig.5.1 shows the results obtained using the POCS and PONICS methods for a 64x64 array. The results are given for a SNR of 0dB and -10dB. Table 5.1 gives comparative figures for the computational complexity and FOM. The FOM is meant merely to compare the results obtained using the POCS and PONICS methods for the same initial conditions. It does not indicate in a proper sense the absolute figure of merit of the solution obtained. Hence it would not be reasonable to compare the FOM values along a column. Notice from Fig.5.1 that for a 64x64 array the results obtained using the POCS and PONICS method do not show appreciable difference. However Table 5.1 shows that an FOM of 95% is attained for nearly all cases of the PONICS method and for hardly any case of the POCS method. Moreover the table also indicates that the PONICS method takes fewer iterations to attain an FOM of 95%. The method of POCS in most cases had to be terminated because the number of iterations exceeded 50. In fact the only instance where the POCS method appears to give better results than the method of PONICS is when the SNR is -10dB and when 16 frequencies are used. For a large signal to noise ratio the bound on the maximum magnitude of the noise is also large. Hence notice that the FOM for -10dB is in general higher than for the corresponding 0 dB case.

Let us also caution that since we are conducting simulation studies the bound on the maximum magnitude of the noise is known precisely. Hence the POCS method, as can be seen from the figure, gives results comparable to those obtained by the method of PONICS. In practice the bound on the noise is only approximately known. To reiterate what was mentioned earlier if the actual bound is more than the estimated bound then the POCS method will not converge even in the l^2 norm. But the PONICS method can be applied even if the known bound is erroneous. At worst it might diverge in the FOM, but will converge in the l^2 norm. In sum, the POCS method was applied under ideal conditions. Even in such case the POCS method does not give significantly better results. Thus these experimental studies indicate that computing a solution by the method of PONICS is better than computing a feasible solution by the method of POCS.

Let us now consider the 32x32 array (down sampled). Fig.5.2 shows the results of the images reconstructed from multispectral noisy holograms by the methods of POCS and PONICS when the SNR is 0dB and -10dB. The figures indicate that the method of PONICS appears to give better results than the method of POCS under the same initial conditions. As in the previous study a table comparing the computational complexity and the FOM for the results obtained using the two methods was made. Table 5.2 shows that whereas the PONICS method attained the desired accuracy within a few iterations, the POCS method failed to converge for the two frequency case or exceeded the prescribed limit on the number of iterations for other cases. For the sake of completion, the figures corresponding to the 16x16 array and 8x8 array are given in Fig.5.3 and Fig.5.4 respectively, although they do not give any useful information even at low noise levels (SNR=0dB and SNR=-10dB).

These studies show that the performance of the method of PONICS for image reconstruction from multispectral holograms in the presence of uniformly bounded noise is in most cases at least as good as the method of POCS for the same initial data. A look at the corresponding values in Table 5.1 to Table 5.4 shows that the method of PONICS converges faster if the samples are

convergence rate falls sharply as the number
fewer. Horeover the amount of
of frequencies is increased from 4 to 16 in the case of a 64x64
array. This indicates that when there is an increasing
inconsistent data the size of the solutachieve the same level of set keeps decreasing
and hence it takes more computation to
FOM.

5.4.3 Comparison of Sequential and Parallel Methods

In our second study we compare the sequential and parallel implementations of the methods of PONICS. We shall consider only multispectral holograms. We also assume a uniform distribution of noise. We did not consider Gaussian distributed noise since the method of PONICS does not make explicit use of the property that noise is Gaussian distributed. In our simulation study we assume that noise is independent and identically distributed at every point. In such a situation the method of PONICS can be applied irrespective of the distribution of noise. The comparative study of the sequential and parallel methods was made using a 32x32 array and for two SNRs, namely, 0dB and -10dB. The results as indicated by Fig.5.5 do not show appreciable difference between the two methods. The termination criterion for the iterative procedures remain the same as in the previous case.

A note regarding the parallel method may be mentioned here. Let $g_i = P_{fi}g$, where P_{fi} denotes the projection onto the set C_{fi}. It is possible to write g_i as

$$g_i = g_o + n_i, \tag{5.55}$$

where n_i is some noise function. In the parallel implementation fewer. Moreover the convergence rate falls sharply as the number of frequencies is increased from 4 to 16 in the case of a 64x64 array. This indicates that when there is an increasing amount of inconsistent data the size of the solution set keeps decreasing and hence it takes more computation to achieve the same level of FOM.

5.4.3 *Comparison of Sequential and Parallel Methods*

In our second study we compare the sequential and parallel implementations of the methods of PONICS. We shall consider only multispectral holograms. We also assume a uniform distribution of noise. We did not consider Gaussian distributed noise since the method of PONICS does not make explicit use of the property that noise is Gaussian distributed. In our simulation study we assume that noise is independent and identically distributed at every point. In such a situation the method of PONICS can be applied irrespective of the distribution of noise. The comparative study of the sequential and parallel methods was made using a 32x32 array and for two SNRs, namely, 0dB and -10dB. The results as indicated by Fig.5.5 do not show appreciable difference between the two methods. The termination criterion for the iterative procedures remain the same as in the previous case.

A note regarding the parallel method may be mentioned here. Let $g_i = P_{fi}g$, where P_{fi} denotes the projection onto the set C_{fi}. It is possible to write g_i as

$$g_i = g_o + n_i, \tag{5.55}$$

where n_i is some noise function. In the parallel implementation we compute $(1/n)\Sigma g_i$. Note that we are in essence computing the time average. From the central limit theorem we know that as n tends to infinity the time average tends to the ensemble average. Since the noise is assumed to have a zero mean the time average can be expected to reduce the noise. In other words $(1/n)\Sigma n_i$ will tend to zero. The implicit assumption here is that g_o is independent of 'i'. This assumption is not strictly true since for a given sparse sensor array data there can be many "correct" solutions. Even if g_o is dependent on 'i', the effect of averaging will be to reduce the noise. Note here that the parallel procedure is similar to the Jacobi iteration for solving a set simultaneous linear equations [26] while the sequential procedure is similar to the Gauss-Siedel iteration. The disadvantage with the parallel method is that it does not update the estimate of the solution each time the projection P_{fi} is computed. Hence the parallel procedure can be expected to take more number iterations to arrive at a prescribed FOM for the solution. In other words, if only a sequential computer is available it is best to use the sequential method since it will converge faster. As we shall soon see the results of our experiments appear to validate our conclusion.

Fig.5.5 shows the results obtained by using the sequential and parallel methods. It can be seen that the quality of the reconstructed images obtained by the two methods are not significantly different. Table 5.5 shows the relative performance of the sequential and parallel methods. As in the previous case, the values for the FOM do not,represent in any absolute sense the quality of the reconstructed image. It is given merely to compare the sequential and parallel methods for the same initial conditions. Notice that while the FOM is nearly equal in most of the cases, the sequential method gives better performance in terms of the number of iterations. However in a parallel machine the parallel method will be speeded up by a factor nearly equal to the number of frequencies. Hence the parallel method will be faster in such a situation.

In this section, we have performed some simulation studies for image reconstruction from digital holograms in the presence of noise. We have considered two methods of image reconstruction from multispectral holograms in the presence of noise. In the first case we attempted to compute a "feasible solution" by the method of POCS. In the second case we applied the method of PONICS. The studies indicate that in many cases the method of PONICS gives better results than the method of POCS. The method of PONICS can be implemented sequentially or in a parallel fashion. We have considered both versions and the studies indicate that the sequential method converges faster than the parallel method in a sequential computer. Hence, unless we have a parallel machine it would be better to use the sequential method.

5.5 Application to other Signal Recovery Problems

In this chapter we discussed the method of projection onto nonintersecting convex sets (PONICS) for image reconstruction from noisy sensor array data. Through simulation studies we have shown its effectiveness in reconstructing a good quality image from multispectral holograms. Simulation studies were conducted to compare the results by both the method of PONICS and the method of POCS. It was found that the method of PONICS gave much better performance in terms of computational complexity than the method of POCS, although the former is not guaranteed to converge to the desired solution while the latter is. Note that the POCS method was applied under ideal conditions and even in such a case the POCS method does not give significantly better results. The PONICS method has both sequential and parallel implementations. Simulation studies reported here do not show any appreciable difference between the two versions. Finally, note that a precise characterisation of the solution computed by the method of PONICS is not known except for the case of two convex sets, when the method was shown to converge to a quasisolution.

There are a number of signal recovery problems that can possibly be dealt with using the method of PONICS. Computer tomography is a good example. Here, as in multispectral digital holography, it is required to find an element of the intersection of a number of convex sets. An empty intersection may result if there is a large amount of noisy data. In such cases one may be tempted to discard part of the data so as to be able to compute a solution by the method of POCS. Using the method of PONICS, however, we can compute a solution that makes use of all the available data.

Table 5.1

Figure of merit versus computational complexity for image reconstruction from multispectral holograms in the presence of uniformly distributed noise for a 64x64 array.

SNR (dB)	#Frequencies	PONICS		POCS	
		#iterations	$\lvert I_f\rvert/\lvert I_p\rvert$	#iterations	$\lvert I_f\rvert/\lvert I_p\rvert$
0	1	2	97.77	50	87.67
0	2	4	95.58	50	87.28
0	4	8	96.26	52	87.69
0	8	56	94.90	56	90.87
0	16	64	95.56	64	84.25
-10	1	7	99.44	11	93.41
-10	2	26	98.72	50	98.11
-10	4	32	96.18	52	95.06
-10	8	40	93.73	56	95.13
-10	16	48	92.53	64	95.30

Table **5.2**

Figure of merit versus computational complexity for image reconstruction from multispectral holograms in the presence of **uniformly** distributed noise for a **32x32** array.

SNR (dB)	#Frequ-encies	PONICS		POCS	
		#itera-tions	$\|I_f\|/\|I_p\|$	#itera-tions	$\|I_f\|/\|I_p\|$
0	1	2	98.31	13	88.37
0	2	4	96.53	42	84.60
0	4	12	97.29	52	81.76
0	8	24	95.69	56	82.39
0	16	48	95.51	64	84.25
-10	1	2	99.42	6	94.82
-10	2	4	99.66	12	93.89
-10	4	8	99.02	36	94.84
-10	8	16	97.93	56	94.66
-10	16	32	95.94	64	94.75

Table 5.3

Figure of merit versus computational complexity for image reconstruction from multispectral holograms in the presence of uniformly distributed noise for a **16x16** array.

SNR (dB)	#Frequ-encies	PONICS		POCS	
		#itera-tions	$\lvert I_f\rvert/\lvert I_p\rvert$	#itera-tions	$\lvert I_f\rvert/\lvert I_p\rvert$
0	1	2	96.49	13	85.94
0	2	6	98.22	16	82.43
0	4	12	97.67	44	80.38
0	8	24	96.83	56	78.62
0	16	48	95.08	64	77.79
-10	1	2	99.61	2	93.75
-10	2	4	98.83	6	93.17
-10	4	8	98.93	16	94.15
-10	8	16	99.37	40	94.05
-10	16	32	99.76	64	94.95

Table 5.4

Figure of merit versus computational complexity for image reconstruction from multispectral holograms in the presence of uniformly distributed noise for an 8x8 array.

SNR (dB)	#Frequencies	PONICS		POCS	
		(iterations	$\lvert I_f\rvert / \lvert I_p\rvert$	#iterations	$\lvert I_f\rvert / \lvert I_p\rvert$
0	1	2	98.44	7	82.82
0	2	4	99.32	18	85.04
0	4	8	99.02	24	82.66
0	8	24	97.37	56	75.98
0	16	48	97.37	64	76.27
-10	1	2	95.32	2	94.22
-10	2	2	96.88	4	94.29
-10	4	8	99.61	8	93.44
-10	8	16	99.61	24	92.66
-10	16	32	99.61	32	94.15

Table 5.5

Comparison of the sequential and parallel methods. Table shows the figure of merit versus computational complexity for image reconstruction from multispectral holograms the presence of uniformly distributed noise for 32x32 array.

SNR	#Frequ-encies	Sequential		Parallel	
		#itera-tions	FOM	#itera-tions	FOM
0	2	4	96.53	8	97.46
0	4	12	97.29	28	96.00
0	8	24	95.69	56	91.45
0	16	48	95.51	64	83.40
-10	2	4	99.66	4	98.78
-10	4	8	99.02	8	96.99
-10	8	16	97.93	16	95.70
-10	16	32	95.94	48	95.83

Initialise:

(1) $g_o(x,y)$ = constant, for (x,y) in region of support,

= 0, otherwise.

(2) $k = 1$; $s = 0.9$

Repeat

(3) For all (x,y) do

$g'(x,y) = g_{k-1}(x,y)$

(4) For i = 1 to n

do steps 5-7

(5) Compute $f(x,y) = g'(x,y)*h(x,y;\lambda_i)$

as in Algoritm 3.1 (Steps 2-5)

(6) For all $(x,y)\in I_p$ do

$f_k(x,y) = f(x,y;\lambda_i)$

(7) Compute $g'(x,y)$ from $f_k(x,y)$

as in Algorithm 3.1 (Steps 6-9)

(8) $k = k + 1$

(9) For all (x,y) do

$g_k(x,y) = g_{k-1}(x,y) + s(g'(x,y)-g_{k-1}(x,y))$

until satisfactory solution obtained.

Algorithm 5.1: The PONICS procedure to reconstruct an image with finite support from hologram data $f(x,y)$ known at a set of points $(x,y)\in I_p$ for n different frequencies.

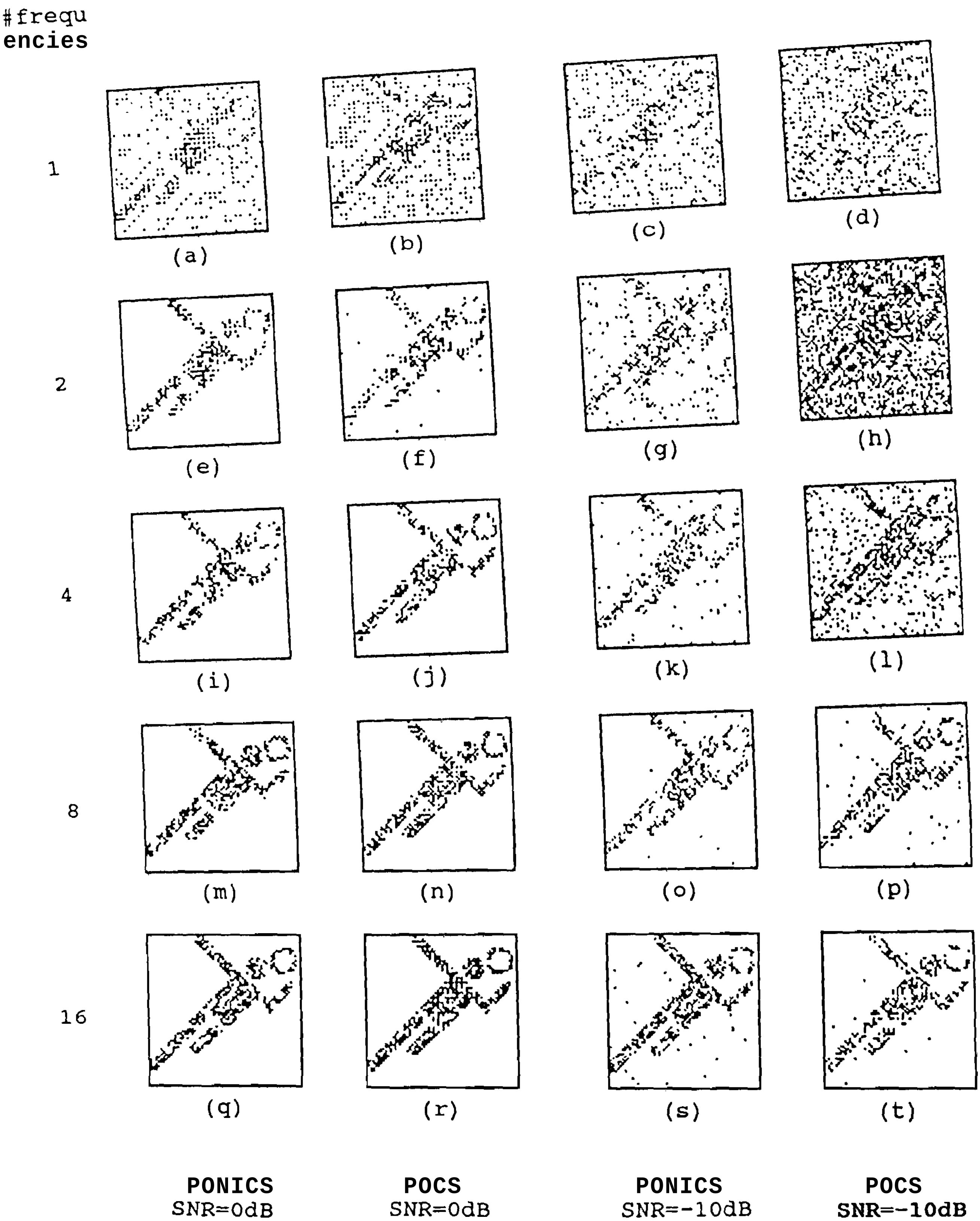

Fig.5.1 Comparison of POCS and PONICS methods for reconstruction of images from noisy sensor array data. Uniformly distributed noise is used. The data is collected from a 64x64 array at different frequencies. Comparison is made for two different SNR's.

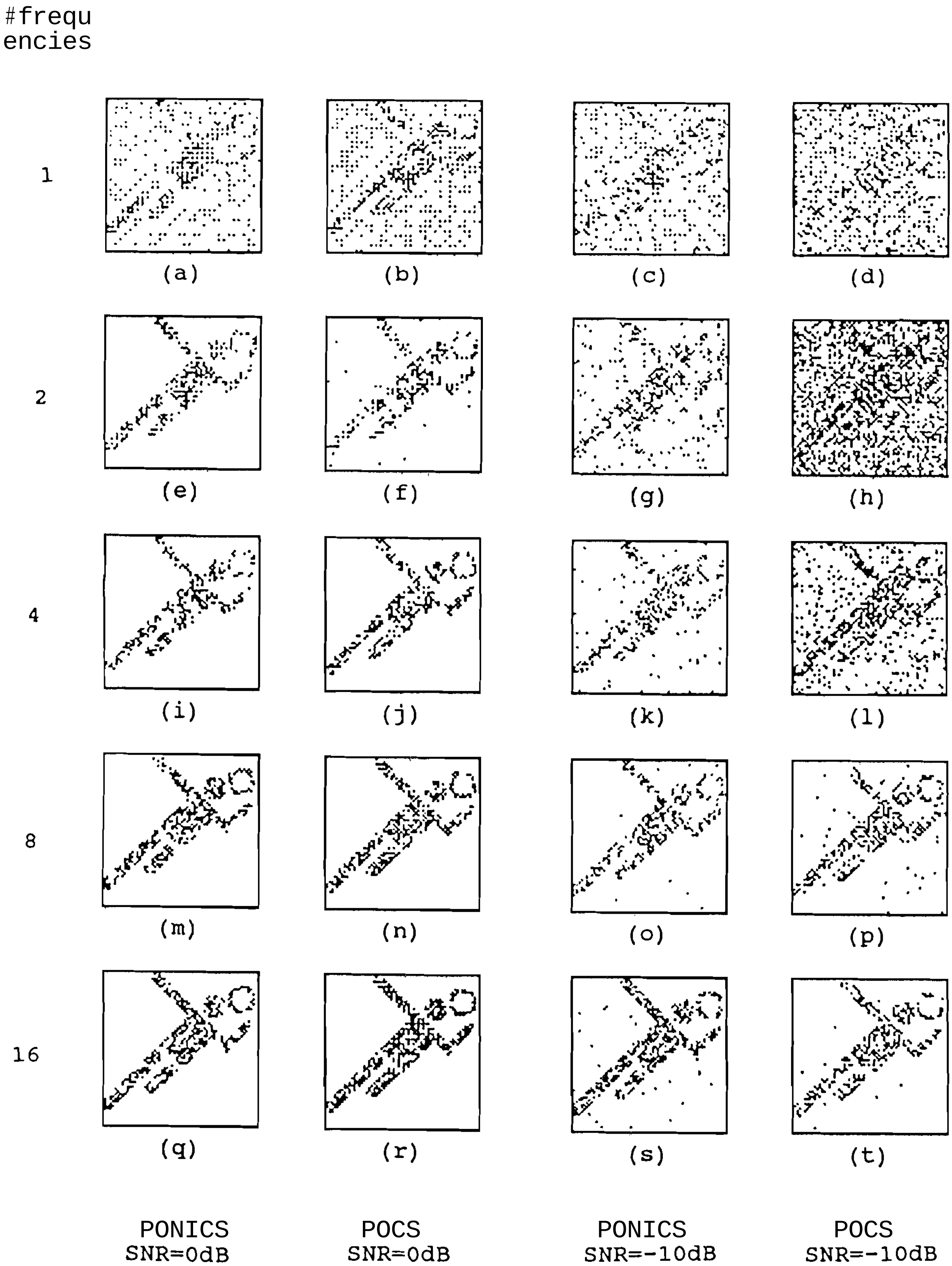

Fig.5.1 Comparison of POCS and PONICS methods for reconstruction of images from noisy sensor array data. Uniformly distributed noise is used. The data is collected from a 64x64 array at different frequencies. Comparison is made for two different SNR's.

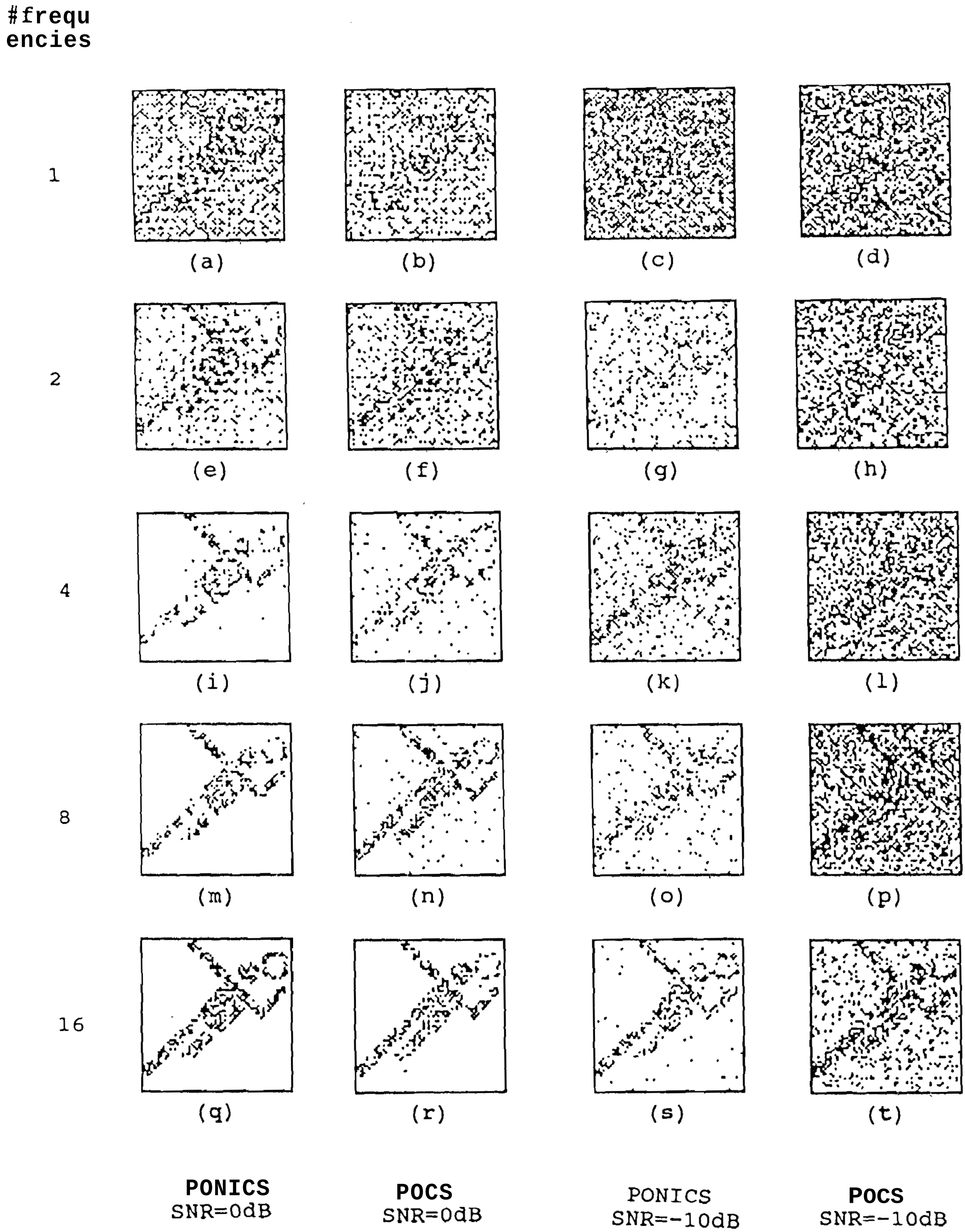

Fig.5.2 **Comparison of POCS and PONICS methods for reconstruction of images from noisy sensor array data. Uniformly distributed noise is used. The data is collected from a 32x32 array at different frequencies. Comparison is made for two different SNR's.**

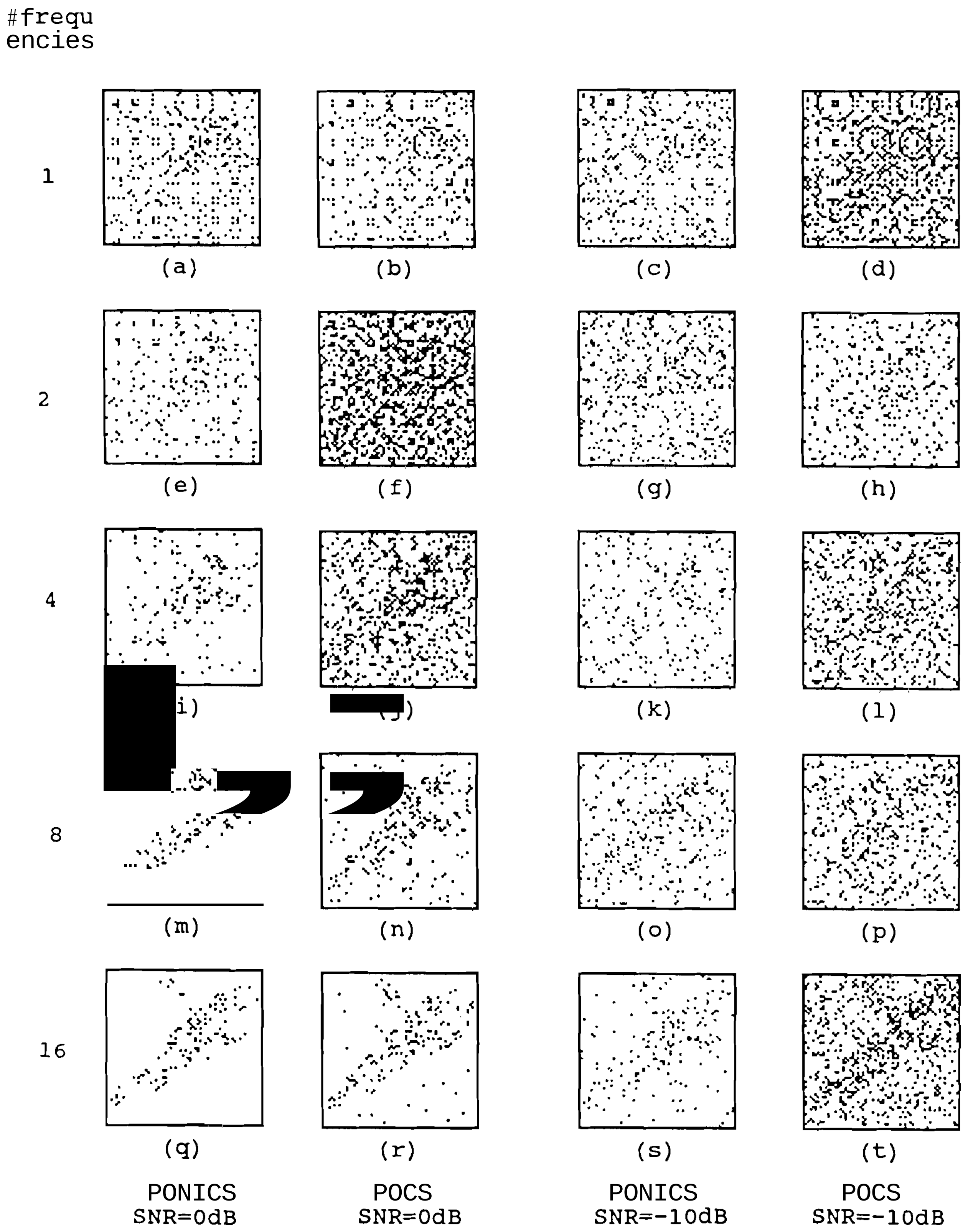

Fig.5.3 Comparison of POCS and PONICS methods for reconstruction of images from noisy sensor array data. Uniformly distributed noise is used. The data is collected from a 16x16 array at different frequencies. Comparison is made for two different SNR's.

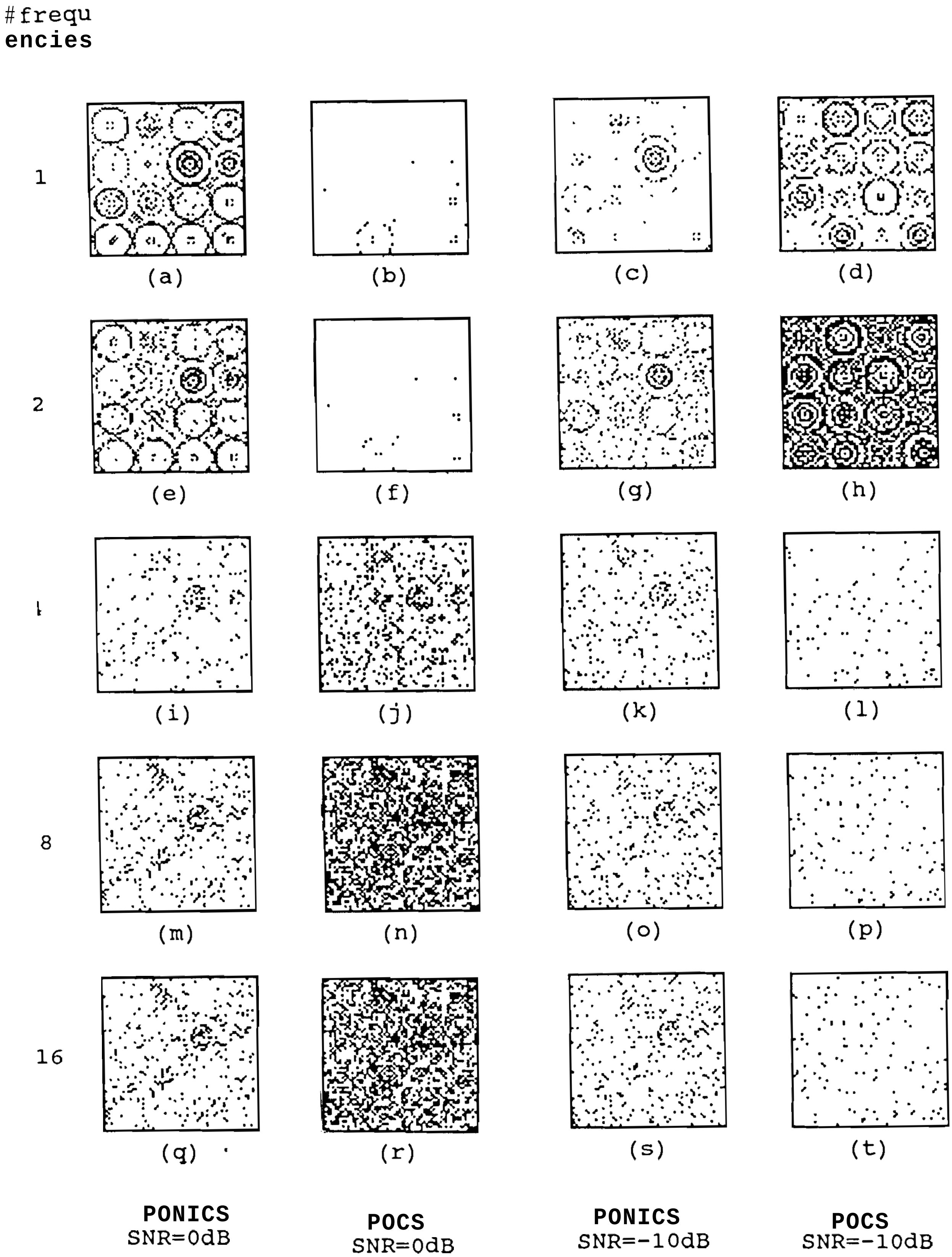

Fig.5.4 Comparison of POCS and PONICS methods for reconstruction of images from noisy sensor array data. Uniformly distributed noise is used. The data is collected from a 8x8 array at different frequencies. Comparison is made for two different SNR's.

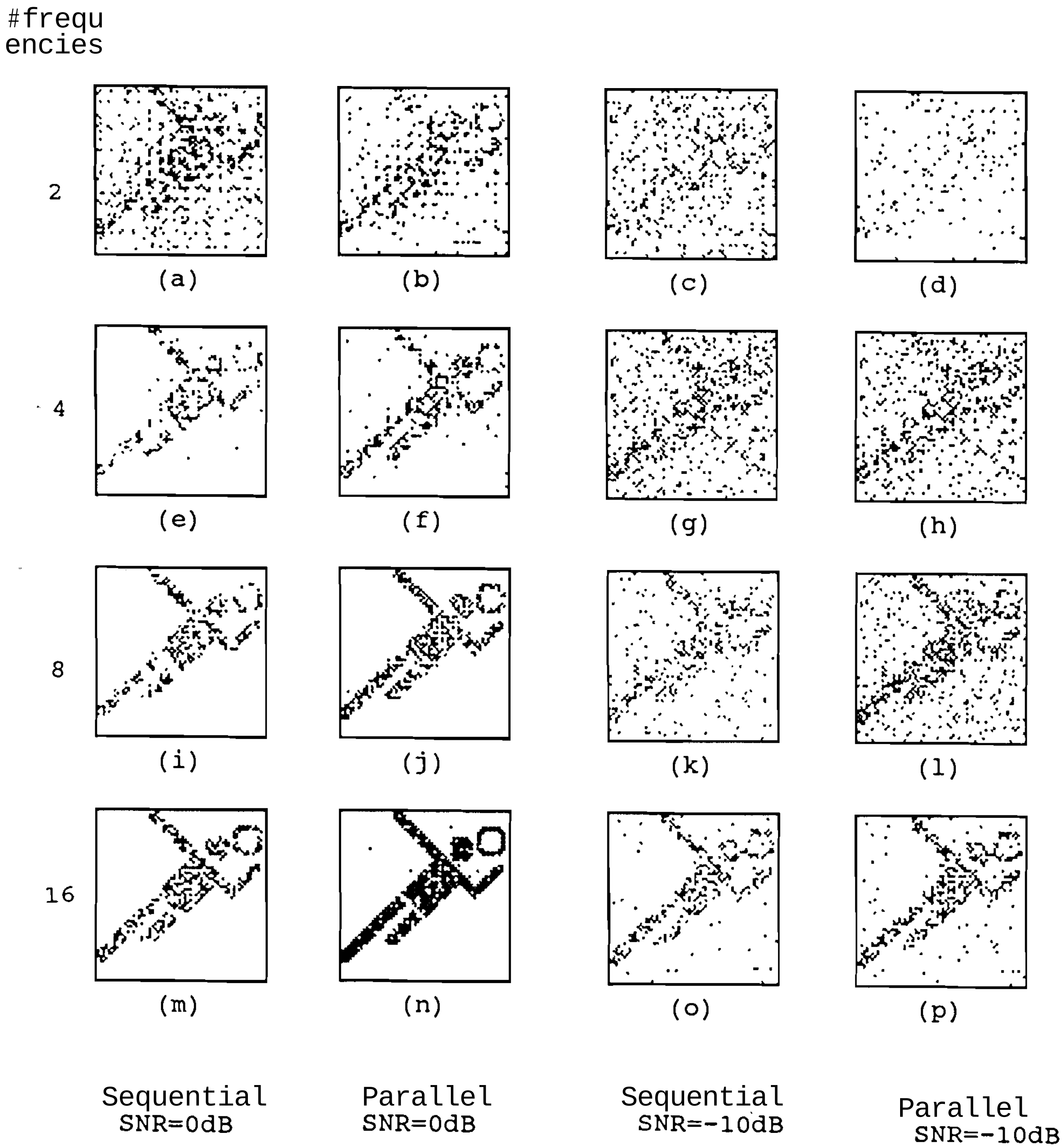

Fig.5.5 Comparison of sequential and parallel methods of PONICS for image reconstruction from noisy (uniformly distributed) multiple frequency hologram data using a 32x32 array for two SNR values (0dB and -10 dB). The figures show the similarity of the results in the sequential and parallel implementation.

Chapter 6

IMAGE RECONSTRUCTION FROM NOISY PHASE

6.1 Problem Statement

61.1 Signal *Reconstruction from Phase*

In the previous three chapters we considered the problems of sparse data and noise. The sparsity of data arose due to the small number of sensors. In this chapter we consider partial data namely phase only data. This problem is similar to the one mentioned in the previous chapter with the added complexity that only the phase of the signal is known. We consider both full phase and quantised phase. An iterative procedure based on the alternating projection theorem is proposed. The **termination** of the procedure is done on the basis of a figure of merit of the solution. Simulation studies show that images can be reconstructed from noisy phase even when the phase is quantised and when only a few sensors are available for collecting the data.

The problem of signal reconstruction from the phase of the Fourier and other linear transforms has of late received wide attention [7],[16],[67]. Signal reconstruction from noisy phase has been considered by Epsy and Lim [11] and Yegnanarayana, et al [67]. In [11] the problem of recontruction of a signal from the noisy phase of its Fourier transform was considered. The noise added to phase was uniformly distributed between $-\Phi$ and $+\Phi$. The closed form solution for signal reconstruction from phase was used. As this solution is valid only for noisefree data, it was found that even for very low noise levels such as $\Phi=\pi/10$ the reconstruction was poor. This method of solution is inadequate in other respects too. First it cannot be easily extended to other transforms. Besides, it does not make explicit use of the fact that the signal has finite duration. This can be done in an iterative procedure, as in [67]. Here the noisy phase is quantised in the hope that the quantised noisy phase is likely to be the same as the quantised noise free phase also. The method of Projection Onto Convex Sets (POCS) can be used to iteratively compute a solution that has finite region of support and that satisfies the known phase data. It was found that reconstruction from quantised phase sometimes produced better quality images than reconstruction from full phase for noisy data. This phenomenon can be explained by considering the angular separation between linear subspaces as discussed below.

6.1.2 Separation between Linear Spaces

Let C_1 and C_2 be two linear subspaces of a Hilbert space H. For $x,y \in H$, define

$$\cos(\psi(x,y)) = |\mathrm{Re}\langle x,y\rangle| / (\|x\| \cdot \|y\|), \tag{6.1}$$

and

$$\cos(\psi(C_1,C_2)) = \sup_{\substack{x\in C_1 \\ y\in C_2}} \cos(\psi(x,y)), \tag{6.2}$$

where $\psi(x,y)$ measures the angular separation between C_1 and C_2 and is nonzero if and only if the zero element is the only element common to both C_1 and C_2 [70].

6.1.3 Noisy Phase

Let us consider the problem of signal reconstruction from phase. Let C_{fsc} denote the set of signals with finite support and let

$$f = Tg = |f|\exp(j\phi), \tag{6.3}$$

where T is a linear transform operator on H. Let

$$C_{\phi} = \{ g: Tg = |Tg|\exp(j\phi)\}, \tag{6.4}$$

for given phase ϕ. By noisy phase we refer to the phase function of Tg + n, where n is some random noise function. If ϕ is noisy then C_{ϕ} and C_{fsc} may have null intersection (having only the zero element) and for high noise levels $\psi(C_{fsc},C_{\phi})$ can also be large. Note here that C_{ϕ} and C_{fsc} can be shown to be closed linear subspaces [43]. Consider now the quantised phase. Let ϕ_q denote the phase quantised to q bits and let

$$C_q = \{g: Tg = |Tg|\exp(j\phi) \text{ and } \phi \text{ when quantised to q bits is } \phi_q\}, \tag{6.5}$$

for a given ϕ_q. C_q includes the set C_{ϕ} and hence $\psi(C_q,C_{fsc}) \leq \psi(C_{\phi},C_{fsc})$. In other words the separation between C_q and C_{fsc} is not more than the separation between C_{ϕ} and C_{fsc}. Moreover the separation is lesser as the quantisation is made finer until it becomes zero. $\psi(C_q,C_{fsc})$ may never attain the zero value for high noise levels and for low noise levels it may be zero for a fine grain quantisation. The POCS method used in [67] converges to a solution such that $\cos(J(g,P_{\phi}g)) = \cos(J(C_{fsc},C_{\phi}))$, where P_{ϕ} is the projection onto the set C_{ϕ}. For high noise levels the quantised phase was found to give better results because the separation between C_{fsc} and C_q is less than that between C_{fsc} and C_{ϕ}. If $\psi(C_{fsc},C_{\phi})$ is zero for some quantisation q then making the quantisation finer will not serve any purpose since the solution set will become larger and hence the varaiance of the estimate of the solution will be large. Ideally, given noisy phase we would like to quantise the phase such that $\psi(c_{fsc},c_q)$ just attains the zero value or use 2-bit quantised phase if it does not attain the zero value. However it is difficult to decide a priori the right level of quantisation.

6.1.4 Figure of Merit for Image Reconstruction from Phase

In an earlier work [67] on image reconstruction from noisy phase of multiple frequency holograms it was shown that for many cases when the noise level is high the image reconstructed from quantised phase is better than the image reconstructed from full phase. In that study only real noise was considered. Here we shall consider complex noise. As we shall soon see, for complex noise also the image reconstructed from full phase is no better than the image reconstructed from quantised phase for high noise levels. However for low levels of noise the image reconstructed using quantised phase is a poor estimate. In this chapter we develop an algorithm based on the method of POCS for image reconstruction from noisy phase. We define a Figure Of Merit (FOM) based on phase that plays a crucial role in terminating the iterative image reconstruction procedure. Simulation studies were conducted to bring out the effectiveness of the proposed algorithm.

The rest of this chapter is organised as follows: In Section 6.2 we review the method of image reconstruction from phase of multiple frequency holograms. Iterative image reconstruction from quantised phase is also described. We define the FOM that is used to develop a condition for terminating the iterative procedure. Simulation studies using the new algorithm are presented in Section 6.3. Studies are also made for image reconstruction from quantised phase. The results show that the differences are small in images reconstructed from full phase and quantised phase even for at noise levels.

6.2 Iterative Reconstruction from Phase

6.2.1 The Method of POCS for Image Reconstruction

The reconstruction procedure is based on the method of POCS which we have seen in Chapter 1. We reproduce it here for ease of reference. Let $C_1, C_2, \ldots C_n$ be a collection of convex sets and let $P_1, P_2, \ldots, P_n$ be the projection operators onto these convex sets. To find a common element of each of these sets the following iteraive procedure may be used:

$$g_K = P_1 P_2 \ldots P_n g_{K-1}. \tag{6.6}$$

Here g_K and g_{K-1} are the estimates at the end of the K-th and (K-1)th iteration respectively. If $C_1, C_2, \ldots C_n$ are closed linear subspaces then there is at least one element namely the zero element that is common to each of these sets. Moreover the above iterative procedure converges strongly [5].

6.2.2 Image Reconstruction from Full Phase

We shall now apply this iterative procedure for image reconstruction from digital holograms. It is required to compute a signal that has finite region of support and that gives rise to the known phase data on the receiver plane at a finite number of points. The phase could be full phase or quantised phase. Let us consider full phase first. The problem may be formally stated as: Find $g(x,y) \in C_{fsc} \cap C_\phi$, where

$$C_\phi = \{g(x,y):\ h(x,y)*g(x,y) = |f(x,y)| \exp(j\phi(x,y))\} \quad (6.7)$$

Here $\phi(x,y)$ is the known phase function and $f(x,y)$ is the unknown magnitude function. It is obvious that C_{fsc} and C_ϕ are closed linear subspaces and the POCS method can be applied to compute the desired solution. The iterative procedure is obtained by substituting $P_1 = P_{fsc}$ and $P_2 = P_\phi$, with n = 2. Here P_{fsc} and P_ϕ are projection operators onto the set C_{fsc} and C_ϕ respectively.

The projection onto C_ϕ is computed as described below. Let

$$P_\phi(g(x,y)) = g_p(x,y) \quad (6.8)$$

and $G_p(u,v)$ be the Fourier transform of $g_p(x,y)$ and $G(u,v)$ the Fourier transform of $g(x,y)$. Now

$$\begin{aligned} G_p(u,v) &= G(u,v), && \text{for } u^2 + v^2 \leq 1/\lambda^2, \\ &= G_o(u,v), && \text{otherwise.} \end{aligned} \quad (6.9)$$

$G_o(u,v)$ is computed as shown below. Let

$$f_p(x,y) = h(x,y) * g(x,y) \quad (6.10)$$

$$= |f_p(x,y)| \exp(j\phi_p(x,y)) \quad (6.11)$$

and

$$\begin{aligned} f_o(x,y) &= |f_p(x,y)|\cos(\phi(x,y) - \phi_p(x,y))\exp(j(\phi_p(x,y))), \\ & \qquad \text{for } \cos(\phi(x,y) - \phi_p(x,y)) > 0, \\ &= 0, \qquad \text{otherwise.} \end{aligned} \quad (6.12)$$

Now

$$G_o(u,v) = F_o(u,v)H(u,v), \quad \text{for } u^2 + v^2 \leq 1/\lambda^2, \quad (6.13)$$

where $F_o(u,v)$ is the Fourier transform of $f_o(x,y)$. If the data $\phi(x,y)$ is known only at a finite set of points I_p then $f_o(x,y)$ may be computed as

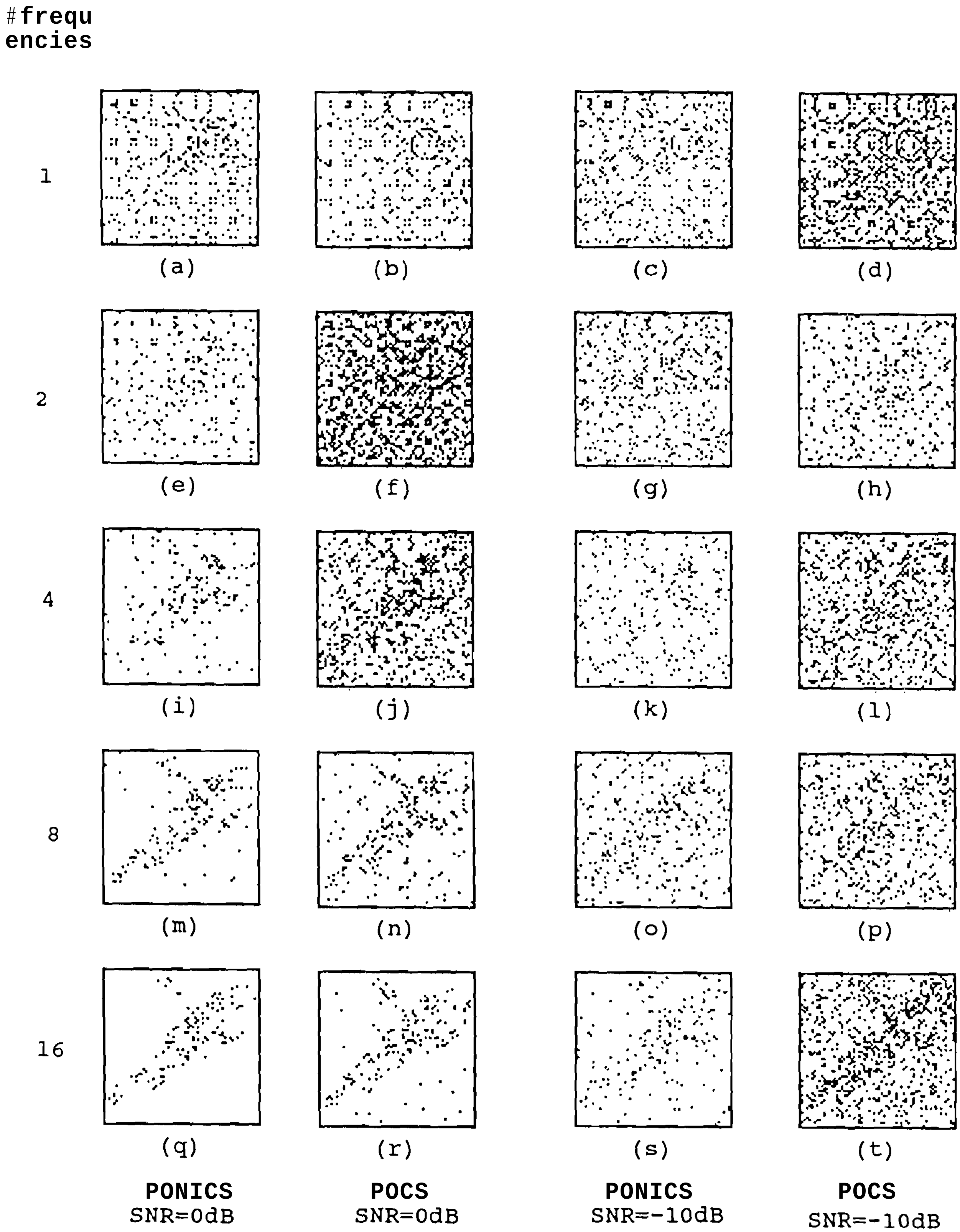

Fig.5.3 Comparison of POCS and PONICS methods for reconstruction of images from noisy sensor array data. Uniformly distributed noise is used. The data is collected from a 16x16 array at different frequencies. Comparison is made for two different SNR's.

$$f_o(x,y) = f_p(x,y), \qquad \text{for } (x,y)\in I_p,$$
$$= f_o'(x,y), \qquad \text{otherwise.} \tag{6.14}$$

Here $f_o'(x,y)$ is $f_o(x,y)$ of (6.12).

6.2.3 Quantised Phase

If only quantised phase ϕ_q is known then our problem is to compute $g(x,y) \in C_{fsc} \cap C_q$, where

$$C_q = \{g(x,y):\ h(x,y)*g(x,y) = |f(x,y)|\exp(j(\phi(x,y))) \text{ and } |\phi(x,y)-\phi_q(x,y)| \le \pi/2^q\} \tag{6.15}$$

Here ϕ_q is given as

$$\phi_q = \pi i/2^{q-1},$$
$$\text{for } \pi i/2^{q-1}-\pi/2^q \le \phi \le \pi i/2^{q-1}-\pi/2^q$$
$$\text{and } i = 0,\ 1,\ \ldots 2^q-1. \tag{6.16}$$

Note that ϕ_q is ambiguously defined for $\phi = \pi i/2^{q-1}-\pi/2^q$. In such cases we choose the lower value of i. The choice is made arbitrarily to maintain consistency. If ϕ_q is defined unambiguously incorporating the above convention then C_q will not be closed. Again it can be easily shown that C_q is a closed linear space. The following iterative procedure can be used to find $g(x,y)\in C_4 \cap C_{fsc}$:

$$g_K = P_{fsc}P_q g_{K-1}. \tag{6.17}$$

Here P_q the projection onto C_q may be computed in the same fashion as P_ϕ except that

$$f_o(x,y) = f_p(x,y),$$
$$\text{for } \phi_q(x,y)-\pi/2^q \le \phi_p(x,y) \le \phi_q(x,y)+\pi/2^q,$$
$$= f_p'(x,y), \qquad \text{otherwise,} \tag{6.18}$$

where

$$f'_p(x,y) = |f_p(x,y)|\cos(\phi_q(x,y)-\pi/2^q-\phi_p(x,y))\exp(j(\phi_q(x,y)-\pi/2^q))),$$

for

$$\cos(\phi_q(x,y)-\pi/2^q-\phi_p(x,y)) > \cos(\phi_q(x,y)+\pi/2^q-\phi_p(x,y))$$

and $\cos(\phi_q(x,y)-\pi/2^q-\phi_p(x,y)) > 0$,

$$= |f_p(x,y)|\cos(\phi_q(x,y)+\pi/2^q-\phi_p(x,y))\exp(j(\phi_q(x,y)+\pi/2^q))),$$

for

$$\cos(\phi_q(x,y)+\pi/2^q-\phi_p(x,y)) > \cos(\phi_q(x,y)-\pi/2^q-\phi_p(x,y))$$

and $\cos(\phi_q(x,y)+\pi/2^q-\phi_p(x,y)) > 0$,

$= 0$, otherwise. (6.19)

The derivation of the above equation is straightforward and has been described with an illustration in Fig.4.3. Notice that θ in Fig.4.3 is $\pi/2^q$ here and ϕ_f is ϕ_q. As in the previous case if ϕ_q is known only at a finite set of points I_p then

$$f_o(x,y) = f_p(x,y), \quad \text{for } (x,y) \notin I_p,$$
$$= f'_o(x,y), \text{ otherwise,} \tag{6.20}$$

where $f'_o(x,y)$ is the same as $f_o(x,y)$ of the previous case.

If the phase data is available at n different frequencies, that is for n different wavelengths, then the iterative procedure to compute $g(x,y) \in C_{fsc} \bigcap_{i=1}^{n} C_{\phi i}$ may be given as

$$g_K = P_{fsc}P_{\phi 1}P_{\phi 2}\cdots P_{\phi n}g_{K-1}, \tag{6.21}$$

where $P_{\phi i}$ is the projection onto the set $C_{\phi i}$ which is the set C_ϕ for a wavelength xi. Similarily if the quantised phase is available for n different frequencies then the iterative procedure to compute $g(x,y) \in C_{fsc} \bigcap_{i=1}^{n} C_{qi}$ may be given as

$$g_K = P_{fsc}P_{q1}P_{q2}\cdots P_{qn}g_{K-1}, \tag{6.22}$$

where P_{qi} is the projection onto the set C_{qi} which is the set C_q for a wavelength λ_i.

6.2.4 Description of Figure of Merit

We have just seen a detailed description of the iterative procedure. Before it can be implemented it is necessary to decide the criterion for terminating the iterative procedure. In [67] the number of iterations was chosen arbitrarily. This is not satisfactory as the number of iterations may be too few or too many to attain a certain accuracy of the result depending on the initial data. Hence we develop a FOM based on phase so that the iterative procedure can be terminated when the FOM of the result attains a predetermined value of FOM. We shall define FOM for full phase and quantised 1-bit and 2-bit phase.

For 1-bit quantised phase the FOM has been proposed in [7]. The FOM for full phase, which we propose shortly, is similar to that for quantised phase. In both cases the intuitive appeal of the FOM is that it gives a measure of how close the reconstructed signal is from the known data. The definition of FOM is based on a notion of phase metric which we shall see below.

Consider first the definition of phase metric for 1-bit quantised phase for one dimension. The result is easily extendible to 2-bit quantisation for two or more dimensions. Let s_f denote the known 1-bit phase quantisation of the received signal $f(x)$ and let s_{fo} denote the 1-bit phase quantisation of $f_o(x)$, where $f_o(x) = h(x) * g_o(x)$ and $g_o(x)$ represents the current estimate of the solution. Recall that the range of the 1-bit quantised phase of $f(x)$ is the set $\{0, \pi\}$. This corresponds to the sign of the real part of f(x). The phase metric can now be defined as

$$E_q(f,f_o) = \int e_q(f,f_o)\, dx \tag{6.23}$$

where

$$e_q(f,f_o) = 1, \quad \text{for } S_f(x) = S_{fo}(x),$$
$$= 0, \quad \text{otherwise.} \tag{6.24}$$

In the discrete case the integral may be replaced by a summation. The phase metric for 2-bit quantised phase may be defined in like manner. Recall that the range of the 2-bit phase function $S''_f(x)$ is the set $\{\pi/4, 3\pi/4, 5\pi/4, 7\pi/4\}$. This corresponds to the sign of the real and imaginary parts of $f(x)$. We can also define $e_q(f,f_o)$ as

$$e_q(f,f_o) = 2, \quad \text{for } |S''_f(x) - S''_{fo}(x)| = \pi/2,$$
$$= 1, \quad \text{for } |S''_f(x) - S''_{fo}(x)| = \pi/4,$$
$$= 0, \quad \text{otherwise.} \tag{6.25}$$

However it was felt that this added complexity will not significantly alter the results for reconstruction from quantised phase. Hence we elect to use the earlier definition (6.24).

Let us now define the phase metric for full phase. Let $\phi_f(x)$ represent the wrapped phase function of $f(x)$. Define the error function e_ϕ as

$$e_\phi(x) = 1, \quad \text{for } |\phi_f(x) - \phi_{fo}(x)| < \theta,$$
$$= 0, \quad \text{otherwise.} \tag{6.26}$$

Here the minus (-) operator represents the minimum phase angle difference and θ is a predetermined value. The phase metric can be defined, as in earlier cases, as an integral or summation of the error function. The choice of the value for θ will be discussed now. Notice that while using quantised 2-bit phase we presume or hope that the true phase could have a variation of $\pi/4$ at most from the known quantised phase. Hence for defining the phase metric for full phase we chose θ to be $\pi/4$.

The FOM may be given as

$$\epsilon = 1 - E(f,f_o)/(\int dx), \tag{6.27}$$

where $E(.)$ is $E_q(.)$ or $E_\phi(.)$ as the case may be. When the hologram is available for n frequencies the FOM may be given as

$$\epsilon = 1 - \sum_{i=1}^{n} E(f_i,f_{oi})/(n(\int dx)) \tag{6.28}$$

Again in the discrete case $\int dx$ may be replaced by the total number of known samples. In [7] the iterative procedure was terminated when FOM attains a value of 95%. Where possible we shall follow the same procedure. However if the phase is noisy the FOM may never attain a predetermined value. Hence, in such cases the iterative procedure is terminated when the FOM falls over successive iterations.

6.3 Simulation Studies

The purpose of simulation study is to demonstrate the effectiveness of the proposed iterative procedure for image reconstruction from noisy phase of multiple frequency holograms and to compare the reconstructions from full phase and quantised phase. Before we present the studies let us first describe the setup. As in previous chapters a 64x64 pixel image shown in Fig.2.1(a) is appended with zeros to form a 128x128 object plane data matrix. The data is transformed using (2.7) to obtain the wavefield distribution on the receiver plane. The distance between the object and receiver planes is 2000 units. The wavelength is 0.25 units and the sampling rate is two samples per unit distance (inter sampling distance along x and y axes is 0.5

units).

In the first of the studies we shall use all the receiver elements (128x128) in the reconstruction of an image. To begin with let us consider noise free data. Fig.6.1(a) and Fig.6.1(e) show the images reconstructed from full phase and 2-bit quantised phase respectively. In both cases the quality of the reconstructed image is good. This shows that 2-bit quantised phase is sufficient to derive the image in most cases. The experiment is repeated with zero mean Gaussian distributed random complex noise added to the signal. We shall consider three noise levels, namely 0dB, -10dB and -30dB. Fig.6.1(b) shows the reconstructed image using phase only when the noise level is 0dB. Fig.6.1(f) shows the reconstruction for the same noise level from quantised 2-bit phase. Fig.6.1(c) and Fig.6.1(g) show the results using full and quantised phase when the noise level is -10dB and Fig.6.1(d) and Fig.6.1(h) show the results using full and quantised phase when the noise level is -30dB. Notice that as the noise level increases the quality of the image reconstructed degrades significantly. Moreover at a high noise level (SNR = -10dB) the image reconstructed from full phase is no better than the image reconstructed from quantised pahse. This goes to confirm our earlier study[67] where a similar result was obtained for real noise.

We will now present the results obtained using noisy sparse data collected at multiple frequencies. Fig.6.2 and Fig.6.4 show the results of using full phase for various array sizes and multiple frequencies for SNR=0dB and SNR=-10dB, respectively. Fig.6.3 and Fig.6.5 show the corresponding results using 2-bit quantised phase for various array sizes and multiple frequencies. The figures show that as the number of frequencies are increased the quality of the reconstructed image improves. Moreover the image reconstructed from 2-bit quantised data is in general no worse than the image reconstructed from full phase data for the same array size and number of frequencies.

Fig.6.2(a) shows the image reconstructed using a 64x64 array with only one frequency (λ=0.25). Fig.6.2(e) shows the image reconstructed using two frequencies (λ=0.25,0.26) for the same array. Fig.6.2(i) shows the result of using four frequencies (λ=0.25,0.26,...0.28). Fig.6.2(m) shows the image reconstructed using eight frequencies and Fig.6.2(q) shows the result of using sixteen frequencies (λ=0.25,0.255,...,0.325). Notice that the quality of the image reconstructed improves as the number of frequencies are increased. Fig.6.2(b), Fig.6.2(f), Fig.6.2(j), Fig.6.2(n) and Fig.6.2(r) show the images reconstructed from full phase using one, two, four, eight and sixteen frequencies respectively with data collected on a 32x32 array. Fig.6.2(c), Fig.6.2(g), Fig.6.2(k), Fig.6.2(o) and Fig.6.2(s) show the images reconstructed from full phase using one, two, four, eight and sixteen frequencies respectively with data collected using a 16x16 array. It can be seen that as the number of samples are reduced the quality of the image reconstructed degrades significantly. In fact with only 16x16 samples the reconstructed image is barely visible even if the number of frequencies are sixteen. The images reconstructed from an 8x8 array is not visible at all even if we use sixteen frequencies as can be seen from Fig.6.2(t). Fig.6.2(d), Fig.6.2(h), Fig.6.2(1), Fig.6.2(p) and Fig.6.2(t) show the images reconstructed from full phase using one, two, four, eight and sixteen frequencies respectively with data collected on a 8x8 array.

Let us now consider quantised phase. Fig.6.3 shows the image reconstructed using 2-bit quantised phase. Fig.6.3(a) to Fig.6.3(t) are the same as Fig.6.2(a) to Fig.6.2(t) except that only 2-bit quantised phase is used. Fig.6.4 and Fig.6.5 show the results using full phase and quantised 2-bit phase respectively for various array sizes and multiple frequencies. The SNR is -10dB in both cases. Note that in most cases the image reconstructed from 2-bit cases is as good as the image reconstructed from full phase.

A study was made for image reconstruction from noisy phase without the use of the FOM. It was found that for sufficiently noisy data the iterative procedure begins to diverge after a few iterations. Specifically, using a 64x64 array with sixteen frequencies the iterative procedure tends to diverge after 20 iterations if the SNR is -10dB or less. For 2-bit quantised phase the divergence in the FOM sense occurs after many more iterations. These studies indicate that it is possible to reconstruct a good quality image from phase only. Moreover the two most significant bits of the phase seem to carry most of the information of the signal. By quantising the phase we appear to be rejecting more noise than signal information. Hence in some cases the image reconstucted using quantised phase gives results that are comparable in quality to that obtained from full phase. However the amount of computation required for obtaining an acceptible quality of the image for 2-bit quantised phase is somewhat higher. But the reduction in measurement complexity due to quantising the phase more than offsets the increase in computation.

6.4 Conclusion

In this chapter we have addressed the problem of image reconstruction from noisy phase with special emphasis on signal recovery from multiple frequency digital holograms. An iterative algorithm based on the method of POCS was applied. A FOM for phase was proposed. This FOM was used to develop a condition for terminating the iterative signal reconstruction procedure. It was pointed out that the iterative procedure converges to a solution (perhaps the trivial solution) in the l^2 norm. Since for noisy data the trivial solution may be the only solution, the iterative procedure was terminated when the FOM fails to improve over succesive iterations.

Simulation studies were conducted using noisy phase. Both full phase and quantised phase were used. It was found that the image reconstructed from 2-bit quantised phase was no worse than that reconstructed from full phase for high noise levels (SNR= -10dB). We also confirmed the earlier reported result [67] that increasing the number of frequencies significantly improves the quality of the reconstructed image. It was verified that after a certain number of iterations the solution tends to diverge if the procedure is continued indefinitely.

The fact that we have not been able to obtain better quality images from full phase than from the same phase quantised to 2 bits indicates that we have not been able to make effective use of full phase information. Hence we conjecture that there must be better algorithms for image reconstruction from noisy phase.

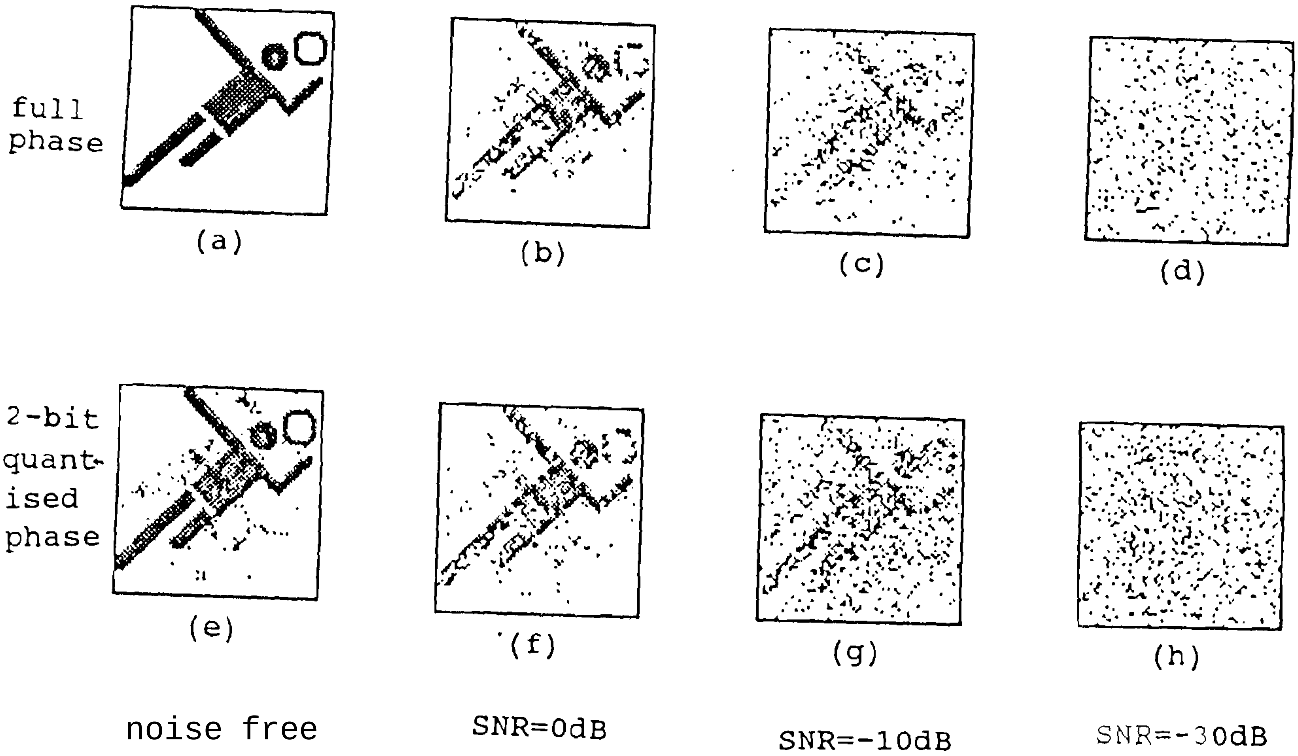

Fig.6.1 Image Reconstruction from full and quantised phase for four different noise levels. All the receiver elements (128x128) are used in the reconstruction. The figure shows that the image reconstructed from quantised phase is as good as the image reconstructed from full phase at high noise levels.

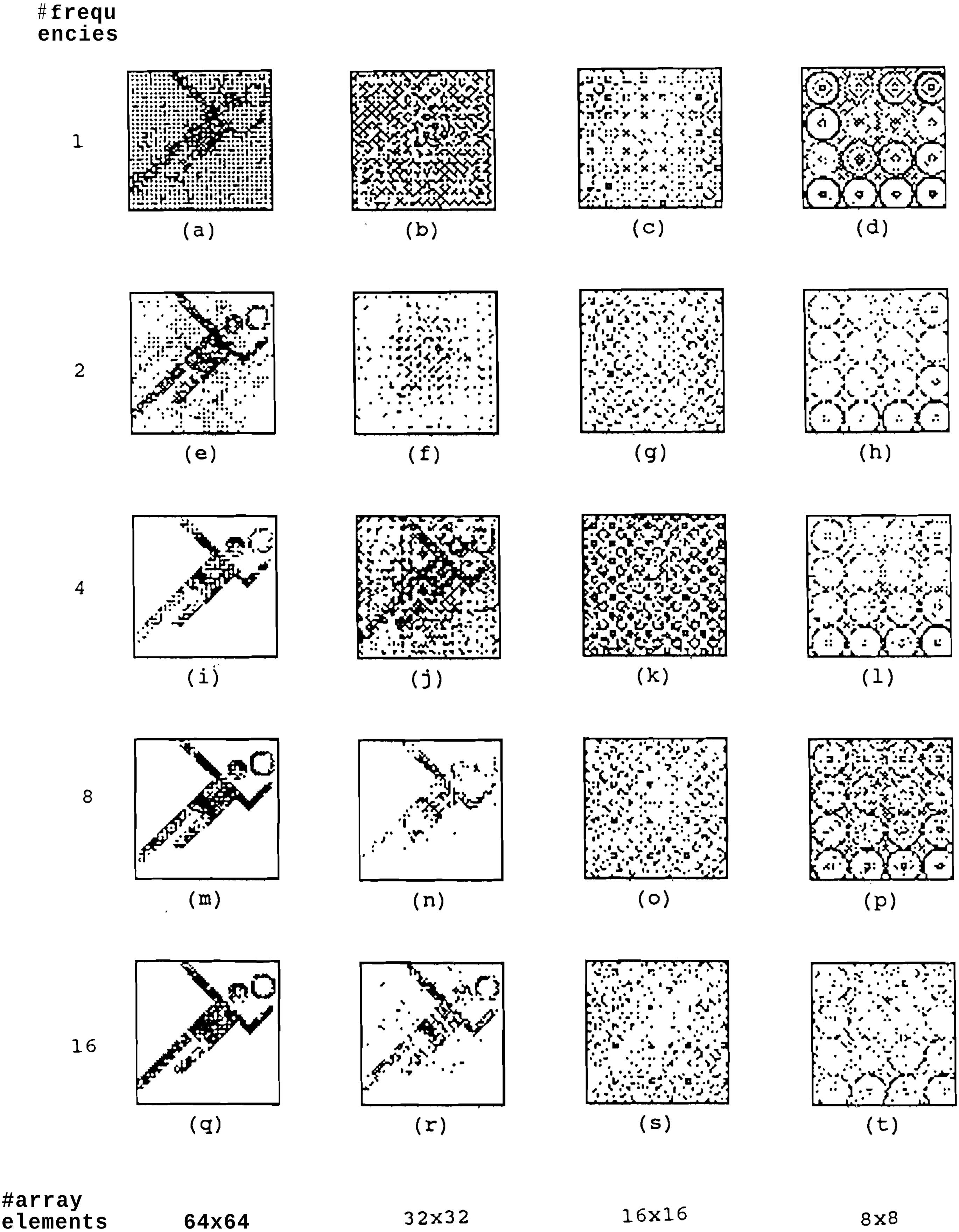

Fig.6.2 Image reconstructed from full phase for SNR=0dB using sparse data collected at multiple frequencies. The figure demonstrates that it is possible to reconstruct an acceptable quality image from phase alone.

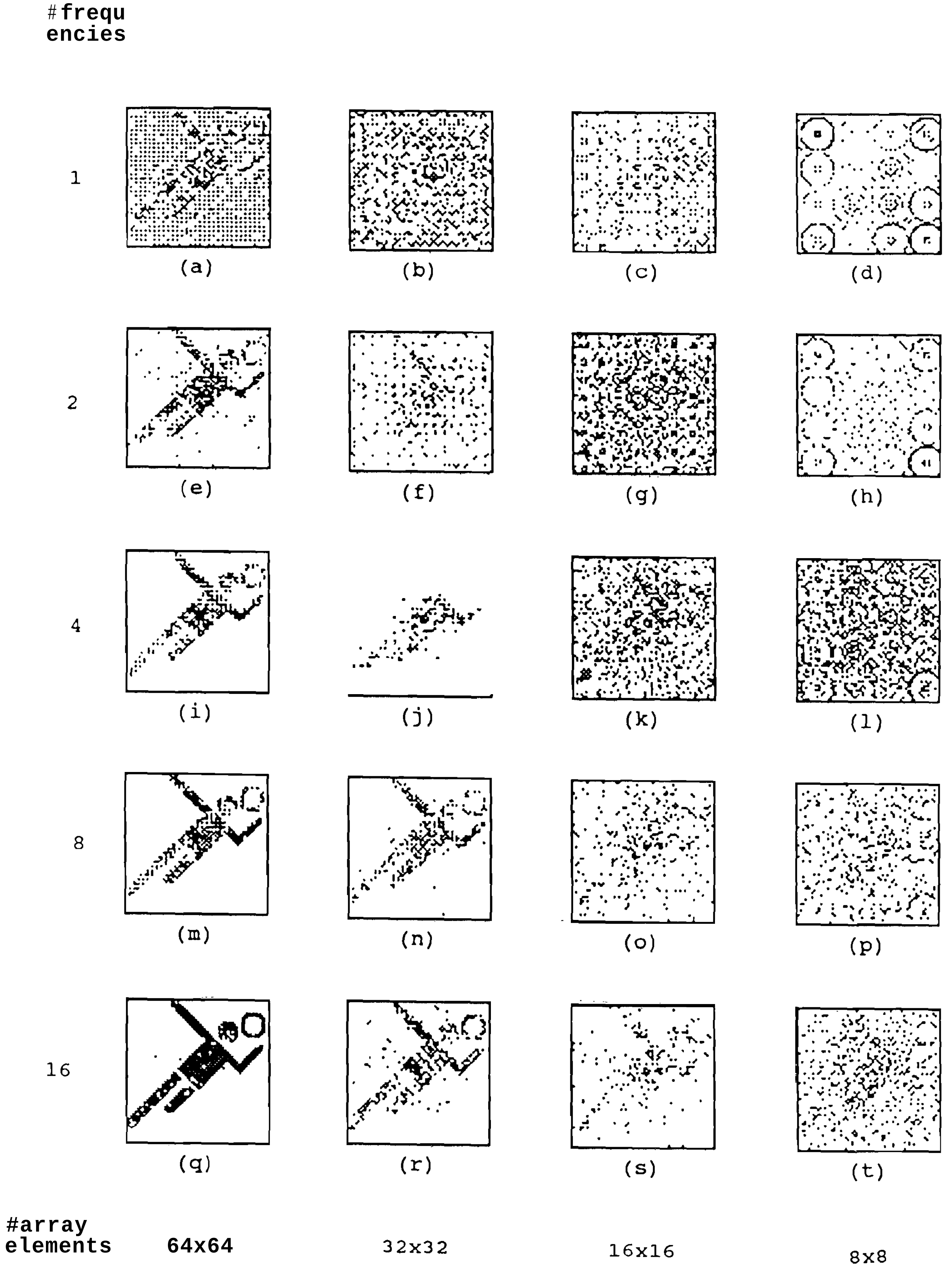

Fig.6.3 Image reconstructed from 2-bit phase for SNR=0dB using sparse data collected at multiple frequencies. The figure demonstrates that it is possible to reconstruct an acceptible quality image from 2-bit quantised phase.

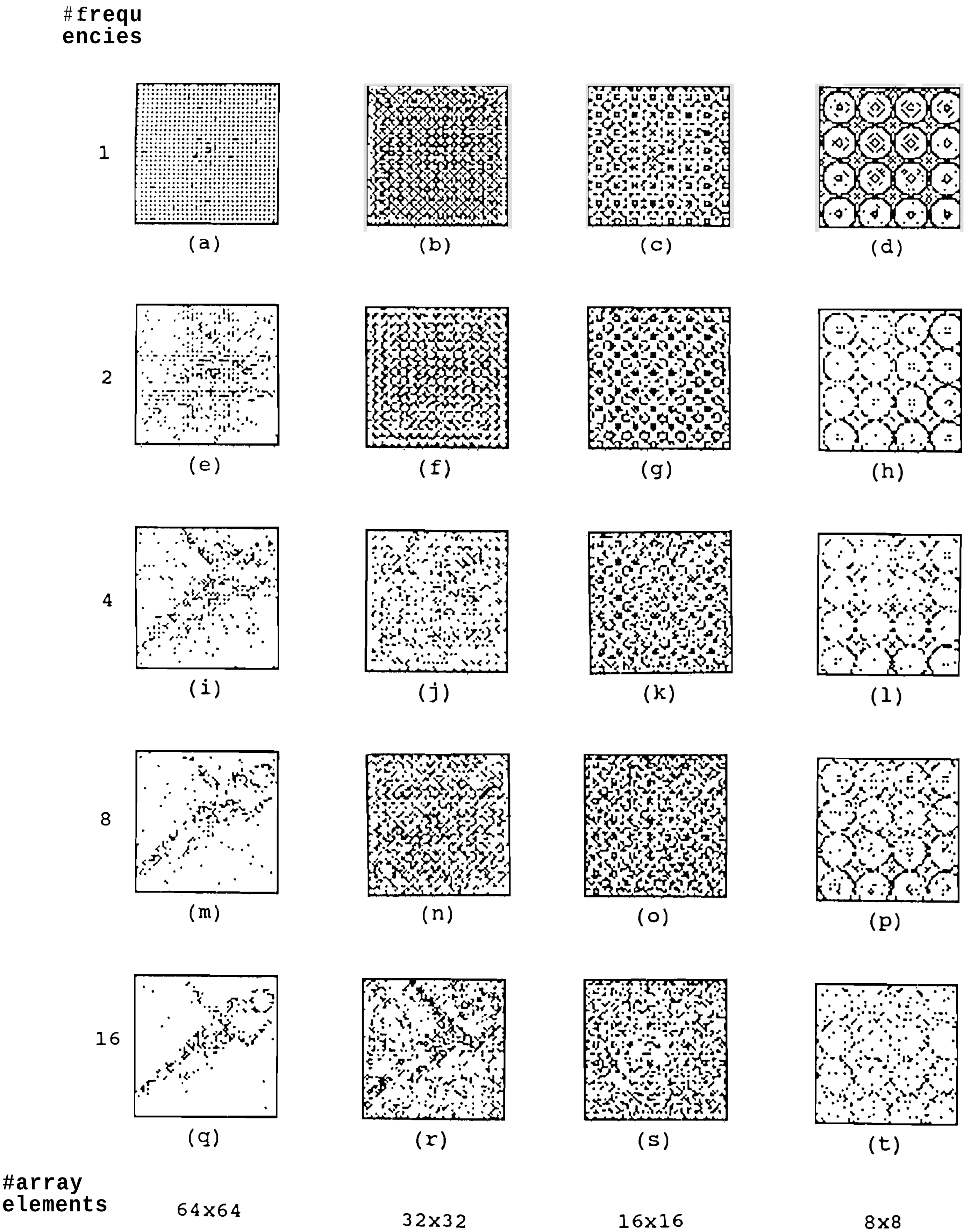

Fig.6.4 Image reconstructed from full phase for SNR=-10dB using sparse data collected at multiple frequencies. The quality of the image reconstructed degrades as the noise level is increased.

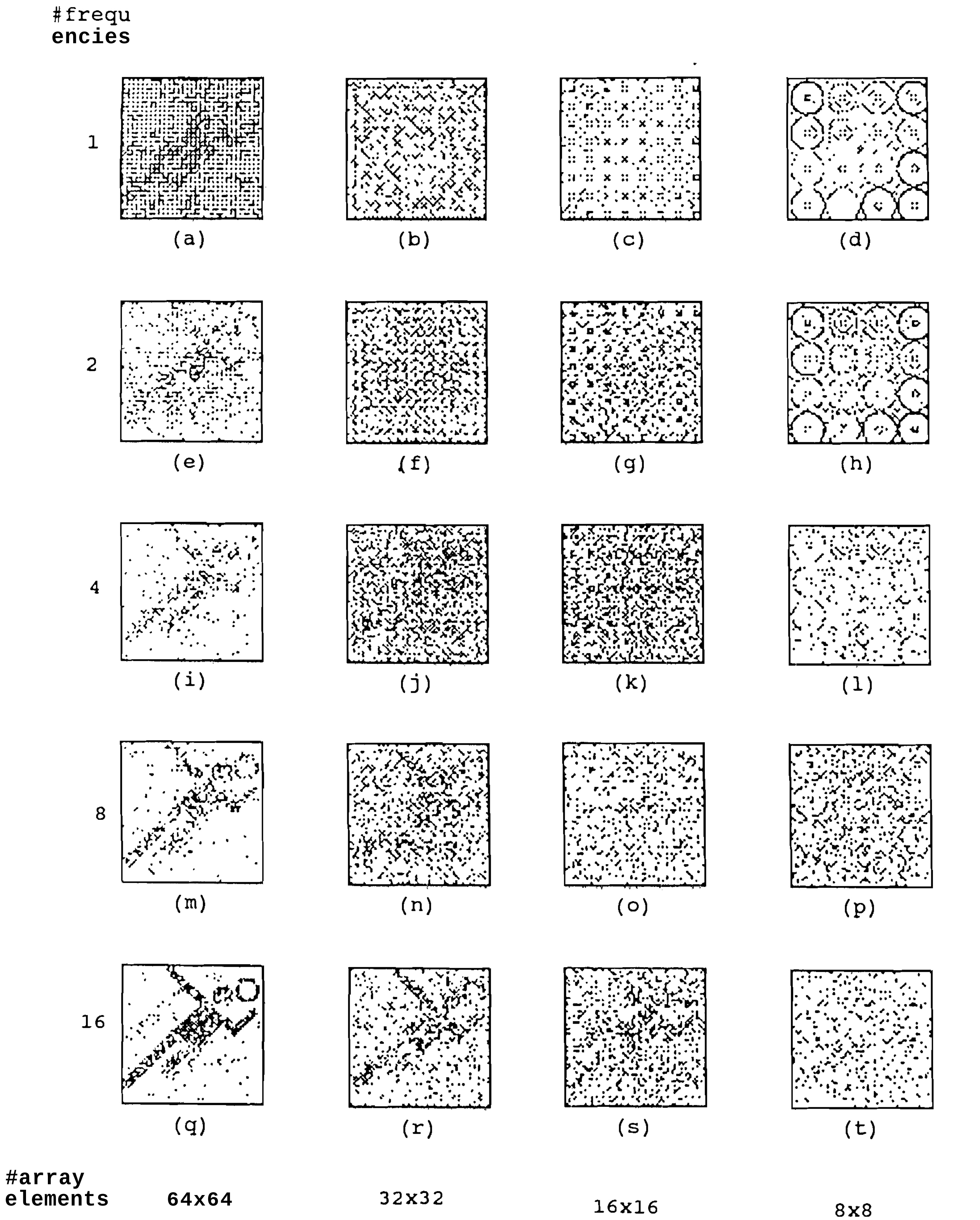

Fig.6.5 Image reconstructed from 2-bit phase for SNR=-10dB using sparse data collected at multiple frequencies. The quality of the image reconstructed from 2-bit quantised phase is no worse than that reconstructed from full phase for most cases.

Chapter **7**

SUMMARY AND CONCLUSIONS

7.1 Problem in Sensor Array Imaging

In this chapter we shall sum up the thesis, point out its achievements and discuss directions for further study. A brief discussion of the main contributions of this work is given in this section. A summary' of the thesis follows in the next section. In the third section we discuss some related issues not addressed in this thesis. Some suggestions to investigate these issues are also given.

The aim of this thesis has been to investigate the problem of information recovery from partial data. Specifically, we have considered the case when the initial data was available in different domains and the knowledge of some characteristic of the signal is known a **priori.** We found that an iterative procedure like POCS could be applied to solve such a problem if a solution existed.

When the initial data is noisy there may exist no solution to the originally stated problem. Hence we have relaxed the constraint that the reconstructed signal should satisfy the initial data exactly. We have computed a feasible solution. The method of PONICS gives another solution to the problem of signal recovery from noisy data. This method was shown to converge even for certain instances when the method of POCS might fail to do so. Our studies on the problem of signal reconstruction from noisy phase show that the existing algorithms are inadequate to recover the information from the given data, since quantised phase in many instances gives better results than full phase. In short, our conclusion is that an iterative procedure like POCS can be applied to compute a solution satisfying some constraints. Note that previous approaches considered a well-posed problem, whereas here we have addressed ill-posed problems.

The problem addressed is one of inverse transformation where the solution set is the space of piecewise continuous functions that vanish outside a compact region of support. The problem could be addressed in one dimension but the aim was to develop algorithms that make use of the characteristics of image function so as to judge if the least squares solution is close to the desired solution from the point of view of human perception. Furthermore the specific problem addressed, namely the digital holography, is related to some practical applications like underwater acoustic imaging and acoustic microscopy. Hence all studies were made with regard to two dimensions.

7.2 Summary of the Thesis

In Chapter 2 we have seen that hologram formation could be viewed as a convolution or a Fresnel/Fourier transform. Although the latter transform is computationally less intensive since it requires the computation of only one Fourier transform, the method of convolution is more suitable for iterative algorithms due to sampling considerations. We have also seen that phase the phase of the received data plays a more important part in the reconstruction than the magnitude.

In Chapter 3 we have considered the problem of sparse data.

We have shown how to combine data from multiple frequencies. Simulation studies show the effectiveness of the proposed method.

In Chapter 4 we have dealt with errors in the measurement of signal. We have shown that the method of POCS which was applied in the previous chapters could be applied here too, though not in the same way. The method as applied in the previous chapters may not converge, as there may exist no signal with the known compact region of support that could have given rise to known data when there is noise in the signal. The method applied here is to obtain a convex set which includes all the functions which could have given rise to the known data subject to some bounded error. This method works well if the error bound is known accurately and fails to work otherwise. This is especially true in the case of multispectral holograms. If the known value of the error bound is larger than the actual value, then the variance of the computed estimate of the signal will be large. If it is less, then the iterations may not converge at all. To take care of such problems the method of PONICS was developed in Chapter 5.

The method of Projection Onto NonIntersecting Convex Sets (PONICS) was meant to deal with the situation when the convex sets are nonintersecting. Consider the example of two convex sets C_1 and C_2, where C_1 is compact. If C_1 and C_2 have nonempty intersection, then the method of POCS will diverge. The aim is to compute a point in C_1 that is closest to an element of C_2. It was shown that such a solution is a quasisolution.

If the number of sets are more than two, then the quasisolution may not be definable. Simulation studies were performed to compare the results obtained by the method of Projection Onto Convex Sets (POCS) and the method of PONICS. The studies have shown that even when the noise statistics are accurately known, the quality of the results obtained by the two methods are not significantly different. Moreover the method of PONICS was found to converge faster. A comparison of the sequential and parallel methods of implementation of PONICS did not bring out any significant difference in the quality of the images reconstructed by the two implementations, although the parallel method was found to converge slower in many cases.

In Chapter 6 the problem of image reconstruction from the noisy phase of digital holograms was addressed. A figure of merit for the goodness of an image reconstructed from full and quantised phase was suggested. It was found that image reconstructed from quantised phase gives results that are as good or even better in quality as those reconstructed from full phase.

7.3 Suggestions for Further Study

A simplified model of digital hologram setup was used in our studies to develop methods for image reconstruction from sparse data. In practice a holographic setup has several problems such as diffraction, medium disturbance, frequency shift, nonlinear effects, etc. Some of these factors may severly affect the performance of the methods developed in the thesis for image reconstruction from partial data. Efforts have to be made to incorporate these factors in a systematic way in simulation studies.

The method of PONICS attempts to solve the problem of signal reconstruction from noisy initial data. It is an extension of the method of POCS to the case when the convex sets have no intersection in common. We have shown that the method converges, although we have not been able to precisely characterise the nature of the solution. It is our belief that no precise characterisation can be given in a general case. However it may be possible to do so for particular instances. Notice that for the case of two convex sets we have shown that the method converges to a quasisolution.

In the problem of signal reconstruction from phase we found that in many cases the image reconstructed from quantised phase is as good as the image reconstructed from full phase. This implies that we have not been able to make full use of the less significant bits of phase information. Hence efforts must be made to find a better solution to this problem.

In this thesis we have examined the problems in image recontruction from sparse data, from noisy sparse data and from partial noisy sparse data. As the data becomes less and less reliable, the problem of image reconstruction becomes more ill-posed. Also it becomes progressively difficult to formally characterise these situations. Therefore one has to rely on visual observation of the image to assess the performance of any method for image reconstruction.

HILBERT SPACES

A brief introduction to the theory of Hilbert Spaces is given here. The depth of treatment will be enough to follow the references to Hilbert Spaces in this work. Most of the material in this section is from [24]. We will first define a metric space. Then we will define a normed space and then state the definition of the L^2 normed space we are dealing with. Finally we will define the Hilbert space.

A metric space is a pair (X,ρ) where X is a set and ρ is a metric on X (also known as distance function), that is, ρ is a real valued function on $X \times X$, such that for all x,y,z in X,

(i) $\rho(x,y) \geq 0$,

(ii) $\rho(x,y) = 0$, if and only if $x = y$

(iii) $\rho(x,y) = \rho(y,x)$ (symmetry)

(iv) $\rho(x,y) \leq \rho(x,z) + \rho(z,y)$ (triangular inequality)

A sequence $\{x_n\}$ in a metric space (X,ρ) is said to be Cauchy if for every $e > 0$ there is an $N = N(e)$ such that

$\rho(x_n,x_m) < e,$ for every $m,n > N$.

The space X is said to be complete if every Cauchy sequence converges to a limit in X.

A vector space is nonernpty space X with two algebraic operations namely vector addition and multiplication of vectors by scalars.

A norm on a vector space is a real valued function whose value at $x \in X$, denoted by $\|x\|$, has the following properties:

(i) $\|x\| \geq 0$

(ii) $\|x\| = 0$, if and only if $x=0$

(iii) $\|a\cdot x\| = |a|.\|x\|$, where a is any scalar

(iv) $\|x + y\| \leq \|x\| + \|y\|$ (triangular inequality).

$\rho(x,y) = \|x - y\|$ is called the metric induced by the norm.

Let $L^2[0,1]$ be the set of all functions square integrable over $[0,1]$. Hence for $x(t)\in L^2[0,1]$, $\|x\|$ is defined as

$$\|x\| = \left(\int_0^1 |x(t)|^2 dt \right)^{1/2} \blacksquare$$

However $L^2[0,1]$ is not a normed space. This can be seen considering two functions x_1, x_2 which differ at a finite or countable number of points. Here $\|x_1-x_2\| = 0$ although $x_1 \neq x_2$.

Let $M = \{x: \|x\|=0\}$. x_1 and x_2 are equivalent, if $(x_1-x_2)\in M$. This equivalence relation induces a partition of $L^2[0,1]$ into pairwise disjoint class of sets. Let y denote a representative of one of these sets. The set of all such y is called the quotient set denoted by $L^2[0,1]/M$. Now $L^2[0,1]/M$ is a normed vector space.

An inner product on X is a mapping of $X\times X$ onto a scalar field (real or complex) and is denoted as $<x,y>$ with the following properties:

(i) $<x+y,z> = <x,z> + <y,z>$

(ii) $<ax,y> = a<x,y>$, where 'a' is a scalar,

(iii) $<x,y> = <y,x>^*$, where * denotes complex conjugate

(iv) $<x,x> \geq 0$

(v) $<x,x> = 0$, if and only if $x = \Theta$.

An inner product on X defines a norm $\|x\|$, given by $\|x\|=<x,x>^{1/2}$. An inner product space is a vector space X with an inner product defined on X. A Hilbert space is a complete inner product space.

REFERENCES

1. C.Andrews and B.R.Hunt, Digital Imase Restoration, Prentice-Hall, New York, 1977.
2. L.M.Bregman, 'Finding the Common Point of Convex Sets by the Method of Successive Projections,' Dokl. Akad. Nauk SSSR, vol.162, no.3, 1965.
3. J.P.Burg, 'Maximum Entropy Spectral Analysis,' in Modern Spectrum Analysis, D.G.Childers, Ed., IEEE Press, pp.34-41, 1978.
4. J.A.Cadzow, 'Signal Enhancement - A Composite Property Mapping Algorithm,' IEEE Trans. Acoust., Speech, Signal Processing, vol.ASSP-36, no.1, Jan. 1987.
5. R.T.Chin, C.-L.Yeh, and W.S.Olson, 'Restoration of Multi-Channel Microwave Radiometric Images', IEEE Trans. Pattern Anal., Mach. Int., vol.PAMI-7, no.4, July 1986.
6. A.J.Devaney, 'Geophysical Diffraction Tomography',IEEE Trans. Geosci., Remote Sensing, vol.GE-22, pp.3-13, Jan. 1984.
7. C.Y.Epsy and J.S.Lim, 'Effects of Additive Noise on Signal Reconstruction from Fourier Transform Phase', IEEE Trans. Acoust., Speech, Signal Processing, vol.ASSP-31, no.4, Aug. 1983.
8. J.R.Feinup, 'Phase Retreival Algorithms : A Comparison,' Appl. Opt., vol.21, pp.2758-2769, 1978.
9. B.R.Frieden, 'Restoring with Maximum Likelihood and Maximum Entropy,' J. Opt. Soc. Amer., vol.62, no.4, pp.511-518, 1972.

R.W.Gerchberg, 'Superresolution Through Error Energy Reduction,' Opt.Acta, vol.21, no.4, Sept. 1974.

11. J.W.Goodman, Introduction to Fourier Optics, McGraw Hill, New York, 1968.

12. J.F.Greenleaf and R.C.Bak,'Clinical Imaging with Transmissive Ultrasonic Computerised Tomography,' IEEE Trans. Biomed. Engg., vol.BME-28, pp177-185, 1981.

13. M.Goldburg and R.J.Marks II, 'Signal Synthesis in the Presence of an Inconsistent Set of Constraints,' IEEE Trans. Circuits Syst., vol.CAS-32, no.7, July 1985.

14. L.K.Gubin, B.T.Polyak and E.V.Raik, 'The Method of Projections for Finding the Common point of Convex Sets,' USSR J. Comp. Math., Math. Phy., vol.7, no.6, 1967.

15. H.F.Harmuth, Acoustic Imaging with Electronic Circuits, Advances in Electronics and Electron Physics, New York, Academic Press, 1979.

16. M.H.Hayes, 'The Reconstruction of a Multi-dimensional Signal from the Phase or Magnitude of its Fourier Transform,' IEEE Trans. Acoust., Speech, Signal Processing, vol.ASSP-30, April 1982.

17. M.H.Hayes, ' The Unique Reconstruction of Multidimensional Sequences from Fourier Transform Phase or Magnitude,' in Imase Recovery: Theory and Applications, H.Stark, Ed., Academic Press, Orlando, 1987.

18. S.Haykin, Adaptive Filter Theory, Prentice-Hall, Englewood Cliffs, New Jersey, 1986.

19. T.T.Huang, J.L.C.Sanz and W.-E. Blanz, 'Image Representation by One-Bit Fourier Phase: Theory, Sampling and Coherent

Image Models,' IEEE Trans. Acoust., Speech, Signal Processing, vol.ASSP-36, Aug. 1988.

20. V.Istracetsu, Fixed Point Theorems, D.Reidel Publishing Co., Dordrecht, Holland, 1981.

21. J.A.Johnson and B.A.Barna, 'Effects of Surface Mapping Corrections with Synthetic Aperture Techniques on Ultrasonic Imaging,' IEEE Trans. Sonics, Ultrason., vol.SU-5, no.5, Sept. 1983.

22. A.C.Kak, 'Tomographic Imaging with Diffracting and NonDiffracting Sources,' in Array Sisnal Processing, S.Haykin, Ed., renti ice-Hall, Englewood Cliffs, New Jersey, 1985.

23. P.N.Keating and T.Savatari, 'Signal Processing in Acoustic Imaging,' Proc. IEEE, vol.67, no.4, Apr. 1979.

24. L.W.Kessler and D.E.Yukas, 'Acoustic Microscopy-1979', Proc. IEEE, vol.67, pp526-536, April 1979.

25. E.Kreysig, Introductory Functional Analysis with Awwlications, John Wiley & Sons, New York, 1979.

26. E.V.Krishnamurthy and A.K.Sen, Numerical Alsorithms, Affliated East-West Press Pvt. Ltd., New Delhi, 1986.

27. H.Lee and G.Wade, 'Phase Only Holograms,' IEEE Sonics, Ultrason., vol.SU-28, June 1987

28. A.Levi and H.Stark, 'Signal Restoration from Phase by Projection Onto Convex Sets', J.Opt.Soc.Amer., vol.73, no.6 June 1983.

29. D.G.Luenberger, Optimization by Vector Space Methods, Wiley, New York, 1969.

30. J.Maeda and K.Murata, 'Image Restoration of Incoherent

Bandlimited Images,' App. Opt., vol.21, pp.2129, 1982.

31. J.Maeda and K.Murata, 'Image Restoration by an Iterative Regularised Pseudo Inverse Method,' Applied. Opt., vol.23, pp.857, 1984.

32. G.A.Merchant and T.W.Parks, 'Reconstruction of Signals from Phase: Efficient Algorithms, Segmentation, and Generalisations,' IEEE Trans. Acoust., Speech, Signal Processing, vol.ASSP-31, no.5, Oct. 1983.

33. Miller K., Complex Stochastic Processes, New York, Prentice-Hall, New Jersey, 1975.

34. R.K.Mueller, 'Acoustic Holography,' Proc. IEEE, vol.59, pp.1319-1335, Sept. 1971.

35. C.E.Morris, M.A.Richards and M.H.Hayes, 'Fast Reconstruction of Linearly Distorted Signals,' IEEE Trans. Acoust., Speech, Signal Processing, vol.ASSP-36, Jul. 1988.

36. J.Nakayama, H.Ogura and M.Fjivara, 'Multiple Frequency Hologram and its Application to Two Dimensional Imaging,' Proc. IEEE, vol.66, no.10, Oct. 1978.

37. A.V.Oppenheim and J.S.Lim, 'The importance of Phase in Signals,' Proc. IEEE, vol.69, no.5, pp.529-541, May 1980.

38. A.Papoulis, Signal Analysis, McGraw Hill, New York, 1975.

39. A.Papoulis, 'A New Algorithm in Spectral Analysis and Bandlimited Signal Extrapolation,' IEEE Trans. Circuits, Syst., vol.CAS-22, Sept. 1978.

40. I.Pitas and A.N.Venetsanopoulos, 'Bayesian Estimation of Medium Properties in Wavefield Downward Extrapolation Problems', IEEE Trans. Acoust., Speech, Signal Processing, vol.ASSP-36, May 1988.

I.Pitas and A.N.Venetsanopoulos, 'Bayeasian Estimation in Seismic Migration,' IEEE Trans. Acoust., Speech, Signal Processing, vol.ASSP-36, Feb. 1988.

42. T.Poggio and V.Torre, '111-Posed Problems and Regularisation in Early Vision,' AI memo-773, Massachussets Institute of Technology, Cambridge, April 1984.

43. J.P.Powers and D.E.Mueller, 'A Computerized Acoustic Imaging Technique Incorporating Automatic Object Recognition,' in Acoustical Holography, vol.5, P.S.Green, Ed., Plenum Press, New York, pp.527-539, 1974.

44. W.L.Root, 'Ill-Posedness and Object Field Reconstruction Problems,' J.Opt.Soc.Amer. A, vol. 4, no. 1, Jan. 1987.

45. A.Rosenfeld, A.C.Kak, Digital Picture Processing, 2nd ed., Vol.1, Academic Press, New York, 1982.

46. Pramod Saini, Algorithms for Imase Reconstruction from Quantised Phase, M.S.Thesis, Dept. of Comp. Sc. and Engg., I.I.T., Madras, May 1988.

47. J.L.C.Sanz and T.S.Huang, 'Unique Reconstruction of a Band-limited Signal from Phase or Magnitude,' J.Opt.Soc. Amer., vol.73, no.11, Nov. 1983.

48. J.L.C.Sanz, F.Cukierman and T.S.Huang, 'Stability of Unique Fourier Transform Phase Reconstruction,' J.Opt.Soc.Amer., vol.73, no.11, Nov. 1983.

49. T.Sato and O.Ikada, 'Superresolution Ultrasonics Imaging Method by Combined Spectral and Synthetic Aperture Synthesis,' J. Acoust. Soc. Amer., vol.62, no.2, Feb. 1977.

50. R.W.Schafer, R.M.Mersereau and M.A.Richards, 'Constrained Iterative Deconvolution Algorithms,' Proc. IEEE, vol.69,

no.2, pp.432-450, April 1980.

51. M.I.Sezan and H.Stark, 'Image Restoration by the Method of Projection Onto Convex Sets: Part 2 - Applications and Numerical Results,' IEEE Trans. Medical Imag., vol.MI-1, no. 2, Oct. 1982.

52. M.I.Sezan and H.Stark, 'Image Restoration by Convex Projections in the Presence of Noise', Applied Optics, vol.22, pp.2782-2789, 1983.

53. D.M.Simmons, <u>Nonlinear Programming for Operations Research</u>, Prentice-Hall, Englewood Cliffs, New Jersey, 1975.

54. H.Stark, D.Cahana and H.Webb, 'Restoration of Arbitrary Finite Energy Optical Objects from Limited Spatial and Spectral Information', J. Opt. Soc. Amer., vol.71, no.6, June 1981.

55. L.Sutton, 'Underwater Acoustic Imaging', Proc. IEEE, vol.74, no.4, April 1979.

56. F.L.Thurstone and H.E.Melton Jr., 'Biomedical Ultrasonics,' IEEE Trans. Ind. Electron., Control, Instrum., vol.IECI-17, pp.167-172, 1970.

57. A.N.Tikhonov and V.Y.Arsenin, <u>Solutions to Ill-Posed Problems</u>, John Wiley, New York,1975.

58. A.N.Tikhonov, A.V.Goncharsky and V.V.Stepanov, 'Inverse Problems in Image Processing,' in <u>Applications of Ill-Posed Problems in Natural Sciences</u>, A.N.Tikhonov, A.V.Goncharsky Ed., Mir Publishers, Moscow, 1987.

59. V.T.Tom, T.F.Quatieri, M.H.Hayes and J.H.McClellan, 'Convergence of Iterative Nonexpansive Signal Reconstruction Algorithms,' IEEE Trans. Acoust., Speech, Signal Processing,

vol.ASSP-29, Oct. 1981.

60. H.J.Trussel and M.R.Civanlar, 'The Feasible solution in Signal Restoration,' IEEE Trans. Acoust., Speech, Signal Processing, vol.ASSP-32, April 1984.

61. P.H.Winston, Artificial Intellisence, Addison-Wesley, New York, 1980.

62. S.J.Wernecke and L.R.D'Adddario, 'Maximum Entropy Image Reconstruction,' IEEE Trans. Comput., vol.C-26, April 1977.

63. N.S.Yaroslavski and L.P.Merzlyakhov, Methods of Digital Holography, Trans. from Russian Consultants Bureau, New York, 1980.

64. B.Yegnanarayana, C.P.Mariadassou and Pramod Saini, 'Signal Reconstruction from Partial Information for Acoustic Imaging Applications,' presented at IEEE ASSP, EURASIP V Workshop on MDSP, Noordjwickout, The Netherlands, Sept. 14-16, 1987.

65. B.Yegnanarayana, C.P.Mariadassou and Pramod Saini, 'Studies on Reducing the Receiver Complexity in Acoustic Imaging,' EUSIPCO, Sept.2-5, 1988.

66. B.Yegnanarayana, C.P.Mariadassou and Pramod Saini, 'Image Reconstruction from Sensor Array Data,' presented at the Indo-US Workshop, Bangalore, India, Jan.11-14, 1988.

67. B.Yegnanarayana, C.P.Mariadassou and Pramod Saini, 'Signal Reconstruction from Partial Data for Acoustic Imaging Applications,' Signal Processing, Feb. 1990.

68. B.Yegnanarayana, D.K.Saikia and T.R.Krishnan, 'Significance of Group Delay Functions in Signal Reconstruction from Spectral Magnitude and Phase,' IEEE Trans. Acoust., Speech, Signal Processing, vol.ASSP-31, no.3, June 1983.

69. K.Yosida, Functional Analysis, Springer-Verlag, New York, 1965.

70. D.C.Youla, 'Generalized Image Restoration by the method of Alternating Orthogonal Projections,' IEEE Trans. Circuits Syst., vol.CAS-25, Aug. 1978.

71. D.C.Youla and H.Webb, 'Image Restoration by the Method of Convex Projections : Part I-Theory', IEEE Trans. Medical Imag., vol.MI-1, no.2, Oct. 1982.

72. D.C.Youla, 'Mathematical Theory of Image Restoration by the Method of Convex Projections,' in Image Recovery: Theory and Applications, H.Stark, Ed., Academic Press, Orlando, 1987.

73. D.C.Youla and V.Velasco, 'Extensions of a Result on the Synthesis of a Signal in the Presence of Inconsistent Constraints,' IEEE Trans. Circuits Syst., vol.CAS-33, no.4, April 1986.

74. X.Zhuang, E.Østevold and R.M.Haralick, 'A Differential Equation Approach to Maximum Entropy Image Reconstruction,' IEEE Trans. Acoust., Speech, Signal Processing, vol.ASSP-35, no.2, Feb. 1987.

LIST OF FIGURES

each point is random within the limits specified.

Fig.2.7 Effect of random noise in the measured complex field data for three different cases of signal to noise ratios(SNR): (a) for SNR=10 dB (b) for SNR= 0 dB and (c) SNR=-10 dB. Since both magnitude and phase are affected, there is a progressive degradation in the quality of the reconstructed image as SNR decreases.

Fig.2.8 Image reconstruction from sparse data for four different cases: (a) from 64x64 points of received data, (b) from 32x32 points of received. data, (c) from 16x16 points of received data and (d) from 8x8 points of received data. The data is created by appropriate down- sampling and setting the values in between to zero. As expected, there is a systematic degradation as the number of samples of data are decreased.

Fig.2.9 Image reconstruction from partial data: (a) reconstruction from magnitude only and (b) reconstruction from phase only. The results show that significant features of the original image are preserved in the reconstruction from phase, indicating that phase is more important than magnitude.

Fig.3.1 Effect of poor sampling of the received data on the reconstructed image. The complete received data consists of 128x128 samples. The figure shows the image reconstructed for four different types of sampling and for four sets of under sampled values. The unknown sample values are set to zero.

Fig.3.2 Effect of multiple frequency data on the image reconstructed from sparse receiver array. The data consists of 64x64 samples. The figure shows the image reconstructed for four types of sampling and four cases of multiple frequencies.

Fig.3.3 Effect of multiple frequency data on the image reconstructed from sparse receiver array. The data consists of 32x32 samples. The figure shows the image reconstructed for four types of sampling and four cases of multiple frequencies. The quality of the image reconstructed improves as the number of frequencies are increased.

Fig.3.4 Effect of multiple frequency data on the image reconstructed from sparse receiver array. The data consists of 16x16 samples. The figure shows the image reconstructed for four types of sampling and four cases of multiple frequencies.

Fig.3.5 Effect of multiple frequency data on the image reconstructed from sparse receiver array. The data consists of 8x8 samples. The figure shows the image reconstructed for four types of sampling and four cases of multiple frequencies. The figure shows that even for very low sampling rate it is possible to get a good image provided the number of frequencies are large(16).

Fig.4.1 Effect of noise on the solution set.

Fig.4.2 Projection onto C_t. The hatched region denotes the set set $H(C_t)$ and Qg is the projection of Rg onto C_t. Note that the magnitude difference between Qg and Rg is 'e' in every dimension. In other words, if N denotes the number of dimensions

$$Ne = \Sigma|Hg[n]-f[n]| - t.$$

Fig.4.3 Projection onto C_ϕ. The hatched region denotes the set C_ϕ. The point closest to Rg in C_ϕ is Qg. Hence Qg may be given by

$$Qg = |Rg| \cos(\phi_{Rg} - (\phi_f + i)) \exp(j(\phi_f + i)).$$

Fig.5.1 Comparison of POCS and PONICS methods for reconstruction of images from noisy sensor array data. Uniformly distributed noise is used. The data is collected from a 64x64 array at different frequencies. Comparison is made for two different SNR's.

Fig.5.2 Comparison of POCS and PONICS methods for reconstruction of images from noisy sensor array data. Uniformly distributed noise is used. The data is collected from a 32x32 array at different frequencies. Comparison is made for two different SNR's.

Fig.5.3 Comparison of POCS and PONICS methods for reconstruction of images from noisy sensor array data. Uniformly distributed noise is used. The data is collected from a 16x16 array at different frequencies. Comparison is made for two different SNR's.

Fig.5.4 Comparison of POCS and PONICS methods for reconstruction of images from noisy sensor array data. Uniformly distributed noise is used. The data is collected from a 8x8 array at different frequencies. Comparison is made for two different SNR's.

Fig.5.5 Comparison of sequential and parallel methods of PONICS for image reconstruction.from noisy (uniformly distributed) multiple frequency hologram data using a 32x32 array for two SNR values (OdB and -10 dB). The figures show the similarity of the results in the sequential and parallel implementation.

Fig.6.1 Image Reconstruction from full and quantised phase for four different noise levels. All the receiver elements (128x128) are used in the reconstruction. The figure shows that the image reconstructed from quantised phase is as good as the image reconstructed from full phase at high noise levels.

Fig.6.2 Image reconstructed from full phase for SNR=0dB using sparse data collected at multiple frequencies. The figure demonstrates that it is possible to reconstruct an acceptible quality image from phase alone.

Fig.6.3 Image reconstructed from 2-bit phase for SNR=0dB using sparse data collected at multiple frequencies. The figure demonstrates that it is possible to reconstruct an acceptible quality image from 2-bit quantised phase.

Fig.6.4 Image reconstructed from full phase for SNR=-10dB using sparse data collected at multiple frequencies. The quality of the image reconstructed degrades as the noise level is increased:

Fig.6.5 Image reconstructed from 2-bit phase for SNR=-10dB using sparse data collected at multiple frequencies. The quality of the image reconstructed from 2-bit quantised phase is no worse than that reconstructed from full phase for most cases.

LIST OF ALGORITHMS

LIST OF TABLES

LIST OF SYMBOLS

ρ_F	metric on the space of functions F
F,G	metric spaces
H	Hilbert space
Q,T	transform operators
D	stabilising functional
f,g,h	functions
f,g,n	vectors
P	projection operator
C	(i) closed convex set
	(ii) closed linear manifold
R	Fredholm's operator of the first kind
$\perp C$	orthogonal complement of a linear set C
ϕ	phase function
ϕ_q	quantised phase
R_{gg}	autocorrelation of a vector g
R_{nn}	autocorrelation of a noise vector **n**
f(x,y)	field distribution on the receiver plane
g(x,y)	field distribution on the object plane
h(x,y)	impulse response of system
*	convolution
n(x,y)	noise function
F(u,v)	Fourier transform of f(x,y)
G(u,v)	Fourier transform of g(x,y)
H(u,v)	Fourier transform of h(x,y)
C_p	region of support
I_p	set of sampling points
C_{fsc}	set of signals with finite region of support
B_w	bandwidth
λ	wavelength
$\Delta x, \Delta y$	sampling interval on the receiver plane
$\Delta x_o, \Delta y_o$	sampling interval on the object plane

B_p	set of bandlimited signals
C_ϕ	set of signals with prescribed transform phase
C_q	set of signals with prescribed quantised phase
C_{fo}	set of object field distributions that could have given rise to a given receiver field distribution
C_{fi}	set of object field distributions that could have given rise to a given receiver field distribution for a wavelength λ
z	distance between object and image plane
s	real number in $(0,1)$
s_1, s_2	real numbers in $(0,2)$
$\Vert\cdot\Vert$	norm
C°	interior of a set C
$\bar{C}$	complement of a set C
Q_R	projection onto the range of R
C_d	$\{g(x): \rho_C(f, Rg) \leq d\}$
C_r	$\{g(x): \rho_{L2}(f,Rg) \leq r\}$
C_t	$\{g(x): \rho_{L1}(f,Rg) \leq t\}$

LIST OF PUBLICATIONS

1. B.Yegnanarayana, C.P.Mariadassou and Pramod Saini, 'Signal Reconstruction from Partial Information for Acoustic Imaging Applications,' presented at IEEE ASSP, EURASIP V Workshop on MDSP, Noordjwickhout, The Netherlands, Sept. 14-16, 1987.
2. B.Yegnanarayana, C.P.Mariadassou and Pramod Saini, 'Image Reconstruction from Sensor Array Data,' presented at the Indo-US Workshop, Bangalore, India, Jan.11-14, 1988.
3. B.Yegnanarayana, C.P.Mariadassou and Pramod Saini, 'Studies on Reducing the Receiver Complexity in Acoustic Imaging,' EUSIPCO, Grenoble France, Sept.2-5, 1988.
4. B.Yegnanarayana, C.P.Mariadassou and P.Saini, 'Signal Reconstruction from Partial Data for Acoustic Imaging Applications,' Signal Processing, Feb.1990.
5. C.P.Mariadassou and B.Yegnanarayana, 'Image Reconstruction from Noisy Holograms,' IEE-Proc. Part F (accepted for publication).
6. C.P.Mariadassou and B.Yegnanarayana, 'Signal Processing Issues in Sensor Array Imaging,' submitted to Proc. IEEE.
7. C.P.Mariadassou and B.Yegnanarayana, 'Iterative Methods for Image Reconstruction from Digital Holograms,' submitted to IEE-Proc. Part F.